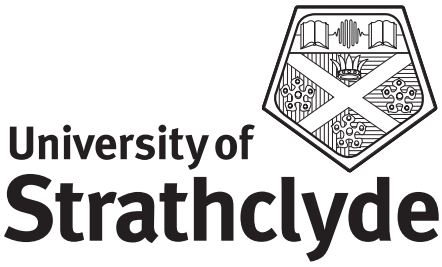

Effects of Fractional Time Derivatives in Predator-Prey Models

Zuhur Moraya Alqahtani
Department of Mathematics and statistics
University of Strathclyde
Glasgow, UK
July 2020

This thesis is submitted to the University of Strathclyde for the degree of Doctor of Philosophy in the Faculty of Science.

Acknowledgements

Above all, I would like to thank God without whom I could not have completed this thesis.

Without my supervisor, Professor Nigel Mottram, this thesis would not exist. His knowledge, explanations, support, kindness, understanding and most of all his dedication to his field, have been an inspiration to me. By challenging and encouraging me, he has inspired me and helped me to become a better researcher. I would also like to thank my internal supervisor, Dr. El-Shahed, at Al Qassim University, who offered his invaluable expertise and guidance.

I also want to thank my parents who have kept me in their thoughts and prayers during this journey. They have offered their unconditional support, love and guidance continuously without asking anything for themselves. I want to thank my children, Raneem and Mohammed, for their understanding, patience, and kindness while I have been completing my research. My husband, Ayed, has been supportive and patient during my research. I want to thank my sisters and brothers who freely provided their guidance when I asked them.

This acknowledgement cannot encompass the many people who deserve thanks who have not hesitated to help me when I needed help, including my colleagues at Princess Nourah bint Abdulrahman University.

I would also like to take this opportunity to thank the University of Strathclyde for accepting me as a PhD candidate and providing academic support, and Princess Nourah bint Abdulrahman University for providing the funding for me to complete my PhD.

Abstract

This thesis is concerned with the effects of fractional derivatives in predator-prey-like systems, including models of plant water interaction. In Chapter 3, a fractional order predator-prey model is introduced, and we show how fractional derivative order can change the system from monostable to bistable. The observable domains of attraction of the two stable points will also be considered, in particular how they change as the fractional order is changed. In Chapter 4, we will generalise the predator-prey model studied in Chapter 3 by considering different fractional orders for each species. This system is referred to as an incommensurate system. We will explain how the different fractional orders affect the stability of this model. Then, in order to see if this change in stability is a more general result, we will consider a plant-herbivore incommensurate system and study the stability of this system. We will also find an approximate analytical solution for the characteristic equation of the incommensurate system when the two fractional orders α and β are similar and both close to the critical value of the fractional order of the commensurate system. In this case, we are able to map out the stable and unstable boundary as a function of both parameters. We will compare the analytical and numerical solutions in these two incommensurate systems. In Chapter 5, we consider two different models of the interaction between surface water, soil water and plants. The first is similar to the model of Dagbovie and Sherratt, without spatial derivatives. We study the steady states of this model and observe the effect of adding the fractional order on the system. In the second model the soil water equation is replaced with the more realistic the Richards equation. In this model, we will also study the steady state and dynamic behaviour in the integer model and then consider the incommensurate fractional system. In this case, we see that a fractional order can affect the transient behaviour of the system.

Contents

List of Figures

List of Tables

Chapter 1

Introduction

Mathematical models allow us to describe the real world by translating from fields such as experimental physics, chemistry, environment science or the social sciences into mathematical equations. Models have been used by mathematicians for thousands of years to improve our understanding of the world and how their components are interrelated. They have been used to model and predict various systems in fields such as meteorology, biomedicine and other real-life disciplines [9]. When a mathematical model can be made to mimic real-life systems accurately and reliably, they can help us to develop our understanding of science, enable us to assess the effects of changes to a system, and help us to plan and make decisions strategically [122].

Once formulated, a model can provide qualitative and quantitative results. Qualitative results demonstrate the behaviour of the system without finding the exact solution. On the other hand, quantitative results depend on finding the solution of the mathematical model and then studying these solutions, which are sometimes only relevant to specific conditions. A motivation for using models in the ecological system we will study is that modelling is easier than experimentation or field trials and we cannot often do experiments over large scales and time [122].

In this thesis we consider ecological models which include competition, cooperation, and predator-prey interactions. They model the dynamics of populations by using ordinary and partial differential equations. The models we consider are based on the classical Lotka-Volterra model, which was introduced in [39], and is comprised of two ordinary differential equations representing interactions of the predator and prey species. The classical Lotka-Volterra model is probably the simplest form of prey-predator interaction and can be written as two coupled differential equations, namely

$$\frac{dx}{dt} = ax - bxy,$$

$$\frac{dy}{dt} = dxy - cy,$$

where x is the number or proportion of prey, y is the number or proportion of predators and a, b, c and d are positive real parameters describing the evolution and interaction of the two species. This model assumes that the prey population increases without the presence of predators at a rate a, that the predator population will die out without the presence of prey species at a rate c, that predators can consume an unlimited amount of the prey species modelled by the parameters b and d, and that there are no complicating environmental factors that would interfere with these interactions.

Researchers have introduced many other models based on the Lotka-Volterra system to model the interactions of herbivores and plants and other systems of interaction such as plants and water. These extended models may consider other variables and other methods of interactions, and they can contain more than two interacting species. They often extend the Lotka-Volterra system to improve how growth, death, predation, harvesting and multiple species are modelled. Traditionally, all biological models have used the integer first order derivative as shown above and there is a huge literature dealing with such models; some of which can be found in the reviews [56, 123] the references therein. In this thesis we will consider a way of incorporating memory into the behaviour of biological populations.

In general, integer derivative models do not include memory effects, and calculate the rate of change of dependent variables using time derivatives evaluated at the present time [38, 63, 79]. However, some integer models do address memory using delay differential equations, where delayed effects or variations in the state of the current system depend on the state of the system at a specific time in the past. In predator-prey models, which consider aspects of population (i.e. conception, gestation and reproduction), the use of delayed differential equations is effective [38, 63, 79]. In fact, some of the dynamics that occur in ecological systems are more dependent on the past state than the current, so consideration of the past time is certainly necessary to understanding these processes in the system [37, 56]. In addition, systems with multiple delays (i.e. birth-death, gestation-reproduction) can be modelled using a system of such delayed differential equations [40]. However, if one or more of the species have some form of memory, fractional differentiation, which has a non-local property, can be a way of including memory [22, 28, 62, 78, 91].

Fractional calculus, the theory of integrals and derivatives of arbitrary orders [57], has been in use for more than 300 years, but it is only recently that it has been applied to physics, engineering and other fields of study. It has recently been shown that, in some situations, fractional derivatives in dynamical systems can more accurately describe real-life situations [118]. Before introducing the

modelling systems that use fractional derivatives, we will first introduce a short historical review of fractional calculus.

From an early age, we learn that exponents represent the idea of algebraic or numerical quantities that are multiplied repeatedly. When we consider exponents of non-integer value, the concept of multiplying a number by itself, i.e. 2.6 times, is more difficult to imagine. In the 17th century, mathematicians wondered if it is possible to find a derivative of a fractional order and in 1695, Leibniz wrote to L'Hopital and considered the meaning of derivatives, when generalised to non-integer order. In that letter, L'Hopital asked about the meaning of the 1/2 order derivative, and Leibniz responded by saying the answer would be logically unacceptable but he predicted that "useful consequences" would arise from it one day [62]. This famous discussion marked the beginning of fractional calculus.

During the next three centuries, many great mathematicians would make significant contributions to this new field of study. In the 18th and early 19th centuries, Euler, Lagrange, Laplace, Lacroix and Fourier introduced definitions of fractional derivatives for any non-integer order. In 1738, when Euler generalised the factorials of a number to the Gamma function, he noticed that the derivative $d^p x^a/dx^p$ can have a meaning when p is non-integer [109]. In 1772, Lagrange similarly noticed that the law of exponents for differential operators of integer order can be extended to any arbitrary order [78]. In 1812, Laplace's work followed Euler's with a detailed definition of the fractional derivative [78] and, in 1819, Lacroix developed the nth derivative for the function $f(x) = x^n$ by generalising the factorial used for the Gamma function and gave the order 1/2 derivative for the function $f(x) = x$ [78]. In 1822, Fourier then provided a more practical definition for derivatives of both the power function and then for any function [78].

After these initial investigations into the theoretical nature of fractional derivatives, Abel, Liouville, Riemann, Grunwald and Letnikov used fractional operators to solve specific physical applications. In 1823, Abel used fractional operations to solve a physical problem, the tautochrone problem, which concerns the determination of the curve for which the time taken for a particle to reach a point is independent of its initial position [21]. Abel combined integration and differentiation and extended it to a non-integer order in order to solve this problem. Then, in 1832, Liouville provided a detailed study of fractional derivatives defined in the form of an infinite series, and applied these derivatives to solve various linear differential equations [109]. In 1847, Riemann introduced a form of fractional integration, although not published until 1876, where he generalised a Taylor series in formulating his definition. After that, Grunwald and Letnikov approached fractional differentiation as the limit of a sum based on their use of finite differences [109].

By the late 19th century, Riemann and Liouville's definitions had become the most well-known and well-used definitions in the literature. A combination of these definitions is the Riemann-Liouville fractional derivative and was introduced in Sonin's 1869 paper entitled "On differentiation with arbitrary index" [78]. Although other definitions for fractional derivatives or integrals were also detailed, i.e. by Laurent in 1884, Nekrassov in 1888, and Krug in 1890 [62], the most notable subsequent definition has been the Caputo derivative introduced in 1967 [16]. We will further discuss the Caputo definition below and in the next chapter.

We will also see in the next chapter that modelling systems using fractional derivatives can generalise integer models in order to include information from past time. Since integer order derivatives do not consider memory effects, and in fact can produce incomplete explanations when researchers have attempted to use them in this way, fractional differential equations have been employed [89, 90], often using the Caputo fractional derivative, to do this. The Caputo derivative is a particularly effective form of fractional derivative because the derivative of any constant is zero and it allows the use of the usual initial and boundary conditions to frame problems [8]. The former property means that the equilibrium states in a Caputo fractional derivative system are exactly the same as the equilibria of the integer order system.

There are many examples where mathematicians and other researchers have modelled real world processes using the Caputo fractional derivative. In the field of engineering, one example is the study of viscoelastic fluids which introduces the tautochrone problem, which has been described earlier in this section [21]. Two studies demonstrate the usefulness of the Caputo derivative in fractional advection-dispersion equation in the field of groundwater hydrology where they were used to model the movement of solutes added to water to trace its flow within a porous medium [8, 47]. In addition, Caputo and other researchers studied diffusion in a porous biomembrane [18, 19] by introducing a derivative of fractional order, the Caputo derivative, to the Fick equation. The Caputo derivative allowed them to determine the concentration profile's dependency on time, in biophysical processes within the cell, in order to produce a simplified model that can be useful where the role of drug release is a major factor in drug delivery systems. Further, the Caputo derivative was used to model sedimentation in water reservoirs [20] in order to improve reservoir efficiency and to enable hydrologists to predict reservoir lifetime. This was done by generalizing the diffusion equation through the introduction of a distributed order fractional derivative which allowed the measurement of changes in sediment deposit over time. Also, in the field of geophysics and fluid mechanics, a modified Caputo derivative was used in constitutive equations to model a type of plastic media (i.e. any material that remains in the changed state after removing resistance) for the purpose of determining its usefulness in disposing of radioactive waste [17]. In this study, the addition of a form of the Caputo derivative

generated constitutive memory equations that allowed them to analyze different properties of a plastic media, namely polycrystalline halite. In all these studies, the Caputo fractional derivative has been used where memory must be considered [96] and demonstrates the usefulness of fractional calculus in practical applications.

Some other examples of practical applications of fractional derivatives in various fields are considered here. In mathematical medicine and biology, researchers have used fractional order models to study immune response to HIV infection, where changes to the fractional order reflect changes in the patients' epidemic status. Infection and proliferation rates of immune response cells were also simulated accurately in the study [90]. The same researchers also used a different fractional order model to study coinfection rates of HIV and TB in relation to a multi-drug resistant strain of TB and treatments to coinfected patients. They calculated the reproduction number and undertook numerical simulations of relevant parameters to conclude that the fractional order in this model was linked to patients' health history [89]. Furthermore, two models of biological systems, showing the behaviour of immune system response to tumours and HIV infection, were investigated by formulating fractional models and where the threshold parameter R_0, the minimum infection parameter, was used to obtain the stability of the systems. They determined that fractional order derivatives added additional complexity to the behaviour of the models. As a result, researchers of infectious disease have used them to model additional parameters in relation to tumour response [102]. Further investigation of tumours led researchers in one study to compare two Gompertz tumour growth models, one using an integer derivative and one using a fractional derivative, to study immune system response to long-term tumour growth in mice. It was determined that the fractional model better fit their experimental data on tumour growth by comparing the predictive capability of the models [12]. In another study, researchers studied the immune response to the long-term growth of tumours in a human population [7]. In this study, according to Arshad et al., the fractional model was determined to best fit their data because these types of equations can describe past evolution of the function. They conclude that additional advantages of the fractional model over the integer model were the ability to track the progression of the growth of different tumours and to adjust the model to each patient's medical needs. In epidemiology, researchers studied the spread of influenza type A, a type of flu virus which can lead to global pandemics, through human populations by developing a fractional order SIRC model using the Caputo derivative based on a SIRC model developed using ordinary differential equations [36]. They state that like the original, this model takes into account susceptible, infected, recovered and cross-immune individuals, but takes advantage of the non-local property of fractional differential equations to consider memory effects, by studying the qualitative behaviour of the model, and then simulating and finding a numerical solution [36]. Further work in epidemiology has been done by researchers studying a 2009 dengue epidemic in west Africa. They reformulated

a SIR model from a system of ordinary differential equations to a fractional one using the Riemann-Liouville derivative to provide a more realistic model that considers memory effects [92]. In their study, both the original and the modified model account for susceptible, infected and recovered individuals in the area. The researchers compared the results for both models using numerical simulation and found that the fractional model provided more accurate results [92]. In psychology, researchers investigated the type of memory that can be modeled with a fractional derivative by taking test data from other researchers and showing that the model can be used effectively to study human memory [33]. They determined that there are two types of memory, one of which can be modeled using fractional derivatives, and they studied two aspects of human memory retention using this model [33]. A more in-depth review of each model that has been considered in our work will be provided in the appropriate chapters within this thesis.

This thesis is organized in the following way. Chapter 2 covers the basic concepts and mathematical principles of fractional derivatives on which our work is founded. The chapter outlines approaches and specific functions that are needed to understand the properties of fractional calculus. In Chapter 3 we consider the behaviour of a fractional order predator-prey model and study the static and dynamic properties of the system, where nonlinear interactions between the two species can lead to multiple stable states. We find that this multistability depends upon the fractional order of the time derivative. These results yield richer dynamics compared to the integer order model, and we find that the parameters and memory effect of the species contribute to important behaviour that may be realistically observed. The work done in Chapter 3 has also been published in Letters in Biomathematics as "Derivative-order-dependent stability and transient behaviour in a predator–prey system of fractional differential equations" [4]. In Chapter 4, we consider the case where the fractional orders of the predator and prey populations are different, which is termed an incommensurate system. We found an approximate analytical solution for the characteristic equation of the incommensurate system using a perturbation from the solution of the characteristic equation of the commensurate system found in Chapter 3. The stability condition in the incommensurate fractional system is found to be a function of the two fractional orders, and an approximate analytical solution for the stability boundary is determined. We use a numerical method to find the solution of the incommensurate system and compare with the analytical results for two different predator prey systems. The first incommensurate system we investigate is the same model we discussed in Chapter 3 and we illustrate how the stability of this system changes if the fractional orders are not the same. The second incommensurate system, a plant-herbivore model, was then studied in a similar way.

Chapter 5 continues the work of the final model in Chapter 4 by considering two further, and more complex models of plant biomass. The first model is that of

Dagbovie and Sherratt [24] but with no spatial dimensions, which includes three differential equations representing plant biomass, surface water and soil water. We then investigated the effect of a fractional derivative included in the biotic element, the plant biomass. The second model also includes the three elements of biomass, surface water and soil water, but the soil water is modelled using the classical Richards' equation and the biomass equation includes a term that depends on the total water uptake rate by roots within the soil depth. For this system, we have investigated the effect of the fractional derivative on the dynamics of the biomass as the rainfall changes. The behaviour of the steady state solution for this model was presented at the 2018 British Applied Mathematics Colloquium. Finally, Chapter 6 summarises significant results from this thesis and discusses how they may be developed and extended in future research.

Chapter 2

Theoretical Background of Fractional Derivatives

2.1 Introduction

In this chapter, the basic concepts and definitions of fractional derivatives, will be introduced, in order to form the basis of the material presented in the following chapters. Here we include the main results that are relevant to this thesis, but a more complete introduction to fractional calculus can be found in references [78, 91], from which much of the material in this chapter is taken.

2.2 Basic Definitions

In this section, various definitions that are needed in the rest of this chapter are highlighted. We start by listing special functions that will be used in the definitions and analysing of fractional derivatives.

2.2.1 Special Functions

The Euler Gamma function [13] is a generalised form of the factorial function and is defined by

$$\Gamma(z) = \int_0^\infty t^{z-1} e^{-t} dt,$$

where $\mathrm{Re}(z) > 0$. The Gamma function can be extended to negative numbers through analytic continuation. For our work the important properties of the Gamma function are that it reduces to the factorial function for integer z, $\Gamma(n+1) = n!$ for all $n \in \mathbb{N}$, and satisfies $\Gamma(z+1) = z\Gamma(z)$.

The Mittag-Leffler function [48] plays an important role in fractional differential equations since it is the basis for the eigenfunctions of fractional derivatives,

and therefore is a generalisation of the exponents function e^z in integer systems.

The Mittag-Leffler function is defined as,

$$E_\alpha(z) = \sum_{k=0}^{\infty} \frac{z^k}{\Gamma(\alpha k + 1)},$$

where $z \in \mathbb{C}$, $\alpha > 0$. If $\alpha = 1$, we see that $E_1(z) = e^z$. The two-parameter Mittag-Leffler function $E_{\alpha,\beta}(z)$, generalises this function and is defined by

$$E_{\alpha,\beta}(z) = \sum_{k=0}^{\infty} \frac{z^k}{\Gamma(\alpha k + \beta)},$$

where $z \in \mathbb{C}$, $\alpha > 0$ and $\beta > 0$.

2.2.2 Fractional Derivatives and Fractional Integrals

In this section we firstly consider the classical integer order derivative and then consider how this can be generalised to a fractional order derivative.
The first derivative of a function $f(x)$ is defined as

$$f'(x) = Df(x) = \lim_{h \to 0} \frac{f(x) - f(x-h)}{h},$$

and the nth derivative can then be calculated by iterating the first derivative n times to obtain,

$$f^{(n)}(x) = D^n f = \lim_{h \to 0} h^{-n} \sum_{k=0}^{n} (-1)^k \binom{n}{k} f\left(x - kh\right), \tag{2.1}$$

where the binomial coefficient is $\binom{n}{k} = \frac{n!}{k!(n-k)!}$. The summation upper limit is n although, since the binomial coefficient is zero for $k > n$ the upper limit could be replaced by infinity. Using (2.1) we can generalise the derivative to a fractional order by replacing the integer n with any positive real number α, to define the αth derivative. In this way we obtain the Grünwald-Letnikov [62] fractional derivative given by

$$f^{(\alpha)}(x) = D^\alpha f(x) = \lim_{h \to 0} h^{-\alpha} \sum_{k=0}^{\infty} (-1)^k \binom{\alpha}{k} f\left(x - kh\right), \tag{2.2}$$

where $\binom{\alpha}{k} = \frac{\Gamma(\alpha+1)}{\Gamma(k+1)\Gamma(\alpha-k+1)}$. The summation upper limit is now infinity since the Gamma function is defined for all values of k. Note that, while $f'(x)$ only takes information from $f(x)$ and $f(x-h)$, the derivative $f^{(\alpha)}(x)$ takes information

from an infinite number of times before.

For integration, which can be defined as negative derivatives, we have

$$D^{-1}f(x) = If(x) = \int_a^x f(t)dt,$$

where we here set $t = a$ as the lower integral limit.

Using Cauchy's formula for repeated integration [83, 91], we then obtain

$$\begin{aligned} D^{-n}f(x) = I^n f(x) &= \int_a^x dx_1 \int_a^{x_1} dx_2 ... \int_a^{x_{n-1}} f(t)dt \\ &= \frac{1}{(n-1)!}\int_a^x (x-t)^{n-1} f(t)dt. \end{aligned}$$

We can then generalise the derivative of order $-n$, i.e. the integral of order n, by replacing n in Cauchy's formula with α. This leads to a definition of the fractional integral,

$$I_a^\alpha f(x) = \frac{1}{\Gamma(\alpha)}\int_a^x \frac{f(t)}{(x-t)^{1-\alpha}}dt, \tag{2.3}$$

where $x > a$ and $\alpha > 0$, which is termed the Riemann-Liouville fractional integral [62]. This form of fractional integral is popular, and has been used many times, because it has many similar properties to the standard integral [78]. This includes the identity property, $I_a^0 f(x) = f(x)$, linearity, $I_a^\alpha(\lambda f(x) + \gamma g(x)) = \lambda I_a^\alpha f(x) + \gamma I_a^\alpha g(x)$, where λ and $\gamma \in \mathbb{C}$, and the composition and commutative properties $I_a^\alpha(I_a^\beta f(x)) = I_a^\beta(I_a^\alpha f(x)) = I_a^{\alpha+\beta}(f(x))$ and a useful Laplace transform $L(I_a^\alpha f(x))(s) = F(s)/s^\alpha$.

The fractional derivatives which are most commonly used are both based on the Riemann-Liouville fractional integral and are termed the Riemann-Liouville fractional derivative and the Caputo fractional derivative. The Riemann-Liouville fractional derivative [78], for the function $f(x)$ is defined by ${}^{RL}D_a^\alpha f(x)$, for $x > a$ and $\alpha > 0$, and is equivalent to the composition of a $(n-\alpha)$th-order integration and a nth order differentiation thus,

$${}^{RL}D_a^\alpha f(x) = D^n I^{n-\alpha} f(x).$$

Equivalently, we have

$${}^{RL}D_a^\alpha f(x) = \begin{cases} \dfrac{1}{\Gamma(n-\alpha)}\dfrac{d^n}{dx^n}\displaystyle\int_a^x (x-t)^{n-\alpha-1} f(t)dt & \text{if } n-1 < \alpha < n,\ n \in \mathbb{N} \\ \dfrac{d^n}{dx^n} f(x) & \text{if } \alpha = n. \end{cases} \tag{2.4}$$

The Riemann-Liouville fractional derivative also has many similar properties to the standard integer derivative [57] such as the identity property, ${}^{RL}D_a^\alpha(I_a^\alpha f(x)) =$

$f(x)$, ${}^{RL}D_a^0 f(x) = f(x)$, the property of composition with integer order derivative, ${}^{RL}D_a^n({}^{RL}D_a^\alpha(f(x))) = {}^{RL}D_a^{n+\alpha}(f(x))$, and linearity, ${}^{RL}D_a^\alpha(\lambda f(x) + \gamma g(x)) = \lambda {}^{RL}D_a^\alpha f(x) + \gamma {}^{RL}D_a^\alpha g(x)$, where λ and $\gamma \in \mathbb{C}$. However, some other properties are not in general the same as the integer derivative, such as commutativity with the integer order derivative, ${}^{RL}D_a^n({}^{RL}D_a^\alpha(f(x))) \neq {}^{RL}D_a^\alpha({}^{RL}D_a^n(f(x)))$. Also, ${}^{RL}D_a^\alpha(c) = \dfrac{c}{\Gamma(1-\alpha)}(x-a)^{-\alpha}$, where c is a constant, so that the derivative of a constant is not zero; ${}^{RL}D_a^\alpha(x-a)^\gamma = \dfrac{\Gamma(\gamma+1)}{\Gamma(\gamma-\alpha+1)}(x-a)^{\gamma-\alpha}$; ${}^{RL}D_a^\alpha(e^{\lambda x}) = x^{-\alpha}E_{1,1-\alpha}(\lambda x)$ where $E_{1,1-\alpha}$ is the two-parameter Mittag-Leffler function and

$$L({}^{RL}D_0^\alpha(f(x)))(s) = s^\alpha F(s) - \sum_{k=0}^{n-1} s^k({}^{RL}D_a^{\alpha-k-1}(f(0))),$$

where L is the Laplace transform operator. Although the Riemann-Liouville fractional derivative has many useful properties, and is often used, the fact that the derivative of a constant is not zero means that the evaluation of equilibria in dynamical systems becomes more complicated.

The other often used fractional derivative is the Caputo fractional derivative [16] which is defined as

$${}^{c}D_a^\alpha f(x) = I^{n-\alpha}D^n f(x),$$

where $x > a$ and $\alpha > 0$ or equivalently

$${}^{c}D_a^\alpha f(x) = \begin{cases} \dfrac{1}{\Gamma(n-\alpha)}\displaystyle\int_a^x (x-t)^{n-\alpha-1} f^{(n)}(t)dt & \text{if } n-1 < \alpha < n,\ n \in \mathbb{N} \\ \dfrac{d^n}{dx^n} f(x) & \text{if } \alpha = n. \end{cases} \tag{2.5}$$

The Caputo fractional derivative also has many similar properties to the standard integer derivative [57] such as the identity property, ${}^{c}D_a^0 f(x) = f(x)$, the property of composition with integer order derivatives, ${}^{c}D_a^\alpha({}^{c}D_a^n(f(x))) = {}^{c}D_a^{\alpha+n}(f(x))$, linearity, ${}^{c}D_a^\alpha(\lambda f(x) + \gamma g(x)) = \lambda {}^{c}D_a^\alpha f(x) + \gamma {}^{c}D_a^\alpha g(x)$, where λ and $\gamma \in \mathbb{C}$. However, some other properties are not in general the same as the integer derivative, such as the commutativity with integer order derivative, ${}^{c}D_a^\alpha({}^{c}D_a^n(f(x))) \neq {}^{c}D_a^n({}^{c}D_a^\alpha(f(x)))$, ${}^{c}D_a^\alpha(x-a)^\gamma = \dfrac{\Gamma(\gamma+1)}{\Gamma(\gamma-\alpha+1)}(x-a)^{\gamma-\alpha}$ where $\gamma > -1$, ${}^{c}D_a^\alpha(e^{\lambda x}) = \lambda^n x^{n-\alpha}E_{1,n-\alpha+1}(\lambda x)$, where $E_{1,1}$ is the two-parameter Mittag-Leffler function and $L({}^{c}D_0^\alpha(f(x)))(s) = s^\alpha F(s) - \sum_{k=0}^{n-1} s^{\alpha-k-1}(D_a^k(f(0))), n-1 < \alpha \leq n$ where L is the Laplace transform operator. However, the key property that leads to the Caputo derivative being useful is that ${}^{c}D_a^\alpha(c) = 0$ for a constant c.

The Riemann-Liouville fractional derivative and the Caputo fractional deriva-

tive are related by [68],

$$ {}^{c}D_{a}^{\alpha}(f(x)) = {}^{RL}D_{a}^{\alpha}(f(x)) - \sum_{k=0}^{n-1} \frac{x^{k-\alpha}}{\Gamma(k+1-\alpha)} f^{(k)}(0), $$

and when $f^{(k)}(0) = 0$, we obtain

$$ {}^{c}D_{a}^{\alpha}(f(x)) = {}^{RL}D_{a}^{\alpha}(f(x)), $$

and so, in this case, the Riemann-Liouville and Caputo derivatives are equal. For both classical and fractional equations, additional conditions to generate solutions must be determined. While the Caputo fractional derivative conditions, which are the same as the ones for classical ordinary differential equations, are state initial conditions, the ones for Riemann-Liouville fractional derivatives are made up of fractional derivatives which cannot be easily compared to real life. Therefore, the Riemann-Liouville fractional derivative is less often useful for modelling real world phenomena [31]. Also, as mentioned above when we need to study the steady state of a system, the Caputo derivative is useful in finding an equilibrium point since the derivative of the constant is zero [57]. For these reasons, the Caputo fractional derivative will be selected in this thesis in the differential equations. As we will see in the next sections, in this thesis we will generalise first order derivatives by fractional derivatives of order $\alpha \in (0, 1]$, so that $n = 1$, and where we take $a = 0$ so that memory effects are included through the fractional derivative by including information for all t from zero to present time. As the fractional order α approaches zero we can see from (2.2) that the factor $h^{-\alpha} \begin{pmatrix} \alpha \\ k \end{pmatrix}$ means means that the fractional derivative receives more weight or influence from the system state further as we go back in time. Thus variations of α will model changes in memory, from long term ($\alpha \to 0$) to short term ($\alpha \to 1$).

2.3 Fractional Order Dynamical Systems

Many biological systems possess a distributed form of memory rather than memory of discrete moments in the past. Therefore, integer order or time delay models may not be as realistic or effective as fractional models, as mentioned in [7, 102]. The general form of any fractional model is

$$ D^{\alpha_k} y_k(t) = f_k(y_1, y_2, ..., y_n), \tag{2.6} $$

with initial conditions $y_k(t_0) = b_k$, $k = 1, ..., n$. The y_k are the species populations, the α_k are the fractional derivative orders, the f_k are functions of y_k, and the b_k are the initial values of the populations y_k at time $t = t_0$.

Fractional dynamical systems such as (2.6) are a generalization of classical classical dynamical systems of integer order, i.e. where $\alpha = 1$. When all the species are biological organisms and have the same memory parameterised by the fractional derivative order α, the system is called commensurate. When the species are biological organisms but have different memory, or when some of the species are biological organisms and others are non-biological, the system is called incommensurate.

The functions f_k in (2.6) model changes in the species y_k and in interactions between the species over time. One of the most common components of f_k is the term that describes the logistic growth [121], which has been used to model many different biological systems [80, 87]. Logistic growth can be described as the limited physical growth of a population y_k taking the form $f_{\text{growth}} = ry_k\left(1 - \frac{y_k}{K}\right)$, where r is the growth rate and K is the carrying capacity. As Figure 2.1(a) shows, in this case the growth rate is only positive for populations between 0 and K, and if the prey population goes above K, the growth rate is negative because there is not enough food to support all the prey, and as a result some die. The solution of a logistic growth differential equation is characterised by the logistic function, which show exponential growth rate, until a population reaches carrying capacity, and is shown in Figure 2.1(b).

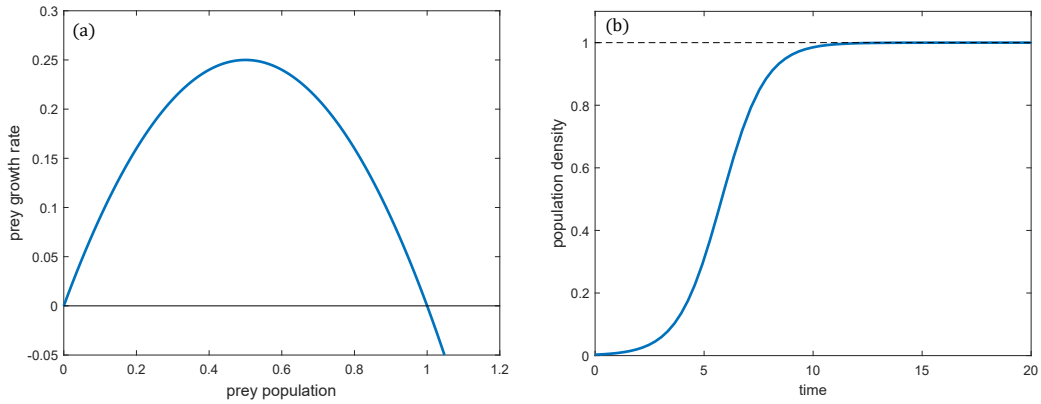

Figure 2.1: The logistic growth function. (a) The growth rate of prey. (b) The solution to a logistic growth equation.

A common function used to model the interaction between two species through predation, specifically between a population of prey and predators, was introduced by Holling [54, 55] and includes three possible response forms, Holling type I, Holling type II and Holling type III [26], see Figure 2.2. They are all of the form $f_{\text{pred}} = g(y_{k-1})y_k$, where f_{pred} is a term in f_k for the predator species y_k, the prey species are y_{k-1}, and where $g(y_{k-1})$ is the growth due to predation rate that can

take any one of the Holling type functions. The form of $g(y_{k-1})$ is chosen depending on the response of the predator to a given prey supply, as can be seen in the Lotka–Volterra predator–prey model [51].

Holling type I behaviour assumes a linear increase in consumption with prey density. It also assumes that there is no delay between the time when a predator consumes a prey and then consumes another. Moreover, it assumes that the consumption of prey does not affect the predator's search for more prey. It is the simplest of the functional responses and has the form $g(y_{k-1}) = ay_{k-1}$, where a is the predation rate. For this type, the rate at which prey y_{k-1} is captured and consumed by the predator y_k is directly proportional to the density of the prey. This type of functional response was used by Lotka and Volterra in their classical work.

A Holling type II relationship models a continually decreasing consumption rate with increasing prey density and where prey consumption eventually reaches a constant value [26] due to the predator's limited capacity to process food. A type II relationship is similar to a type I except that each predator requires handling time for each individual of the prey species that is consumed which reduces the available time to search for more prey [26]. The predation interaction can be of the form $g(y_{k-1}) = \dfrac{ay_{k-1}}{y_{k-1} + b}$ where a/b is the predation rate when the levels of prey, y_{k-1}, are small and a is the maximum growth rate of the predator species when there are many available prey. The parameter b is the half saturation point, i.e. the value of y_{k-1} at which the predation rate is half the maximum value.

A Holling type III function is similar to the type II behaviour at high levels of prey density, but for low prey numbers the form of predation rate reduces to zero, modelling the learning, searching and prey switching behaviour of predators. Learning and searching in predator behaviour refers to the way they naturally improve their efficiency in finding and attacking prey as prey density increases. Prey switching occurs in ecosystems where there are two or more prey species and one predator species. If the prey species are at equal densities, the predator will prey on either one randomly. However, if the density of one of the prey species decreases, the predator will switch to the other more common species more often. The form of predation rate decreasing to zero can be explained by the predator finding prey so rarely that it has not had enough experience to enhance its ability to capture and kill prey species. This response is represented by $g(y_{k-1}) = \dfrac{ay_{k-1}^2}{y_{k-1}^2 + b^2}$, where b is again the half saturation point.

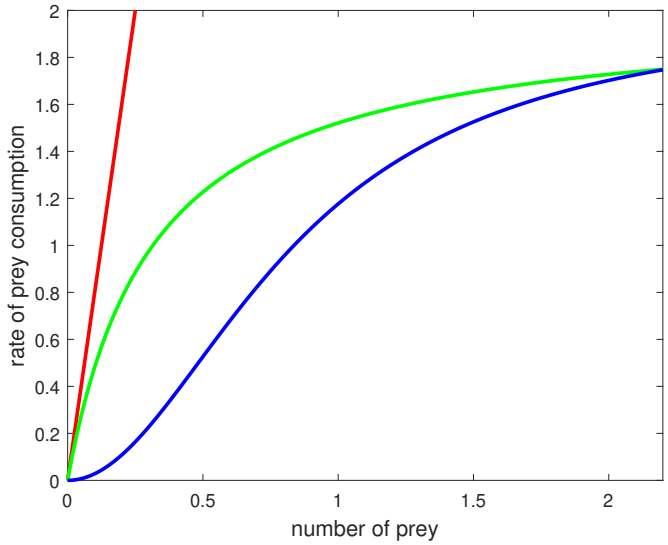

Figure 2.2: Holling type functional responses where Holling type I (red curve), Holling type II (green curve) and Holling type III (blue curve).

Here we have just highlighted a few of the terms that commonly contribute to the predator-prey functions f_k. There are many other terms that are used to model the complex interactions of species, but we will describe those when we meet them in later chapters.

In this thesis, it will often be necessary to solve the system of fractional differential equations using a numerical method. For this we use a method based on the Adams-Bashforth-Moulton method [29, 30, 32]. This method uses a Volterra integral equation form of the initial value problem and a time-iterative scheme. Standard quadrature techniques are used to solve the integrals, which alone is called the one-step Adams Moulton method, with an explicit time stepping method, known as the one-step Adams-Bashforth method. The combination of these two schemes is known as the Adams-Bashforth-Moulton method. Full details of this method are given in [30]. For a more complete discussion on this numerical method, an error analysis and stability result are covered by Sweilam et al. [115] and Garrappa [42]. Also, the work of Leedle [65] that contains a summary of results for standard and higher order Adams-Bashforth-Moulton methods, including the result that the error is proportional to $h^{1+\alpha}$, where h is the time step value and $\alpha < 1$.

In this thesis, the Matlab code flmm2 [43] (Matlab version 2018), which employs the Adams-Bashforth-Moulton suggested by Lubich in [71] and studied in [44], is used for solving the commensurate system. This code utilizes three implicit generalised methods including the trapezoidal rule, the Newton-Gregory formula and a backward differentiation formula. Finally, the behaviour of the incommensurate system is investigated by using the code FDE-PI1-Ex.m which was also

introduced by Garrappa in [45].

2.3.1 Stability in Fractional Dynamical Systems

As is standard, we consider a point $(y_1^*, y_2^*, ..., y_n^*)$ to be an equilibrium point of the system when the Caputo fractional time derivatives are zero, i.e. when $f_k(y_1^*, y_2^*, ..., y_n^*) = 0$. A stable equilibrium is then characterized by all solutions with a nearby initial condition remaining nearby. In all other cases, an equilibrium point is unstable. An asymptotically stable equilibrium is characterized by a stable equilibrium where the system state approaches the equilibrium point asymptotically as time approaches infinity. Although the position of equilibria is exactly the same as in the integer derivative case, the stability is determined by a criterion that can depend on the orders of the fractional derivatives.

For integer systems, stability is determined through the eigenvalues of the Jacobian J evaluated at the equilibrium point, as is standard. However for a fractional derivative system, the eigenfunction of the system is not the exponential function $e^{\lambda t}$ but the Mittag-Lefler function $E_\alpha\left((\lambda t)^\alpha\right)$ [3, 23, 28, 69, 73]. Using this eigenfunction, the stability of a commensurate system is then determined by finding the eigenvalues λ from the equation

$$\det\left(J - \lambda^\alpha I\right) = 0. \tag{2.7}$$

This means that, if Λ are the eigenvalues from the equivalent system of integer differential equations, so that $\det(J - \Lambda I) = 0$, then λ can be determined from the relationship $\Lambda = \lambda^\alpha$.

For a stable equilibrium point the condition is $\mathrm{Re}(\lambda) < 0$, or equivalently $|\arg(\lambda)| > \pi/2$ for the fractional system. Therefore, since $\Lambda = \lambda^\alpha$ the condition of the stability of the commensurate system can be written in terms of the eigenvalues of the integer system, Λ, where Λ must satisfy $|\arg(\Lambda)| > \alpha\pi/2$. A representation of this condition is given in Figure 2.3. It is clear from Figure 2.3 that for real eigenvalues, i.e. those lying in the real axis, the value of α will not affect whether the eigenvalues lie in the stable or unstable region. However, for complex eigenvalues, so that $\mathrm{Im}(\lambda) \neq 0$, the value of α will determine whether λ lies in the stability region.

Crucially, if α is reduced towards zero, none of the eigenvalues λ will be within the unstable region. We therefore expect that reducing α will, in general, tend to stabilise the system.

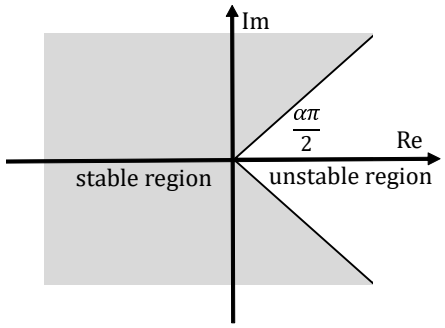

Figure 2.3: The region of the stability for a fractional system, $|\arg(\Lambda)| > \alpha\pi/2$ (coloured gray), $0 < \alpha < 1$.

In terms of the stability of the incommensurate system, the condition of the stability is required that all the roots of the following characteristic equation

$$\det\left(J - \operatorname{diag}\left[\lambda^{\alpha_1}, \quad \lambda^{\alpha_2}, \ldots, \lambda^{\alpha_n}\right]\right) = 0, \tag{2.8}$$

have negative real parts. The characteristic equation (2.8) can then be transformed to an integer-order polynomial equation if all values of α_i are rational numbers. So, assuming $\alpha_i = v_i/u_i$, where the greatest common divisor for u_i and v_i equals 1, and $\lambda = \Lambda^M$, where M is the lowest common multiple at the denominators u_i, (2.8) can be written as

$$\det\left(J - \operatorname{diag}\left[\Lambda^{M\alpha_1}, \quad \Lambda^{M\alpha_2}, \ldots, \Lambda^{M\alpha_n}\right]\right) = 0. \tag{2.9}$$

Since all $M\alpha_i$ are then integers, (2.9) is a polynomial. Consequently, if $|\arg\Lambda| > \pi/2M$, then the incommensurate system is asymptotically stable [27].

Chapter 3

A Fractional Order Predator-Prey Model

In this chapter, the static and dynamic behaviour of a fractional order predator–prey model are studied, where the nonlinear interactions between the two species lead to multiple stable states. As has been found in many previous systems, the stability of such states can be dependent on the fractional order of the time derivative, which is included as a phenomenological model of memory-effects in the predator and prey species. However, what is less well understood is the transient behaviour and dependence of the *observed* domains of attraction for each stable state on the order of the fractional time derivative. These dependencies are investigated using analytical (for the stability of equilibria) and numerical (for the observed domains of attraction) techniques. Results reveal far richer dynamics compared to the integer order model. We conclude that, as well as the species and controllable parameters, the memory effect of the species will play a role in the observed behaviour of the system. All the results in this chapter are published in Letters in Biomathematics [4].

3.1 Introduction

In the field of biology, mathematical modeling has been used to consider the interaction between populations of predators and prey. Numerous studies have looked at these systems but perhaps the most influential are those of the chemist and statistician Lotka and the mathematician Volterra [39, 56]. They introduced the first mathematical model of interacting predator-prey populations, which has since been analysed and extended by many authors [39]. More complicated predator-prey models have been introduced, and many researchers have sought to modify the Lotka-Volterra model so that it can be better applied to real-world ecological systems.

For instance, Harrison [52], Magal et al. [72] and Kar et al. [59], have adapted

the Lotka-Volterra model to study prey-predator relationships that exhibit a Holling Type II functional response [26]. Harrison [52] modified the standard predator-prey model and then used experimental data to determine which systems best fit his model's predictions. Magal et al. [72] studied the associated system of equations to consider the predation of leafminers by a parasite, and Kar et al. [59] modified the work done by Magal et al. where Kar et al. introduced harvesting terms and studied the system without diffusion terms.

In this chapter, we consider a fractional derivative generalisation of a relatively standard model of population dynamics and investigate the observed domains of attraction for the various stable equilibrium points as a function of the fractional order of the derivatives. By the term 'observed domains of attraction' we do not consider the true asymptotic domains of attraction, i.e. the sets of initial conditions for which the system achieves each of the equilibrium states at infinite time, but rather we classify the initial conditions as being associated with the equilibrium state they are closest to (using the Euclidean distance in state-space) after a fixed observation time. It is these domains that we investigate while varying the fractional order of the time derivatives. Even though the model of memory is phenomenological, the aim in this chapter is to show that the fractional derivative order can play a significant role in determining the size of the domain of attraction, and thus this effect could be observed in the real-life dynamics of interacting populations. We speculate that changes in fractional order, that may occur when memory functions change in time or through environmental effects, have the potential to alter the long-term dynamics of a system, particularly when there are two possible stable states.

In the next section, we introduce the fractional order differential equations to be considered as a model of a two-species predator–prey system. In Sections 3.3 and 3.4, the equilibrium states and the stability of these states are investigated, and in Section 3.5 numerical solutions of the system, found using an Adams-Bashforth-Moulton predictor-corrector scheme, are presented in order to show the effect of fractional order on the dynamics. Finally, conclusions are provided in Section 3.6.

3.2 Predator-Prey Model

In real life, an ecosystem consists of many different species all interacting with each other to varying degrees. In this chapter we take, as an example model, a two-species predator–prey model that was introduced in [59], where the authors created a model using growth, functional responses and harvesting terms because these terms were thought to mimic the behaviour in a real ecosystem. The dynamics of the population density of the prey (x) and predator (y) were taken to obey the

equations,

$$\frac{dx}{dt} = r_1 x\left(1-\frac{x}{k_1}\right) - \frac{mxy}{1+ax} - h_1 x, \tag{3.1}$$

$$\frac{dy}{dt} = r_2 y\left(1-\frac{y}{k_2}\right) + q\frac{mxy}{1+ax} - h_2 y, \tag{3.2}$$

where $x(t)$ and $y(t)$ are the prey and predator populations at time t, respectively, and we take initial conditions $x(0) = x_0$ and $y(0) = y_0$. In these equations the first terms on the right-hand sides of both equations (3.1) and (3.2) represent the logistic growth of the species with r_1 and r_2 being the intrinsic growth rates and k_1 and k_2 being the respective environmental carrying capacities, that is the maximum values, of the prey and predator populations respectively, if no other effects were present. The second terms on the right-hand sides of (3.1) and (3.2) represent the predation of the prey by the predator through a Holling type II functional response [26], where m is the decrease of prey per time per predator, that is the percentage of prey killed in each unit of time for each predator, which is effectively the efficiency of the predator's ability to capture prey, the parameter a is related to the predator's efficiency in capture and consumption of the prey, and q is an efficiency constant, where $0 \leq q \leq 1$ and represents the proportion of the prey biomass that the predator can utilise for growth. The last terms in (3.1) and (3.2), h_1 and h_2, represent the harvesting rate of the prey and predator population, respectively, although it is possible for these terms to be incorporated into adjusted birth rates and carrying capacities if necessary.

For mathematical simplicity, and to reduce the number of independent parameters in the system, we first nondimensionalise (3.1) and (3.2) using the nondimensionalised independent variables

$$\bar{t} = r_1 t, \quad X = \frac{x}{k_1}, \quad Y = \frac{y}{k_2}.$$

Nondimensionalised time is now relative to the growth rate r_1. Equations (3.1) and (3.2) can now be written as the following equations

$$r_1 k_1 \frac{dX}{d\bar{t}} = k_1 r_1 X(1-X) - \frac{mk_1 k_2 XY}{1+ak_1 X} - h_1 k_1 X,$$

$$r_1 k_2 \frac{dY}{d\bar{t}} = k_2 r_2 Y(1-Y) + \frac{qk_1 k_2 XY}{1+ak_1 X} - h_2 k_2 Y,$$

which simplify to

$$\frac{dX}{d\bar{t}} = X(1-X) - \frac{K_1 XY}{1+IX} - E_1 X, \tag{3.3}$$

$$\frac{dY}{d\bar{t}} = RY(1-Y) + \frac{K_2 XY}{1+IX} - E_2 Y, \tag{3.4}$$

where $E_1 = \frac{h_1}{r_1}, E_2 = \frac{h_2}{r_1}, R = \frac{r_2}{r_1}, K_1 = \frac{k_2 m}{r_1}, K_2 = \frac{k_1 m q}{r_1}$ and $I = a k_1$ are positive nondimensional constants. The constants E_1 and E_2 are the ratios of harvesting to prey birth rate for the prey and predators which, as we will see later, are important to the stability of the populations of each species. Therefore, if the harvesting rate is larger than the growth rate of prey then $E_1 > 1$ and $E_2 > 1$. The constant R is a ratio of the birth rates of the two species and, to a large extent, is responsible for determining the ratio of predator and prey population numbers at equilibrium. The two parameters K_1 and K_2 can be thought of as nondimensionalised carrying capacities for the two species, scaled by the ratio of birth rate and predation factors. The final parameter I is a rescaled and nondimensional version of the parameter a which measures the efficiency of the predator's search and feeding process.

The aim of this chapter is to study the dynamic properties of a generalisation of the system described in (3.3) and (3.4) through the introduction of the Caputo fractional derivative of order α, D_t^α. As indicated in Chapter 2, these fractional derivatives are introduced to model memory effects in the predator and prey populations. We write this generalised system as

$$
\begin{aligned}
{}^cD_t^\alpha X &= X(1-X) - \frac{K_1 XY}{1+IX} - E_1 X, && (3.5)\\
{}^cD_t^\alpha Y &= RY(1-Y) + \frac{K_2 XY}{1+IX} - E_2 Y, && (3.6)
\end{aligned}
$$

with the initial conditions $X(0) = X_0$ and $Y(0) = Y_0$, $\alpha \in (0, 1]$, i.e. such that memory effects are assumed to include all information from an initial time $t = 0$ until the present time t. The model, and the simulations, assume that the system is constant (at the initial condition) for $t < 0$. In (3.5) and (3.6), we have dropped the $^-$ from $\bar{t}$ for convenience.

3.3 Equilibrium Points

Since we know the Caputo derivative of a constant function is zero, we know the equilibrium points for the fractional model are the same as equilibrium points for the integer-order model [59]. The equilibrium points can therefore be found by solving the following steady-state situation for (3.5) and (3.6):

$$0 = X\left(1 - X - \frac{K_1 Y}{1+IX} - E_1\right), \tag{3.7}$$

$$0 = Y\left(R(1-Y) + \frac{K_2 X}{1+IX} - E_2\right). \tag{3.8}$$

Using (3.7), we see that solutions are $X = 0$ or $1 - X - \dfrac{K_1 Y}{1 + IX} - E_1 = 0$. When $X = 0$, (3.8) gives $Y\left(R(1 - Y) - E_2\right) = 0$, so that either $Y = 0$ or $Y = 1 - \dfrac{E_2}{R}$. Considering (3.8), we see $Y = 0$ or $R(1 - Y) + \dfrac{K_2 X}{1 + IX} - E_2 = 0$. If $Y = 0$, then (3.7) gives us $X = 0$ or $X = 1 - E_1$. If $X \neq 0$ and $Y \neq 0$, we therefore have

$$1 - X - \frac{K_1 Y}{1 + IX} - E_1 = 0, \tag{3.9}$$

$$R(1 - Y) + \frac{K_2 X}{1 + IX} - E_2 = 0. \tag{3.10}$$

From (3.10), we have

$$Y = \frac{1}{R}\left[R - E_2 + \frac{K_2 X}{1 + IX}\right], \tag{3.11}$$

which with (3.9), gives us

$$X^3 + C_2 X^2 + C_1 X + C_0 = 0, \tag{3.12}$$

where

$$C_0 = \frac{1}{I^2}(E_1 - 1) - \frac{K_1}{I^2}\left(\frac{E_2}{R} - 1\right), \tag{3.13}$$

$$C_1 = \frac{2}{I}(E_1 - 1) - \frac{K_1}{I}\left(\frac{E_2}{R} - 1\right) + \frac{1}{I^2}\left(\frac{K_1 K_2}{R} + 1\right), \tag{3.14}$$

$$C_2 = (E_1 - 1) + \frac{2}{I}. \tag{3.15}$$

Therefore, the equilibrium points are

$$P_0 = (0, 0) \text{ the extinction state}, \tag{3.16}$$

$$P_1 = (1 - E_1, 0) \text{ the predator-free state}, \tag{3.17}$$

$$P_2 = \left(0, 1 - \frac{E_2}{R}\right) \text{ the prey-free state}, \tag{3.18}$$

$$P_{3i} = (X^*, Y^*) \text{ for } i = 1, 2, 3 \text{ the coexisting population states}, \tag{3.19}$$

where the coexisting population states, i.e. for which $X^* \neq 0$ and $Y^* \neq 0$, satisfies (3.12) and (3.11), respectively.

The extinction state, P_0, where prey and predator populations are zero, the predator-free state, P_1, and the prey-free state, P_2, all always exist but if the predator-free and prey-free states are to be physically meaningful we must have $E_1 < 1$ and $E_2 < R$, respectively. These conditions are equivalent, in dimensional terms, to the limitations that the harvesting rates of the prey and predator are

less than the intrinsic growth rates so that $h_1 < r_1$ and $h_2 < r_2$. The coexistence states, P_{3i}, are more complicated and are now discussed in detail.

From (3.11) we see that, for a physically realistic coexistent state we must, as well as having $X^* > 0$, have that the harvesting of predators is less than an enhanced growth rate of predators, $E_2 < R + K_2X^*/(1 + IX^*)$, to ensure that $Y^* > 0$. For these coexistence states we therefore see that a higher level of harvesting is possible, compared to the prey-free state, because the nonzero prey population can support the presence of a predator population even with relatively high levels of harvesting. In order to determine the number of real roots of (3.12), we will consider the discriminant of the equation (see, for instance, discussion of the Cardano formula in [125]), namely

$$\Delta = C_1^2C_2^2 - 4C_1^3 - 4C_0C_2^3 - 27C_0^2 + 18C_0C_1C_2. \tag{3.20}$$

If $\Delta > 0$, then there are three real roots, and if $\Delta < 0$ then there is only one real root. Because we are interested in the system that has multiple physical equilibrium points, we should determine the number of real and positive roots of (3.12) by using the sign of the discriminant in (3.20) and Descartes' Rule of Signs [5].

We have concentrated on the case with as many existing P_{3i} states as possible, since this case will provide more possibilities to transfer between states. In particular, we will later see that the stability of P_0, P_1 and P_2 are not affected by changing the fractional order α, but a change of stability is possible for P_{3i} by changing α. From the discriminant and using Descartes' Rule of Signs we find that it is possible to have three positive coexistence states, when $\Delta > 0$, and the change of signs in (3.12) is equal to three, i.e. $C_2 < 0$, $C_1 > 0$, $C_0 < 0$, which is equivalent to a condition on the prey harvesting rate, $M_1 < E_1 < \min(M_0, M_2)$, where

$$M_0 = 1 + K_1\left(\frac{E_2}{R} - 1\right), \tag{3.21a}$$

$$M_1 = \ 1 + \frac{K_1}{2}\left(\frac{E_2}{R} - 1\right) - \frac{1}{2I}\left(\frac{K_1K_2}{R} + 1\right), \tag{3.21b}$$

$$M_2 = \ 1 - \frac{2}{I}. \tag{3.21c}$$

It should be noted that these conditions for three coexisting P_{3i} states are necessary but not sufficient, so that even if these conditions are met, we might not have three coexistence states (there could be only one positive root of (3.12)).

3.4 Stability

Determining whether an individual equilibrium point is stable is undertaken by considering the eigenvalues of the Jacobian matrix, $J(X, Y)$ at the equilibrium

point (X, Y). For our system in (3.5) and (3.6) the Jacobian matrix is

$$J(X,Y) = \begin{bmatrix} (1-E_1) - \dfrac{K_1 Y}{(1+IX)^2} - 2X & \dfrac{-K_1 X}{1+IX} \\ \dfrac{K_2 Y}{(1+IX)^2} & (R-E_2) + \dfrac{K_2 X}{(1+IX)} - 2YR \end{bmatrix}. \tag{3.22}$$

The stabilities of the three equilibrium points P_0, P_1 and P_2 have previously been reported [59] but are summarised here for completeness.

The eigenvalues of the Jacobian matrix at the extinction state $P_0 = (0, 0)$ are $\Lambda_1 = 1 - E_1$ and $\Lambda_2 = R - E_2$. If $E_1 > 1$ and $E_2 > R$, then the system will be stable around P_0. This result is to be expected and shows that if the harvesting rates are greater than the intrinsic growth rates of the predator and prey species then the extinction state is stable and that if at least one of the harvesting rates is less than the corresponding growth rate, then the extinction state is unstable.

The eigenvalues of the Jacobian matrix at the predator-free state $P_1 = (1 - E_1, 0)$ are $\Lambda_1 = E_1 - 1$ and $\Lambda_2 = R - E_2 + \dfrac{K_2\,(1-E_1)}{1+I\,(1-E_1)}$. If P_1 is physical, so that $E_1 < 1$, then the condition for stability is $E_2 > R + \dfrac{K_2(1-E_1)}{1+I(1-E_1)}$, i.e. the predator-free state is stable if it exists and the predator harvesting rate is sufficiently large.

The eigenvalues of the Jacobian matrix at the prey-free state $P_2 = (0, 1-E_2/R)$ are $\Lambda_1 = M_0 - E_1$, where M_0 is given in (3.21a), and $\Lambda_2 = E_2 - R$. If the prey-free state P_2 exists, so that $E_2 < R$, then the condition for stability is that the prey harvesting rate is sufficiently large, $E_1 > M_0$ which is equivalent to $E_2 < R\left(1 + \dfrac{E_1 - 1}{K_1}\right)$ i.e. that the predator harvesting rate is sufficiently small.

The results of the stability, shown in Chapter 2, mean that, since the eigenvalues, which are the solutions of the characteristic equation for the integer model, of the extinction state $P_0 = (0, 0)$, the predator-free state $P_1 = (1 - E_1, 0)$ and the prey-free state $P_2 = (0, 1 - E_2/R)$ are all always real, their stability will be unaffected by the fractional derivative order.

We can summarise the existence and stability conditions for P_0, P_1 and P_2 and the existence conditions for P_3 as follows

1. The predator-free and prey-free states, P_1 and P_2, may co-exist, but they will never both be stable.

2. If the prey-free state P_2 is a stable equilibrium point, then the interior equilibrium points P_{3i}, $i = 1, 2, 3$, do not all exist.

3. If the extinction state P_0 is a stable equilibrium point, then the predator-free and prey-free states, P_1 and P_2, do not exist and the interior equilibrium points P_{3i}, $i = 1, 2, 3$, do not all exist. This is because the condition for stability of P_0, $E_1 > 1$, contradicts the condition for having three positive solutions for (3.12).

4. When $E_1 < 1$ and $E_2 > R + \dfrac{K_2(1 - E_1)}{1 + I(1 - E_1)}$, then P_1 is a stable equilibrium point and it is possible for at least one co-existence state to exist because $C_0 < 0$ and $C_2 > 0$ may be positive if $E_1 > 1 - 2/I$.

5. When $E_1 < \min(1, M_0)$ and $E_2 < R + \dfrac{K_2(1 - E_1)}{1 + I(1 - E_1)}$, then P_0, P_1 and P_2 are all unstable, but it is still possible for at least one co-existence state to exist because $E_1 < M_0$ which means $C_0 < 0$. Indeed it is possible to have three positive solutions for (3.12) P_{3i}.

We will now consider the stability of P_{3i}. In contrast to the P_0, P_1 and P_2 states, the stability of the coexistence states P_{3i}, $i = 1, 2, 3$, where the populations of both prey and predator are nonzero, can be affected by the fractional derivative order. The eigenvalues of the Jacobian matrix, (3.22), corresponding to the coexistence equilibrium points P_{3i}, $i = 1, 2, 3$, in (3.19) are the roots of the characteristic equation

$$\Lambda^2 + f\Lambda + g = 0, \tag{3.23}$$

where

$$f = X^* - \frac{K_1 I Y^* X^*}{(1 + IX^*)^2} + RY^*, \tag{3.24}$$

$$g = RY^* X^* + \frac{K_1 Y^* X^*}{(1 + IX^*)^2} \left(\frac{K_2}{1 + IX^*} - RIY^* \right), \tag{3.25}$$

and (X^*, Y^*) is one of the three solutions to (3.11) and (3.12). Therefore, the stability condition of the interior equilibrium points P_{3i} depends on f and g.

We are then able to derive the following results:

(i) If $f > 0$ and $g > 0$, then, by the Routh-Hurwitz criterion, (3.23) has two roots with negative real parts, so the equilibrium point is asymptotically stable for all $\alpha \in (0, 1]$.

(ii) If $f > 0$ and $g < 0$, then $g < f^2/4$, so (3.23) has real roots, and there is one change of sign in the coefficients of (3.23). Therefore, by the Routh-Hurwitz criterion, (3.23) has one root with positive real part and the equilibrium point is unstable for all $\alpha \in (0, 1]$.

(iii) If $g < f^2/4$, then (3.23) has real roots and if $f < 0$, then there is at least one change of sign in the coefficients of the polynomial in (3.23) so that, by the Routh-Hurwitz criterion, there is at least one positive real root and the equilibrium point is unstable for all $\alpha \in (0, 1]$.

(iv) If $g > f^2/4$ and $f < 0$, then (3.23) has two complex conjugate roots with real part $-f/2 > 0$. Then, using the stability criterion for the fractional order system, the condition for stability is $|\arg\Lambda| > \alpha\pi/2, \alpha \in (0, 1]$, so

$$|\arg \Lambda| = \left|\tan^{-1}\left(-\sqrt{\frac{4g}{f^2} - 1}\right)\right| > \frac{\alpha\pi}{2},$$

which can equivalently be written as $\left|\cos^{-1}\left(-\frac{f}{2\sqrt{g}}\right)\right| > \frac{\alpha\pi}{2}$. Because of $\alpha \in (0, 1]$ the condition can be written as $\alpha < \frac{2}{\pi}\cos^{-1}\left(\frac{-f}{2\sqrt{g}}\right)$. Therefore, the maximum value of α for which stability is ensured is

$$\alpha^* = \frac{2}{\pi}\cos^{-1}\left(-\frac{f}{2\sqrt{g}}\right). \tag{3.26}$$

Thus, if $f < 0$ and $g > f^2/4$, the system in (3.5) and (3.6) is asymptotically stable if and only if $\alpha \in (0, \alpha^*)$, and when $\alpha \geq \alpha^*$ the system is unstable with complex eigenvalues. The system therefore undergoes a bifurcation when the fractional order α increases above the critical value α^*.

3.5 Numerical Simulation

In this section, we investigate the numerical solution of the system in (3.5) and (3.6), paying attention to the critical fractional derivative order, α^*, below the value of which one of the unstable equilibrium points becomes stable. We will see that, although for $\alpha > \alpha^*$ only one equilibrium point is stable, for certain initial states the system can remain close to an unstable equilibrium point. As α reduces, the area of initial state space for which the system remains close to this unstable point grows until, when $\alpha = \alpha^*$, the unstable point becomes stable. We therefore see that both above and below this critical value, the transient behaviour and the observed domains of stability for the equilibria can significantly change as a function of the fractional derivative order.

The estimated values of the parameters that are used in the numerical simulation are taken from the models of Harrison [52], where he uses a standard differential equation predator-prey model to qualitatively predict the outcome of a predator-prey experiment, and Magal et al. [72], where they use two differential

equations to model the spread of hosts (leafminers) and parasites in a biological system. Harrison's model is given by the following equations

$$\frac{dx}{dt} = \rho\left(1 - \frac{x}{k}\right)x - \frac{\omega xy}{\Phi + x},$$
$$\frac{dy}{dt} = \frac{\sigma xy}{\Phi + x} - \gamma y,$$

and the parameter values are provided in Table 3.1.

Table 3.1: Values and ecological interpretations of the parameters in Harrison's model [52]. Note that d denotes days and μL denotes microlitres. In [52] the unit of millilitre is used, however, through comparison with Magal et al. [72] it is clear that the units for the density should be per microlitre in our application.

Parameter	Estimated Value	Unit	Interpretation
x and y		$(\mu L)^{-1}$	the density of prey and predator
ρ	$2-3$	d^{-1}	growth rate of prey
k	0.9	$(\mu L)^{-1}$	carrying capacity of prey
ω	$0.01-0.05$	d^{-1}	maximum rate of prey consumption
Φ	$0.003-0.3$	$(\mu L)^{-1}$	half saturation constant
σ	$5-50$	d^{-1}	conversion rate from prey to predator
γ	0.002	d^{-1}	harvesting rate of predator

The model of Magal et al. is

$$\frac{dx}{dt} = r_1 x\left(1 - \frac{x}{k_1}\right) - \frac{Exy}{1 + Ehx},$$
$$\frac{dy}{dt} = r_2 y\left(1 - \frac{y}{k_2}\right) + \frac{E\gamma yx}{1 + Ehx},$$

and Table 3.2 provides values and an ecological interpretation of these parameters.

Table 3.2: Values and ecological interpretations of the parameters in the model of Magal et al. [72]. Parameters are written in units consistent with [52].

Parameter	Estimated Value	Unit	Interpretation
x and y		$(\mu L)^{-1}$	the density of prey and predator
r_1	3	d^{-1}	growth rate of leafminers
r_2	0.1	d^{-1}	growth rate of parasitoids
k_1	1	$(\mu L)^{-1}$	carrying capacity of leafminers
k_2	0.0029	$(\mu L)^{-1}$	carrying capacity of parasitoids
E	200.2	$(\mu L)d^{-1}$	encounter rate
γ	10	no unit	conversion efficiency
h	5	d	harvesting time

Table 3.3: Parameter values used in our numerical simulations where the harvesting rates are taking to be similar to the harvesting rates, h_1 and h_2, in [52].

Parameter	Estimated Value	Unit	Reference	Interpretation
x and y		$(\mu L)^{-1}$		the density of prey and predator
r_1	3	d^{-1}	[72]	growth rate of prey
r_2	0.1	d^{-1}	[72]	growth rate of predator
a	1001	μL	[72]	the rate of consumption of the prey
k_1	1	$(\mu L)^{-1}$	[72]	carrying capacity of prey
k_2	0.0029	$(\mu L)^{-1}$	[72]	carrying capacity of predator
m	200.2	$(\mu L)d^{-1}$	[72]	decreasing rate of prey per predator
q	10	no unit	[72]	efficiency constant
h_1	0.001	d^{-1}	[52]	harvesting rate of prey
h_2	0.01	d^{-1}	[52]	harvesting rate of predator

Table 3.3 gives the values of parameters used in our numerical simulations (which are typical for systems where the size of predator populations are much larger than prey populations such as in parasitic-predation on host prey [6]). The corresponding values of the nondimensionlised parameters are $R = 0.0333$, $K_1 = 0.1935$, $K_2 = 667.3333$, $I = 1001$, $E_1 = 0.0003$ and $E_2 = 0.0033$. Although we write only 4 decimal places, we work to a higher accuracy in our numerical work.

Numerical solutions of (3.5) and (3.6) are found using the Adam-Bashforth-Moulton method for parameter values in Table 3.3, and with a timestep size $h = 2^{-8}$ days. Various possible values of h (from 2^{-5}-2^{-10} days) were investigated and this value, $h = 2^{-8}$ days, was chosen so that the area of the domains of stability changed by less than 5% for timesteps less than this. Smaller values of h could be used, for greater accuracy, but would lead to significantly longer computational times and therefore the value of 5% accuracy was chosen.

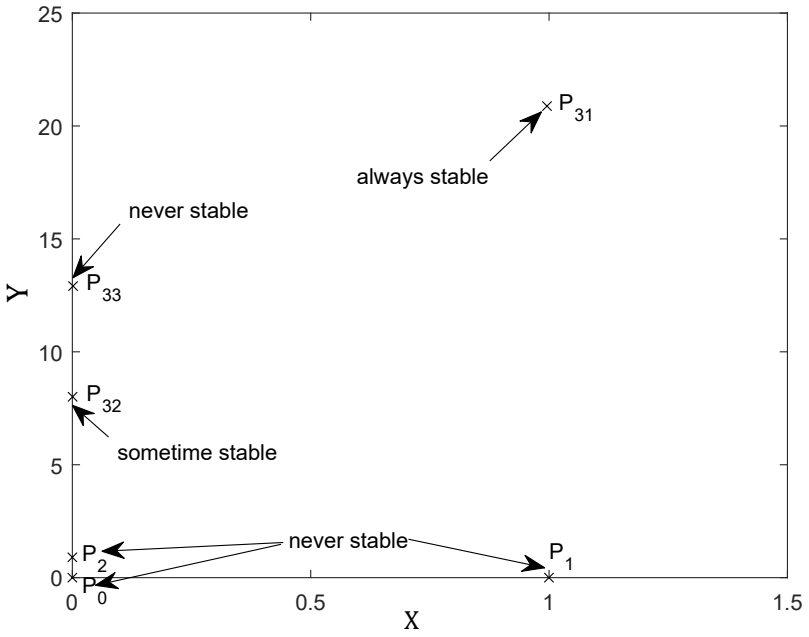

Figure 3.1: The positions and stabilities of the equilibrium points of the system (3.5) and (3.6), using parameter values from Table 3.3.

For these parameter values, the physically relevant equilibrium points are $P_0 = (0, 0)$, $P_1 = (0.9997, 0)$, $P_2 = (0, 0.9009)$, $P_{31} = (0.9956, 20.9009)$, $P_{32} = (0.0005, 8.0015)$ and $P_{33} = (0.0015, 12.9395)$ as shown in Figure 3.1. For the parameters we use, $\Delta = 8.9167 \times 10^{17}$, $M_0 = 0.8256$, $M_1 = -1.0229$ and $M_2 = 0.9980$. Since $\Delta > 0$ and $M_1 < E_1 < \min(M_0, M_2)$, we may have the coexisting population states. Indeed this is what we find. The states P_0, P_1, P_2 and P_{33} are all unstable. The P_{31} equilibrium point is stable for all values of α, with the eigenvalues of the Jacobian matrix at P_{31} being negative $\Lambda_1 = -0.9915$ and $\Lambda_2 = -0.6960$. Also, for the same parameter values, the eigenvalues of the Jacobian matrix at P_{32} are complex conjugates with positive real part, $\Lambda_{1,2} = 0.0436 \pm 0.2372i$, so that for the integer derivative order system the point P_{32} is unstable. As mentioned in Chapter 2, as the derivative order reduces, the region $|\arg(\lambda)| > \alpha\pi/2$ eventually expands to include the P_{32} complex conjugate Jacobian eigenvalues, so that for $\alpha \in (0, \alpha^*)$, where $\alpha^* = 0.88406$, the point P_{32} is stable. This means that for the integer derivative system, i.e. $\alpha = 1$, there is only one stable equilibrium point, P_{31}, a state in which there are significant levels of prey and predator, but for the fractional derivative system with a fractional derivative order less than the critical value $\alpha < \alpha^*$ there exists a further stable equilibrium point P_{32}, a state in which the prey level is almost zero.

We demonstrate this change in stability in Figure 3.2, which shows the evolu-

tion of the system from the same initial condition $X(0) = 0.0005$, $Y(0) = 8.0$ but for two fractional derivative order values, either side of the critical value, for the integer order system $\alpha = 1$ (Figure 3.2(a)) and $\alpha = 0.8$ (Figure 3.2(b)). In Figure 3.2(a), the equilibrium point P_{32} is unstable and the system evolves to the only stable equilibrium point, P_{31}. However, for the lower value of α, Figure 3.2(b) shows that, whilst the equilibrium point P_{31} is still stable, for the same initial values of prey and predator populations the system evolves to the, now stable, equilibrium point P_{32}.

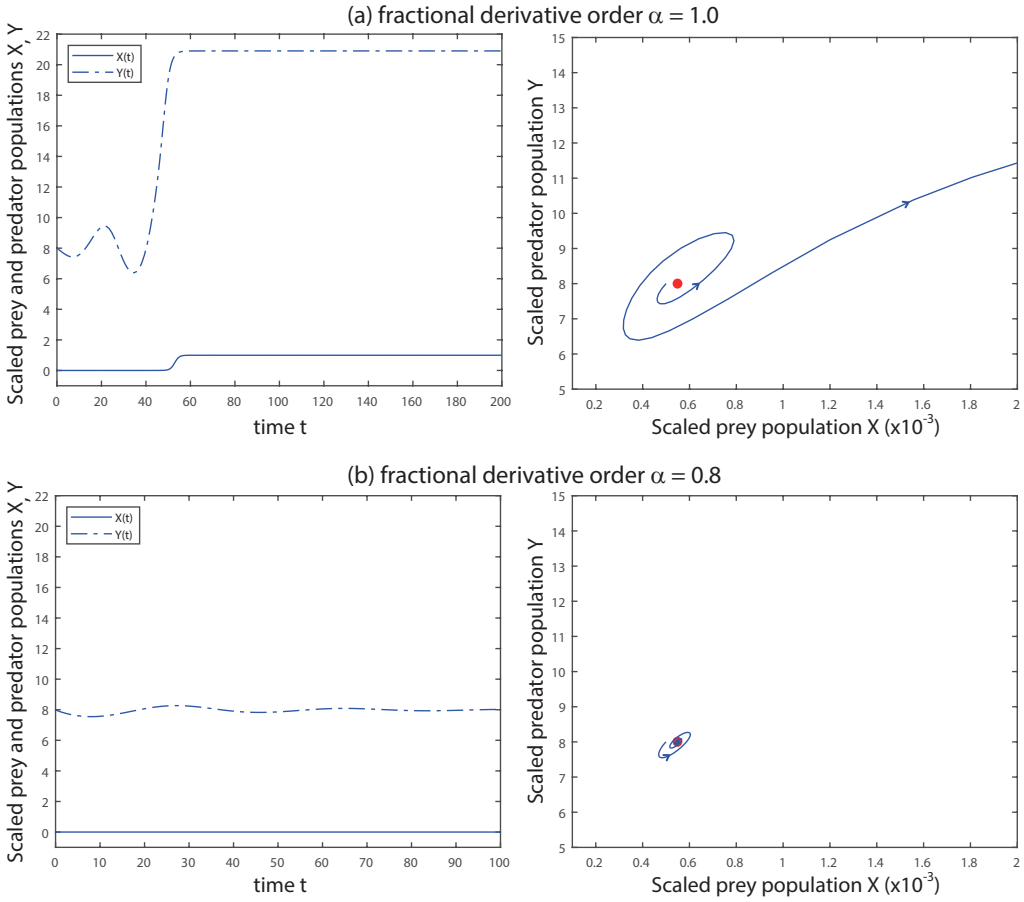

Figure 3.2: The trajectories when (a) $\alpha = 1 > \alpha^*$, where the system evolves to the stable equilibrium point P_{31} (not shown in the trajectory plot), and (b) $\alpha = 0.8 < \alpha^*$, where the system evolves to the fractional-derivative–stabilised equilibrium point P_{32} (red point).

Changing the fractional derivative order therefore gives the possibility of transitioning from a monostable system to a bistable system. This transition occurs though a Hopf-like bifurcation. However, in this fractional derivative system, a limit cycle that would appear during a Hopf bifurcation, does not exist and trajectories in the phase plane can pass across a closed cycle or separatrix. A closed

cycle can exist, although trajectories do not approach this closed cycle asymptotically, so this is not termed a limit cycle.

In Figure 3.3, we show the phase plane trajectories for prey and predator populations from an initial state of $X(0) = 0.0005$ and $Y(0) = 8.0$ for six different values of the fractional derivative order above the critical value $\alpha^* = 0.88406$. In all plots within Figure 3.3, we see that the equilibrium point P_{32} is unstable, with the trajectory eventually reaching the only stable equilibrium point P_{31}. However as the fractional derivative order changes, the transient behaviour, before the system converges to the stable point P_{32}, changes. Even though P_{32} is unstable, the Hopf-like bifurcation leads to oscillations in the prey and predator populations. The number of cycles around P_{32} is seen to increase as the fractional derivative order decreases, as shown in Figure 3.4. Therefore, for a certain amount of time, even if $\alpha > \alpha^*$, the system stays close to P_{32} for a while. When the fractional derivative order has reduced below the critical value α^*, the phase plane trajectory would asymptotically approach P_{32} in an oscillatory fashion, with an infinite number of cycles around the equilibrium point. This approach to an infinite number of cycles is also seen in Figure 3.4.

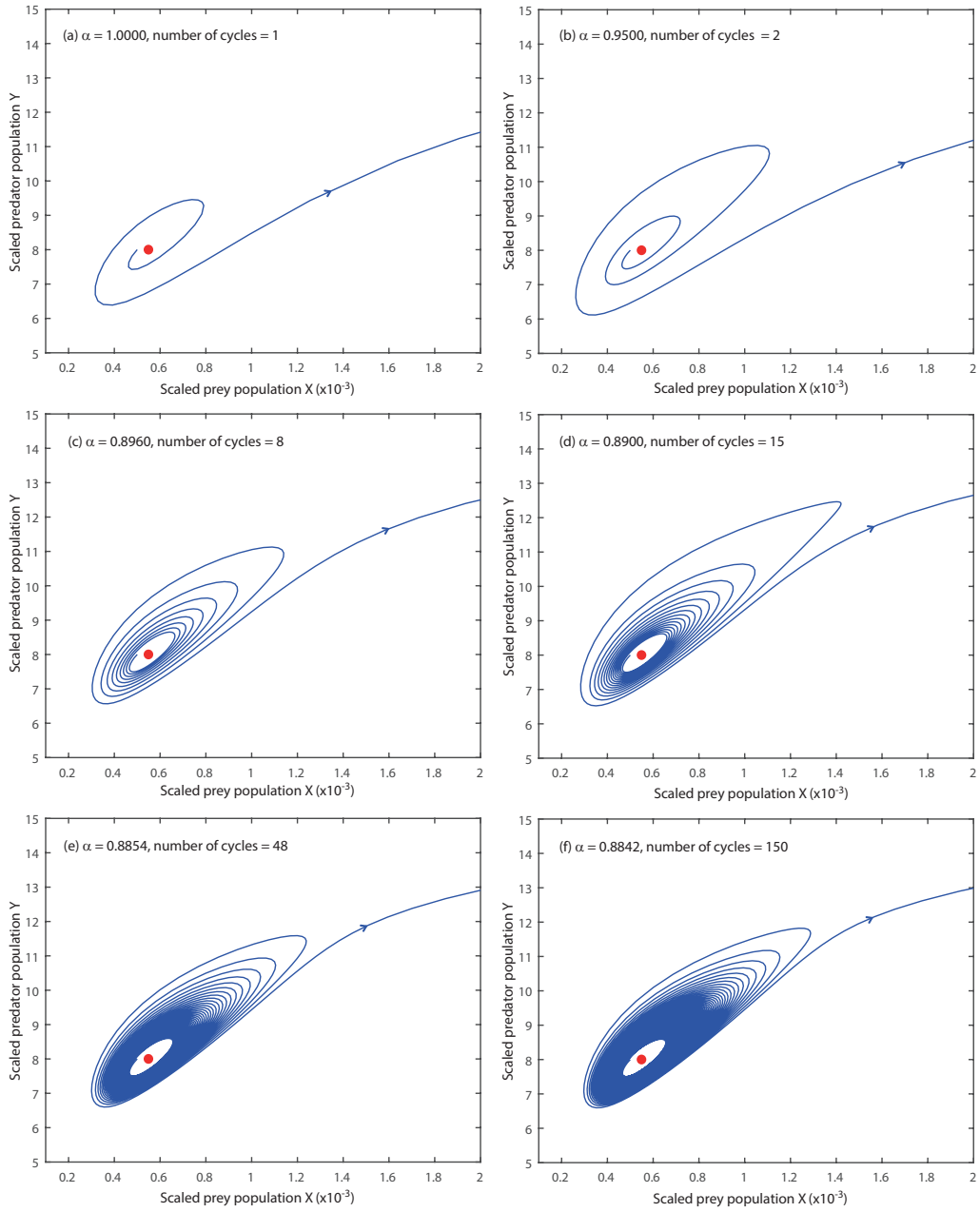

Figure 3.3: Phase plane trajectories for the predator–prey populations for the initial state $X(0) = 0.0005$, $Y(0) = 8.0$ but for various values of the fractional derivative order α. The red point marks the unstable equilibrium point $P_{32} = (0.0005, 8.0015)$. As α decreases (from (a) through to (f)) the number of cycles around P_{32} increases.

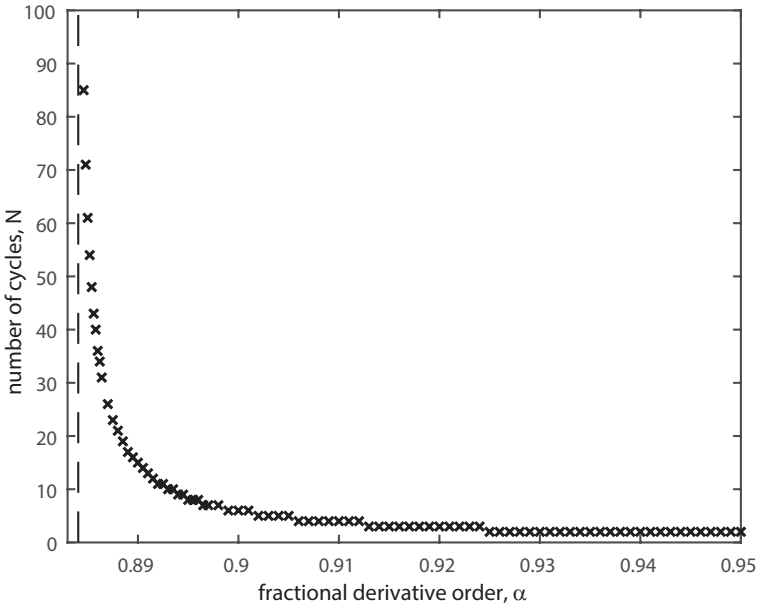

Figure 3.4: The number of cycles around the equilibrium point P_{32} as the fractional derivative order α varies as was illustrated in Fig. 3.3, this number of cycles approach to an infinite number of cycles when α has reduced below the critical value α^*.

The change in transient behaviour can also be seen when we consider the state of the system after a fixed time $t = t_{\text{end}}$. Because we have two equilibrium points, when $\alpha < \alpha^*$, we are interested in finding out when the trajectory goes to either P_{31} or P_{32}, and how these depend on the choice of the initial condition. Figure 3.5 shows this behaviour for only two different initial conditions, where $\alpha = 0.85 < \alpha^*$.

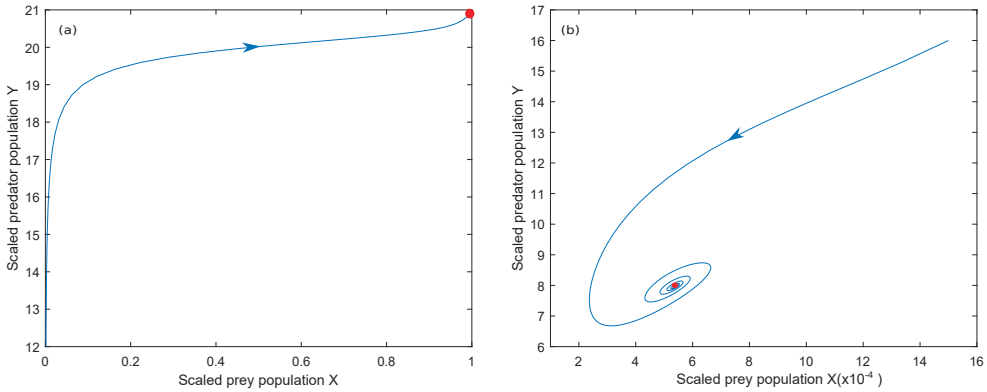

Figure 3.5: Phase plane trajectories for $\alpha = 0.85 < \alpha^*$. (a) $X(0) = 0.0015$, $Y(0) = 12$ and the red point is P_{31}. (b) $X(0) = 0.0015$, $Y(0) = 16$ and the red point is P_{32}.

To illustrate this change in transient behaviour for more initial states, we will now vary the initial state and consider the final state at $t = t_{\text{end}} = 500$ (equivalent to a dimensional $t = 167\,\text{days}$), labelling each initial point depending on whether the final state is closer to P_{31} or P_{32}. Figure 3.6 shows the results of this process of labelling the initial states depending on whether the final state is closer to P_{31} (coloured green) or P_{32} (coloured white). For values of the initial state X_0 greater than 0.1, the system final state, at t_{end}, is always closer to P_{31} and would therefore be coloured green. For the value of the fractional derivative order used for Figure 3.6, $\alpha = 0.75 < \alpha^*$, i.e. below the critical value, we see that both P_{31} and P_{32} are stable, although the domain of attraction of P_{31} is much larger than P_{32}. Figure 3.7 then shows an enlarged version of Figure 3.6, indicating how the domain of attraction of P_{32} changes as the fractional derivative order changes.

From Figure 3.7(d-f) we see that for fractional derivative orders less than the critical value, for which both P_{31} and P_{32} are stable, we have a region of the space of initial states where the system is closer to P_{31} when $t = t_{\text{end}}$ and a region where the system is closer to P_{32}. When the fractional derivative order is greater than the critical value Figure 3.7(a-c) we might expect, since the equilibrium point P_{32} is now unstable, that the white region in these plots would collapse. However, since these regions are labelled after a fixed time $t = t_{\text{end}}$, and because of the Hopf-like bifurcation that leads to oscillatory behaviour around P_{32}, we see that, for a range of initial conditions, the system remains close to P_{32}. It is interesting to note that for relatively large values of the fractional derivative order, i.e. in Figure 3.7(a,b) there are two disconnected white regions.

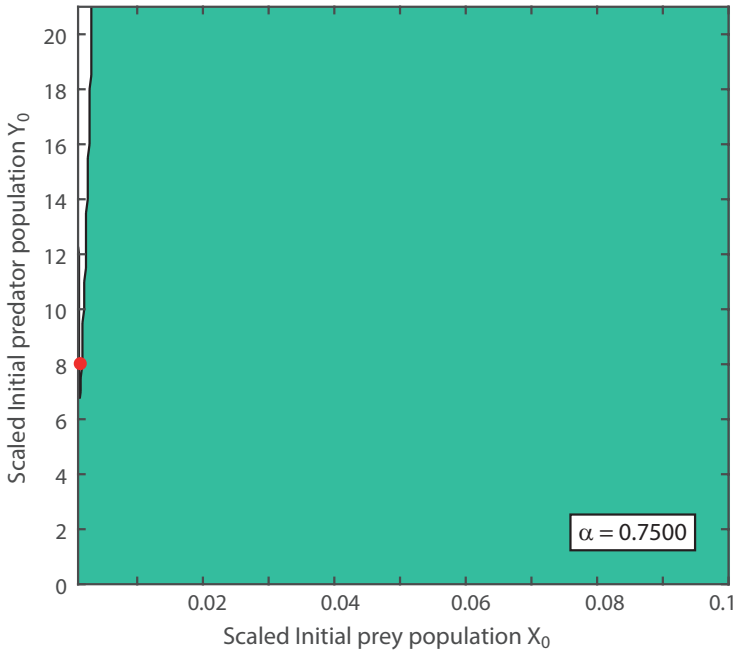

Figure 3.6: Observed domains of attraction for $\alpha = 0.75 < \alpha^*$. If the initial states X_0, Y_0 are chosen from the green region, the system will be closer to the equilibrium point P_{31} at $t = t_{\text{end}}$, and for initial states within the white region, the system will be closer to the equilibrium point P_{32} (red point) at $t = t_{\text{end}}$.

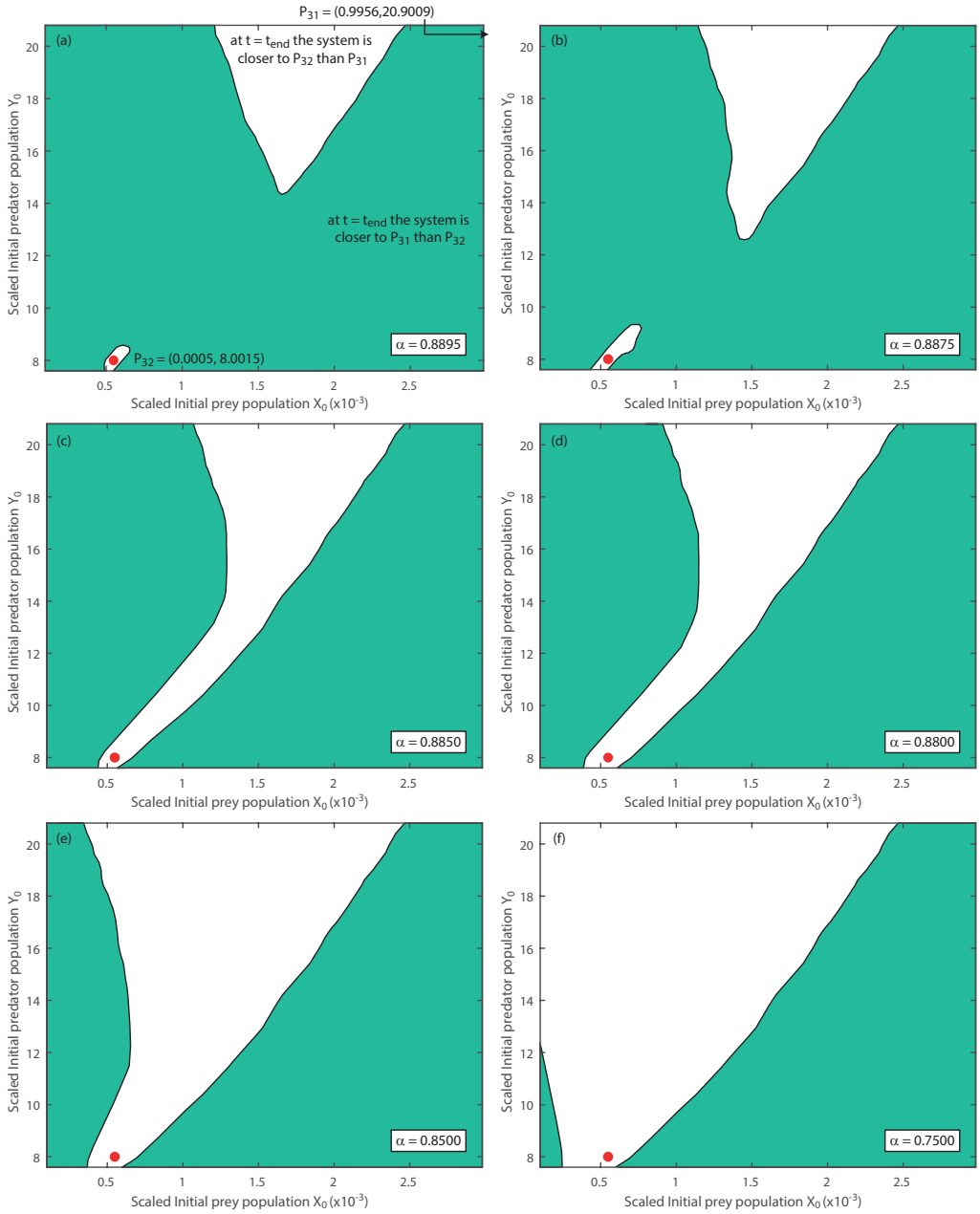

Figure 3.7: Observed domains of attraction for various values of the fractional derivative order α. If the initial states X_0, Y_0 are chosen from the green region, the system will be closer to the equilibrium point P_{31} at $t = t_{\text{end}}$, and for initial states within the white region, the system will be closer to the equilibrium point P_{32} at $t = t_{\text{end}}$. For (a), (b), (c) the value of the fractional derivative order is $\alpha > \alpha^*$ and for (d), (e), (f) $\alpha < \alpha^*$.

3.6 Conclusions

In this chapter, for the predator-prey system that was under consideration, conditions of stability and bifurcation have been obtained and, importantly, it was found that through the variation of the fractional order α it is possible to transition from a monostable system to a bistable system. In the bistable system, the two stable equilibrium points (P_{31} and P_{32}) have very different levels of predator and prey populations - for the parameters used here we find prey/predator ratios of $X/Y = 0.04760$ and $X/Y = 0.00006$ for the two bistable states. The presence of increased memory (corresponding to a reduction in α) in the predator and prey has therefore opened up the possibility of very different stable states and, at the boundary of the domain of attraction, a sensitivity to small variations in system parameters, such as birth, death or harvesting rates, can lead to a drastic change in the prey/predator ratio. Even when the system has only one stable state, the observed domains of attraction (the domains for which the system will remain close to either equilibrium point after a fixed time) can be memory dependent.

We have concentrated on a particular model, with the same parameters as used in [72]. For these parameter values, the domain of attraction for P_{32} is much smaller than that of P_{31} and so may not be readily observable in real life. However, we would suggest that the main effects, on stability and domains of attraction, of altering the fractional derivative order would be present for any similar system where there is more than one stable state possible. A key observation from Figure 3.7 is that, both for fractional derivatives below and above the critical value α^*, the observed domain of attraction changes significantly as α changes.

Further extension of this model, to an incommensurate fractional system, for which the predator and prey populations have different fractional derivative orders, will be dealt with in the next chapter.

Chapter 4

Incommensurate Predator-Prey Model

If we consider a model of two or more interacting species, that may have different levels of memory, i.e. long or short-term memories, one way to represent the system is to model them by using an incommensurate fractional order system of differential equations. As mentioned in Chapter 2, such an incommensurate system will have the following general form

$$D^{\alpha_k} y_k(t) = f_k(y_1, y_2, ..., y_n),$$

where $\alpha_k \in (0, 1]$ is the fractional order for the k^{th} species with $k = 1, ..., n$, and $y_k(t_0) = b_k$, is the initial state for the k^{th} species.

Incommensurate fractional systems such as this have not received as much attention as commensurate fractional systems. There have been a number of papers that study incommensurate systems from the perspective of synchronisation, a phenomenon that may occur when two or more dissipative chaotic systems are coupled [129]. However, this effect is typically only investigated through numerical simulations that are based on the stability criteria of linear fractional order systems, such as the work presented in [84] (and references 19-24 in [84]). In these works, the underlying aim is to control synchronisation in an n-dimensional fractional dynamical system by choosing a suitable control function [2]. Researchers have focused on investigating many kinds of synchronisation such as hybrid projective [61, 132], H-infinity observer-based [127], Q-S [84], master-slave, complete, chaos, and robust [2], although analytic results explaining how incommensurate fractional derivatives affect the systems are lacking. Other researchers have focused on general types of incommensurate dynamical systems. In 2008, Petras [88] analysed the stability criteria of linear and nonlinear fractional systems, using examples to explain how to apply the criteria for the stability of specific values of the fractional orders. In 2012, Datsko and Lucbko [25] investigated the incommensurate system based on the van der Pol-FitzHugh-Nagumo system for different

fractional orders. They showed that the stability behaviour depends on the choice of fractional orders, and that by changing system parameters, different limit cycles will occur. They found a simple limit cycle, limit cycles with intersections, and limit cycles that are similar to strange attractors. In 2016, Yude et al. [58] applied the stability theorem of incommensurate fractional orders systems for two different systems: the Lotka-Volterra predator-prey system [1, 130] and the Chen system [116, 117]. The eigenvalues for each equilibrium point were examined, and the stability results were illustrated numerically. Stability results for a linear system which contains the Caputo derivative were obtained by Brandibur and Kaslik in 2017 [14]. In this work, they focused on the Morris-Lecar neuronal model after replacing the integer derivative in the first equation of the model by the fractional Caputo derivative.

In 2018, Brandibur and Kaslik [15] investigated a fractional derivative form of the FitzHugh-Nagumo model. They explored stability conditions for this system, and how fractional orders affected Hopf-bifurcations. In 2019, El-Saka et al. [34] investigated an incommensurate fractional order version of a predator-prey biological model, first introduced in [70]. Hopf-bifurcations were examined for this system and the theoretical results were verified by several numerical examples. In all these works, very few analytical results were represented.

In this chapter, two incommensurate fractional systems will be considered. In Section 4.1, we find an approximate analytical solution for the characteristic equation of the incommensurate system when the two fractional orders α and β are similar using perturbation theory [81] and the solution of the characteristic equation of the commensurate system. Then, the condition for the stability of the incommensurate fractional system is determined as a function of the two fractional orders, and the approximate analytical solution for the stability boundary is found. The method used to find the numerical solution for this equation for incommensurate fractional orders is also introduced and used to compare to the analytical results. Two incommensurate predator-prey systems are investigated: in Section 4.2.1, the incommensurate system of the same predator-prey model studied in Chapter 3 will be investigated to consider the effect of having two different fractional orders; in Section 4.2.2, an alternative incommensurate system is introduced to compare the results with those found in Section 4.2.1.

4.1 Characteristic Equation of the Incommensurate System

In this section, we will find approximate analytical solutions for the eigenvalues that satisfy the characteristic equation of the incommensurate system, assuming that the fractional orders are similar. We will then consider the stability boundary

based on these eigenvalues. The eigenvalues of the Jacobian matrix are the solution of the characteristic equation, for example if we have two species in the system the Jacobian matrix will be of the form

$$J(X,Y) = \begin{bmatrix} J_{11} & J_{12} \\ J_{21} & J_{22} \end{bmatrix}.$$

The characteristic equation for the incommensurate system is then

$$(\lambda^{\alpha} - J_{11})(\lambda^{\beta} - J_{22}) - J_{12}J_{21} = 0. \tag{4.1}$$

4.1.1 Eigenvalues of the Incommensurate System

The stability of equilibrium points in an incommensurate fractional derivative system is determined by the eigenvalues solutions to the characteristic equation (4.1). Here we now consider solutions of this equation when α and β are similar. We will take fractional orders $\alpha, \beta \in (0,1)$, such that $\alpha = n_1/m_1$ and $\beta = n_2/m_2$ are rational numbers. Since the rational numbers are dense in the real numbers, we need only consider rational values of α and β. We set a common denominator $\alpha = n/M$ and $\beta = m/M$, and the characteristic equation (4.1) can then be written as

$$\left(\lambda^{\frac{n}{M}} - J_{11}\right)\left(\lambda^{\frac{m}{M}} - J_{22}\right) - J_{12}J_{21} = 0. \tag{4.2}$$

We will now consider values of α and β that are similar, specifically that $m = n+1$, so that with the substitution $\Lambda = \lambda^{\frac{1}{M}}$, we obtain

$$\left(\Lambda^{n} - J_{11}\right)\left(\Lambda^{n+1} - J_{22}\right) - J_{12}J_{21} = 0. \tag{4.3}$$

The difference between α and β is therefore $1/M$ and so, if we take that M is large enough, we are able to allow β to be arbitrarily close to α. As M increases then, since α is fixed, so must n increase. Therefore, the limit $\beta \to \alpha$ is equivalent to $n \to \infty$, or $1/n \to 0$. For a commensurate system, with $\alpha = \beta = \dfrac{n}{M}$, the system reverts to

$$(\Lambda^{n} - J_{11})(\Lambda^{n} - J_{22}) - J_{12}J_{21} = 0. \tag{4.4}$$

Comparing these two equations we see that (4.3) has $2n+1$ solutions while (4.4) has $2n$ solutions. In the following section, we will first find the $2n$ solutions of (4.3) that are close to the solutions of (4.4), and then find the one extra solution. After that, the stability boundary for equilibrium, as a function of α and β, will be found.

Since $\beta \to \alpha$ as $n \to \infty$, we expect $2n$ of the $2n+1$ solutions of (4.3) to tend to the $2n$ solutions of (4.4) as $n \to \infty$. We will therefore look for $2n$ solutions of (4.3), Λ, as perturbations of the roots of (4.4), which we denote by Λ^*. The standard form of perturbation would be $\Lambda = \Lambda^* + \dfrac{1}{n}\bar{\Lambda}_1 + \dfrac{1}{n^2}\bar{\Lambda}_2 + \ldots$ although for ease of computation we have chosen the similar form (4.5). We therefore set

$$\Lambda^{n} = (\Lambda^*)^n + \frac{1}{n}(\bar{\Lambda}_1)^n + \frac{1}{n^2}(\bar{\Lambda}_2)^n + O\left(\frac{1}{n^3}\right), \tag{4.5}$$

and we seek the analytic forms of $\bar{\Lambda}_1$ and $\bar{\Lambda}_2$. An approximate perturbation solution is then obtained by truncating the series and keeping only the first three terms, the leading order solution, the first-order perturbation correction and the second-order perturbation correction.

For simplicity, let $\Delta = \Lambda^n$, so that $\Lambda^{n+1} = \Delta^{1+\frac{1}{n}}$, and we can rewrite (4.3), and (4.4) as the following equations:

$$(\Delta - J_{11})\left(\Delta^{1+\varepsilon} - J_{22}\right) - J_{12}J_{21} = 0, \tag{4.6}$$

$$(\Delta - J_{11})(\Delta - J_{22}) - J_{12}J_{21} = 0, \tag{4.7}$$

where $\varepsilon = 1/n$. In this case, the up-to second order perturbation of (4.5) can be written in the following form

$$\Delta = \Delta^* + \varepsilon\bar{\Delta}_1 + \varepsilon^2\bar{\Delta}_2, \tag{4.8}$$

where Δ^* derives from one of the $2n$ solutions of (4.4). Rewriting (4.6) as

$$\Delta^{\varepsilon+1}(\Delta - J_{11}) - J_{22}\Delta + J_{11}J_{22} - J_{12}J_{21} = 0, \tag{4.9}$$

and using (4.8), we obtain

$$\begin{aligned}\left(\Delta^* + \varepsilon\bar{\Delta}_1 + \varepsilon^2\bar{\Delta}_2\right)^{\varepsilon+1}\left(\left(\Delta^* + \varepsilon\bar{\Delta}_1 + \varepsilon^2\bar{\Delta}_2\right) - J_{11}\right) =& J_{22}\left(\Delta^* + \varepsilon\bar{\Delta}_1 + \varepsilon^2\bar{\Delta}_2\right) \\ &- J_{11}J_{22} + J_{12}J_{21}.\end{aligned} \tag{4.10}$$

Using the Taylor expansion for $\left(\Delta^* + \varepsilon\bar{\Delta}_1 + \varepsilon^2\bar{\Delta}_2\right)^{\varepsilon+1}$ about $\varepsilon = 0$, (4.10) can be written as

$$\begin{aligned}&\left(\Delta^* + \left(\bar{\Delta}_1 + \Delta^*\ln\Delta^*\right)\varepsilon + \left(2\bar{\Delta}_2 + 2\bar{\Delta}_1 + 2\bar{\Delta}_1\ln\Delta^* + \Delta^*\left(\ln\Delta^*\right)^2\right)\frac{\varepsilon^2}{2!} + \ldots\right) \\ &\times\left(\left(\Delta^* + \varepsilon\bar{\Delta}_1 + \varepsilon^2\bar{\Delta}_2\right) - J_{11}\right) = J_{22}\left(\Delta^* + \varepsilon\bar{\Delta}_1 + \varepsilon^2\bar{\Delta}_2\right) - J_{11}J_{22} + J_{12}J_{21}.\end{aligned} \tag{4.11}$$

The leading order, $O(1)$, terms in (4.11), disappear because Δ^* satisfies (4.7). By comparing the coefficients of ε on both sides of (4.11), we obtain

$$\Delta^*\bar{\Delta}_1 + \left(\bar{\Delta}_1 + \Delta^*\ln\Delta^*\right)\Delta^* - J_{11}\left(\bar{\Delta}_1 + \Delta^*\ln\Delta^*\right) = J_{22}\bar{\Delta}_1,$$

thus the first order correction term is

$$\bar{\Delta}_1 = \frac{\Delta^*\ln\Delta^*\left(J_{11} - \Delta^*\right)}{2\Delta^* - J_{11} - J_{22}}. \tag{4.12}$$

Comparing coefficients of ε^2 on both sides of (4.11), we obtain

$$\begin{aligned}&\Delta^*\bar{\Delta}_2 + \left(\bar{\Delta}_1 + \Delta^*\ln\Delta^*\right)\bar{\Delta}_1 + \left(2\bar{\Delta}_1 + 2\bar{\Delta}_2 + 2\bar{\Delta}_1\ln\Delta^* + \Delta^*(\ln\Delta^*)^2\right)\frac{\Delta^*}{2} \\ &\quad - \left(2\bar{\Delta}_2 + 2\bar{\Delta}_1 + 2\bar{\Delta}_1\ln\Delta^* + \Delta^*(\ln\Delta^*)^2\right)\frac{J_{11}}{2!} = J_{22}\bar{\Delta}_2,\end{aligned}$$

and thus the second order correction term is

$$\bar{\Delta}_2 = \frac{-\bar{\Delta}_1^2 - \bar{\Delta}_1 \Delta^* \ln \Delta^* - (\Delta^* - J_{11}) \left(\bar{\Delta}_1 + \bar{\Delta}_1 \ln \Delta^* + \dfrac{\Delta^* (\ln \Delta^*)^2}{2} \right)}{2\Delta^* - J_{11} - J_{22}}, \quad (4.13)$$

which, using (4.12) becomes

$$\bar{\Delta}_2 = \frac{1}{2\left(J_{11} - 2\Delta^* + J_{22}\right)^3} \Big[\Delta^* \ln \Delta^* (J_{11} - \Delta^*) \Big[\ln \Delta^* (J_{11}^2 - 2J_{11}\Delta^* - J_{22}^2 + 2\Delta^{*2}) + 2(J_{11} - \Delta^*)(J_{11} - 2\Delta^* + J_{22}) \Big] \Big]. \quad (4.14)$$

From (4.12) and (4.14), the approximate analytical form (4.8) can be written as

$$\Delta = \Delta^* + \varepsilon \left[\frac{\Delta^* \ln \Delta^* \left(J_{11} - \Delta^*\right)}{2\Delta^* - J_{11} - J_{22}} \right] + \varepsilon^2 \left[\frac{1}{2\left(J_{11} - 2\Delta^* + J_{22}\right)^3} \Big[\Delta^* \ln \Delta^* (J_{11} - \Delta^*) \Big[\ln \Delta^* (J_{11}^2 - 2J_{11}\Delta^* - J_{22}^2 + 2\Delta^{*2}) + 2(J_{11} - \Delta^*)(J_{11} - 2\Delta^* + J_{22}) \Big] \Big] \right]. \quad (4.15)$$

We know that $\Delta = \Lambda^n = \lambda^{\frac{n}{M}} = \lambda^\alpha$ and $\Delta^* = (\Lambda^*)^n = (\lambda^*)^{\frac{n}{M}} = (\lambda^*)^\alpha$, therefore (4.15) can be written as

$$\lambda^\alpha = (\lambda^*)^\alpha + \varepsilon \frac{(\lambda^*)^\alpha \ln(\lambda^*)^\alpha (J_{11} - (\lambda^*)^\alpha)}{2\left(\lambda^*\right)^\alpha - J_{11} - J_{22}} + \varepsilon^2 \frac{1}{2(J_{11} - 2(\lambda^*)^\alpha + J_{22})^3} \Big[(\lambda^*)^\alpha \ln(\lambda^*)^\alpha (J_{11} - (\lambda^*)^\alpha) \Big[\ln(\lambda^*)^\alpha \left(J_{11}^2 - 2J_{11} \left(\lambda^*\right)^\alpha - J_{22}^2 + 2\left(\left(\lambda^*\right)^\alpha\right)^2 \right) + (J_{11} - (\lambda^*)^\alpha)(J_{11} - 2(\lambda^*)^\alpha + J_{22}) \Big] \Big], \quad (4.16)$$

where λ^* is a solution for the commensurate system, i.e.,

$$(\lambda^*)^\alpha = \frac{J_{11} + J_{22} \pm \sqrt{{J_{11}}^2 + {J_{22}}^2 - 2J_{11}J_{22} + 4J_{12}J_{21}}}{2}. \quad (4.17)$$

In order to find the extra root of (4.3), we consider the functions

$$f_{2n}(\Lambda) = \Lambda^{2n} - (J_{11} + J_{22})\Lambda^n + J_{11}J_{22} - J_{12}J_{21},$$

and

$$f_{2n+1}(\Lambda) = \Lambda^{2n+1} - J_{11}\Lambda^{n+1} - J_{22}\Lambda^n + J_{11}J_{22} - J_{12}J_{21}.$$

Assuming, as in the last section, that $2n$ roots of f_{2n+1} are close to the roots of f_{2n} we can find the sign of the additional root by using Descartes' Rule of Signs

[5]. The number of the changes of signs of terms in f_{2n} will be compared to the number of the changes of signs of terms in f_{2n+1}. If f_{2n} and f_{2n+1} have the same number of the changes of signs (the same number of positive roots modulo 2), then the single extra root for f_{2n+1} will necessarily be negative, and thus will not alter the stability of the system.

The first and last coefficients in f_{2n} and f_{2n+1} are identical, thus, we will focus on the other coefficients which depend on J_{11} and J_{22}. There are four different possibilities for the signs of these coefficients. $J_{11}, J_{22} > 0$; $J_{11}, J_{22} < 0$; $J_{11} < 0 < J_{22}$; $J_{22} < 0 < J_{11}$.

If J_{11} and J_{22} are both positive or are both negative, then the number of the changes of signs has not increased, so that the number of positive roots has not increased and therefore, the extra root cannot be positive. For the other two cases, the sign of $J_{11} + J_{22}$ affects the number of positive roots. Table 4.1 shows all the possibilities of the number of roots that we could get. We see from Table 4.1 that, in going from f_{2n} to f_{2n+1}, we may have either zero or two additional positive roots. However, only one root is added in going from f_{2n} to f_{2n+1}. Therefore we have proven that the extra root cannot be positive. The extra root does not, therefore, affect the stability of the system.

	$J_{11}+J_{22}$	$J_{11}J_{22}-J_{12}J_{21}$	$f_{2n}=$ $f_{2n+1}=$	Λ^{2n} Λ^{2n+1}	$-J_{11}\Lambda^{n+1}$	$-(J_{11}+J_{22})\Lambda^{n}$ $-J_{22}\Lambda^{n}$	$+J_{11}J_{22}-J_{12}J_{21}$ $+J_{11}J_{22}-J_{12}J_{21}$	number of signs changing
$J_{11}<0<J_{22}$	$+$	$+$	f_{2n}	$+$		$-$	$+$	two
			f_{2n+1}	$+$	$+$	$-$	$+$	two
	$+$	$-$	f_{2n}	$+$		$-$	$-$	one
			f_{2n+1}	$+$	$+$	$-$	$-$	one
	$-$	$+$	f_{2n}	$+$		$+$	$+$	zero
			f_{2n+1}	$+$	$+$	$-$	$+$	two
	$-$	$-$	f_{2n}	$+$		$+$	$-$	one
			f_{2n+1}	$+$	$+$	$-$	$-$	one
$J_{22}<0<J_{11}$	$+$	$+$	f_{2n}	$+$		$-$	$+$	two
			f_{2n+1}	$+$	$-$	$+$	$+$	two
	$+$	$-$	f_{2n}	$+$		$-$	$-$	one
			f_{2n+1}	$+$	$-$	$+$	$-$	three
	$-$	$+$	f_{2n}	$+$		$+$	$+$	zero
			f_{2n+1}	$+$	$-$	$+$	$+$	two
	$-$	$-$	f_{2n}	$+$		$+$	$-$	one
			f_{2n+1}	$+$	$-$	$+$	$-$	three

Table 4.1: All the possibilities for the signs of coefficients in f_{2n} and f_{2n+1}.

4.1.2 Stability Boundary

In this section, we focus on the $2n$ eigenvalues solutions of (4.16) since the extra root investigated in the last section will never cause the system to be unstable. We will consider situations when we have complex eigenvalues in the commensurate case, so that stability is alpha-dependent, and then assume that the incommensurate system has complex eigenvalues, which will at least be the case when the system is close to commensurate. Therefore, by using (4.17), we can rewrite the solution of the commensurate system as $(\lambda^*)^\alpha = x \pm iy$, where

$$x = \frac{J_{11} + J_{22}}{2} \quad \text{and} \quad y = \frac{1}{2}\left(-{J_{11}}^2 - {J_{22}}^2 + 2J_{11}J_{22} - 4J_{12}J_{21}\right)^{\frac{1}{2}}.$$

To determine the stability of the equilibrium point we are interested in $|\arg\lambda|$ and therefore we may consider just one of the complex conjugate solutions, $(\lambda^*)^\alpha = x + iy$. The form of λ^α is then

$$\lambda^\alpha = (x + iy) + \varepsilon\,(x_1 + iy_1) + \varepsilon^2\,(x_2 + iy_2)\,, \tag{4.18}$$

where x_1, y_1, x_2 and y_2 are related to J_{11}, J_{12}, J_{21} and J_{22} which we provided in Appendix A.1. The condition for stability is $|\arg\lambda| > \dfrac{\pi}{2}$. Therefore, from (4.18), if we consider only the first order correction, the condition for stability is

$$|\arg\left((x + \varepsilon x_1) + (y + \varepsilon y_1)\,i\right)| > \frac{\pi}{2}\alpha. \tag{4.19}$$

Using the Taylor series expansion for $\dfrac{y + \varepsilon y_1}{x + \varepsilon x_1}$, we have

$$\arg\left((x + \varepsilon x_1) + i\,(y + \varepsilon y_1)\right) = \tan^{-1}\frac{y + \varepsilon y_1}{x + \varepsilon x_1} = \tan^{-1}\left[\frac{y}{x} + \left(\frac{y_1}{x} - \frac{x_1 y}{x^2}\right)\varepsilon + \cdots\right].$$

Using the Taylor series expansion for $\tan^{-1}$, we obtain

$$\arg\left((x + \varepsilon x_1) + i\,(y + \varepsilon y_1)\right) = \tan^{-1}N_1 + \frac{N_2}{1 + {N_1}^2}\varepsilon,$$

where $N_1 = \dfrac{y}{x}$ and $N_2 = \dfrac{y_1}{x} - \dfrac{x_1 y}{x^2}$. Since $\varepsilon = \dfrac{\beta}{\alpha} - 1$, (4.19) can be written as

$$\left|\tan^{-1}N_1 + \frac{N_2}{1 + {N_1}^2}\left(\frac{\beta}{\alpha} - 1\right)\right| > \frac{\pi}{2}\alpha, \tag{4.20}$$

which is the condition for the stability, dependent on α and β. If we consider the second order correction, the stability condition is

$$\left|\arg\left((x + \varepsilon x_1 + \varepsilon^2 x_2) + \left(y + \varepsilon y_1 + \varepsilon^2 y_2\right)i\right)\right| > \frac{\pi}{2}\alpha, \tag{4.21}$$

which, again using Taylor series, becomes

$$\arg\left(\left(x+\varepsilon x_1+\varepsilon^2 x_2\right)+i\left(y+\varepsilon y_1+\varepsilon^2 y_2\right)\right) = \tan^{-1}N_1+\frac{N_2}{1+{N_1}^2}\varepsilon + \frac{2N_3+2N_3{N_1}^2-2N_1{N_2}^2}{\left(1+{N_1}^2\right)^2}\varepsilon^2,$$

where $N_3=\left(\frac{y_2}{x}-\frac{x_1y_1+x_2y}{x^2}+\frac{x_1^2y}{x^3}\right)$. This condition, as a function of α and β, can then be written as

$$\left|\tan^{-1}N_1+\frac{N_2}{1+{N_1}^2}\left(\frac{\beta}{\alpha}-1\right)+\frac{2N_3+2N_3{N_1}^2-2N_1{N_2}^2}{\left(1+{N_1}^2\right)^2}\left(\frac{\beta}{\alpha}-1\right)^2\right|>\frac{\pi}{2}\alpha. \tag{4.22}$$

Equations (4.20) and (4.22) now give us approximations for the boundary of the stability region, $\beta=\beta(\alpha)$, close to the critical order for the commensurate system α^*. Those two critical curves, derived from (4.20) and (4.22), respectively, are

$$\beta=\beta_1(\alpha)=\alpha\left(D_1\alpha+D_2\right), \tag{4.23}$$

and

$$\beta=\beta_2(\alpha)=\left(\left(1-\frac{M_2}{2M_1}\right)\mp\sqrt{\left(1-\frac{M_2}{2M_1}\right)^2-\frac{1}{M_1}\left(M_1-M_2-\frac{\pi}{2}\alpha+\tan^{-1}N_1\right)}\right)\alpha, \tag{4.24}$$

where

$$\begin{aligned} D_1 &= \frac{\pi}{2}\left(\frac{1+N_1^2}{N_2}\right),\\ D_2 &= 1-\frac{1+N_1^2}{N_2}\tan^{-1}N_1,\\ M_1 &= \frac{2N_3+2N_3{N_1}^2-2N_1{N_2}^2}{\left(1+{N_1}^2\right)^2},\\ M_2 &= \frac{N_2}{1+{N_1}^2}. \end{aligned}$$

4.2 Numerical Solution

In this section, we will numerically find the solution of (4.1) using Matlab (fsolve) for particular predator-prey systems, and compare the stability boundary for a particular equilibrium point to the approximate analytical results (4.23) and (4.24).

4.2.1 Predator-Prey Incommensurate System

The first system we will consider is the incommensurate version of the predator-prey system that was introduced in Chapter 3, namely

$$
\begin{aligned}
{}^{c}D_{t}^{\alpha}X &= X(1-X) - \frac{K_1XY}{1+IX} - E_1X, && (4.25)\\
{}^{c}D_{t}^{\beta}Y &= RY(1-Y) + \frac{K_2XY}{1+IX} - E_2Y, && (4.26)
\end{aligned}
$$

with the initial conditions $X(0) = X_0$ and $Y(0) = Y_0$, where $0 < \alpha < 1$ and $0 < \beta < 1$.

In Chapter 3, we found that the commensurate system is asymptotically stable around the equilibrium point P_{32} for all fractional derivative orders in the interval $(0, \alpha^*)$ where α^* can be determined from the system parameters. In this section, we will investigate how α^* changes as β is allowed to change for the same parameter values used in the previous chapter.

Using the command fsolve in Matlab, we consider changes in the eigenvalue $\lambda_0 = 0.0436 + 0.2372\text{i}$, which is the eigenvalue that leads to the instability in the integer system ($\alpha = 1$, $\beta = 1$) at P_{32}, as α and β change. Two example situations are given below after which we consider a more general case. If we retain integer order prey dynamics but allow fractional order predator dynamics, so that $\alpha = 1$ and $0 < \beta < 1$, then the complex eigenvalue of the system is shown in Figure 4.1(a, b). The real part of the eigenvalue is always positive and so the system, (4.25) and (4.26), will never be stable around P_{32} for any value of β when $\alpha = 1$. If we retain integer order predator dynamics but allow fractional order prey dynamics, so that $\beta = 1$ and $0 < \alpha < 1$, then the complex eigenvalue of the system (see Figure 4.1(c, d)) swaps from having positive real part to negative real part. The system (4.25) and (4.26), can therefore be stable when $\beta = 1$ if α reduces below a critical value $\alpha^* = 0.8922$.

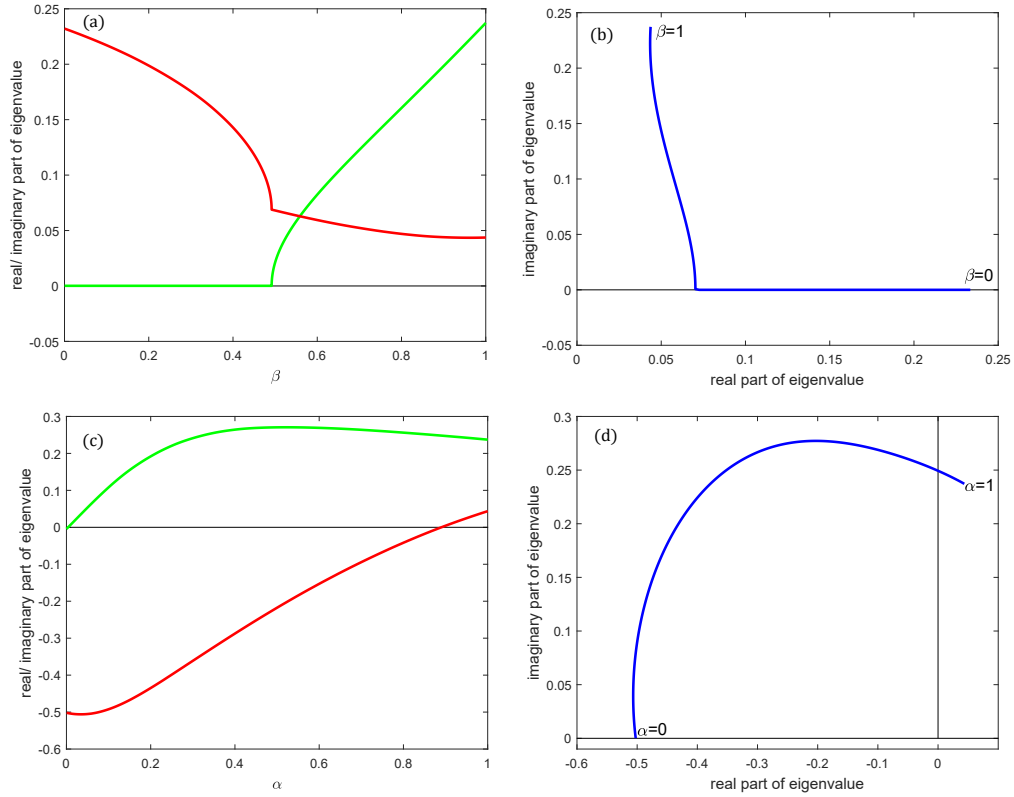

Figure 4.1: One of the complex conjugate solutions (eigenvalues) to the characteristic equation (4.1) for the incommensurate system, (4.25) and (4.26) at the equilibrium point P_{32}. In (a) and (c) the real parts (red line) and the imaginary parts (green line), while (b) and (d) show the Argand diagram.

The more general situation, when both α and β vary is shown in Figure 4.2. In Figure 4.2 the green region indicates that the equilibrium point P_{32} is unstable, i.e. there is an eigenvalue with positive real part. The white region in Figure 4.2 indicates that P_{32} is stable, i.e. all eigenvalues have negative real part. Therefore, for values of the prey fractional order, α, close to one, the incommensurate system will not be stable, but as we reduce α we move to the white region, and we can get a stable equilibrium point. The dashed line in Figure 4.2 shows that the unstable region (green) can be separated into two sub-regions depending on the kind of instability the incommensurate system exhibits around P_{32}. For (α, β) above the dashed line in the green region, the unstable eigenvalue is complex and so the trajectories will spiral around the equilibrium point as they evolve away from P_{32}, and when (α, β) is below the dashed line in the green region, the unstable eigenvalue is real and so the trajectories will not spiral around the equilibrium point as they evolve away from P_{32}. In Figure 4.2 the line $\alpha = \beta$, i.e. the commensurate system is shown as well as the point α^*, the critical value of the fractional order below which the commensurate system is stable.

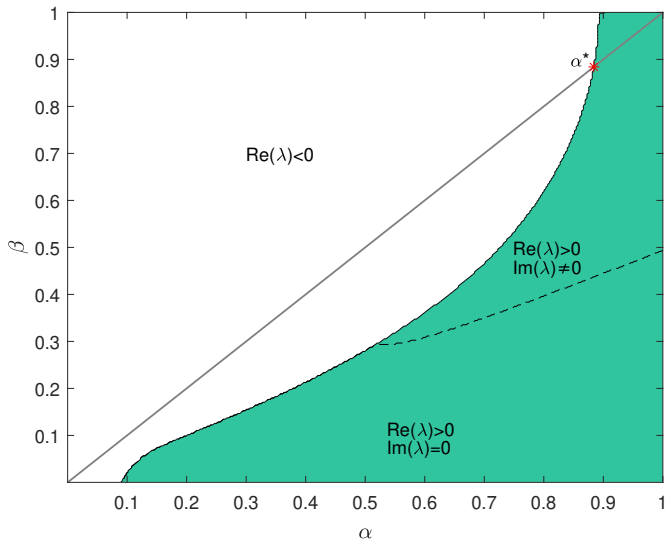

Figure 4.2: The regions of stability for various values of the fractional derivative order. For fractional orders, for the incommensurate system (4.25) and (4.26) chosen from the white region, the system will be stable around the equilibrium point P_{32}. For fractional orders chosen from the green region, the system will be unstable around the equilibrium point P_{32}. The line $\alpha = \beta$, i.e. the commensurate system is shown as well as the point α^*, the critical value of the fractional order below which the commensurate system is stable.

As we proved in the previous chapter, for $\alpha > \alpha^*$, the commensurate system ($\alpha = \beta$) is unstable around the equilibrium point P_{32}. However, from Figure 4.2 we see that the incommensurate system might be stable when $\alpha > \alpha^*$ and $\beta > \alpha^*$ if α and β are chosen to be in the white region. This is illustrated in Figure 4.3(a) when $\alpha = 0.89 > \alpha^*$, where P_{32} is stable for $\beta > \beta_2$ and the form of the unstable behaviour changes upon passing β_1. Figure 4.3(b-d) indicates how the stability around the equilibrium point vary as β changes. If $\beta = 0.95$, the incommensurate system can be stable when $\beta > \beta_2$, see Figure 4.3(b). If $\beta = 0.6$, i.e. above the dashed line in the green region, the incommensurate system will be unstable around trajectories that spiral around the equilibrium point as they evolve away from P_{32}, see Figure 4.3(c). If $\beta = 0.3$, below the dashed line in the green region, the incommensurate system will also be unstable but does not spiral around the equilibrium point as it evolves away from P_{32}, see Figure 4.3(d).

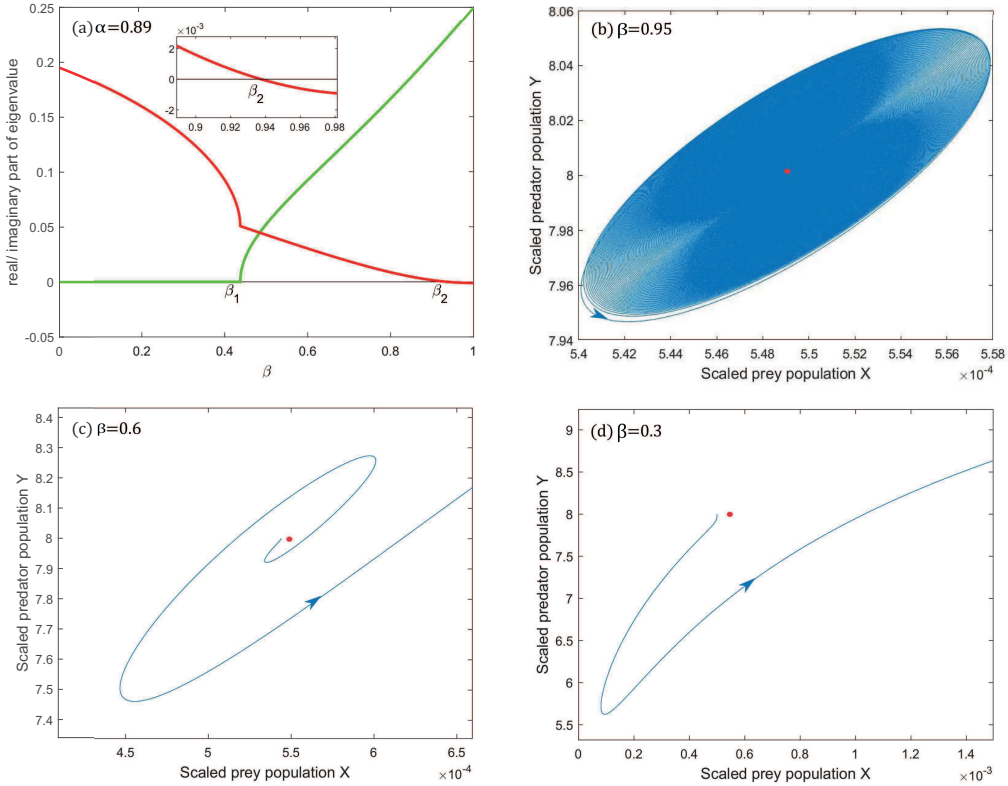

Figure 4.3: The behaviour of the incommensurate system, (4.25) and (4.26), when $\alpha = 0.89 > \alpha^*$. (a) One of the complex conjugate solutions (eigenvalues) to the characteristic equation (4.1) at the equilibrium point P_{32}. The real parts (red line) and the imaginary parts (green line). (b), (c) and (d) illustrate the phase plane trajectories when $\beta = 0.95$, $\beta = 0.6$ and $\beta = 0.3$, respectively, where the red point is P_{32}.

In the commensurate system when $\alpha < \alpha^*$, the system is stable around the equilibrium point P_{32}. However, when $\alpha \neq \beta$ it is possible for the incommensurate system to be unstable for $\alpha < \alpha^*$ if β is chosen to be small enough, so that (α, β) is in the green region of Figure 4.2. Figure 4.4(a) illustrates this behaviour when $\alpha = 0.60 < \alpha^*$, where we see a change in behaviour as β reduces. The form of the unstable behaviour changes when passing β_1 and P_{32} is stable for $\beta > \beta_2$. If $\beta = 0.95$, the incommensurate system is stable, as seen in Figure 4.4(b), and if $\beta = 0.35$, above the dashed line in the green region, the incommensurate system will be unstable and will spiral away from the equilibrium point, see Figure 4.4(c). If $\beta = 0.2$, under the dashed line in the green region, the incommensurate system will also be unstable without spiralling around the equilibrium point P_{32}, see Figure 4.4(d).

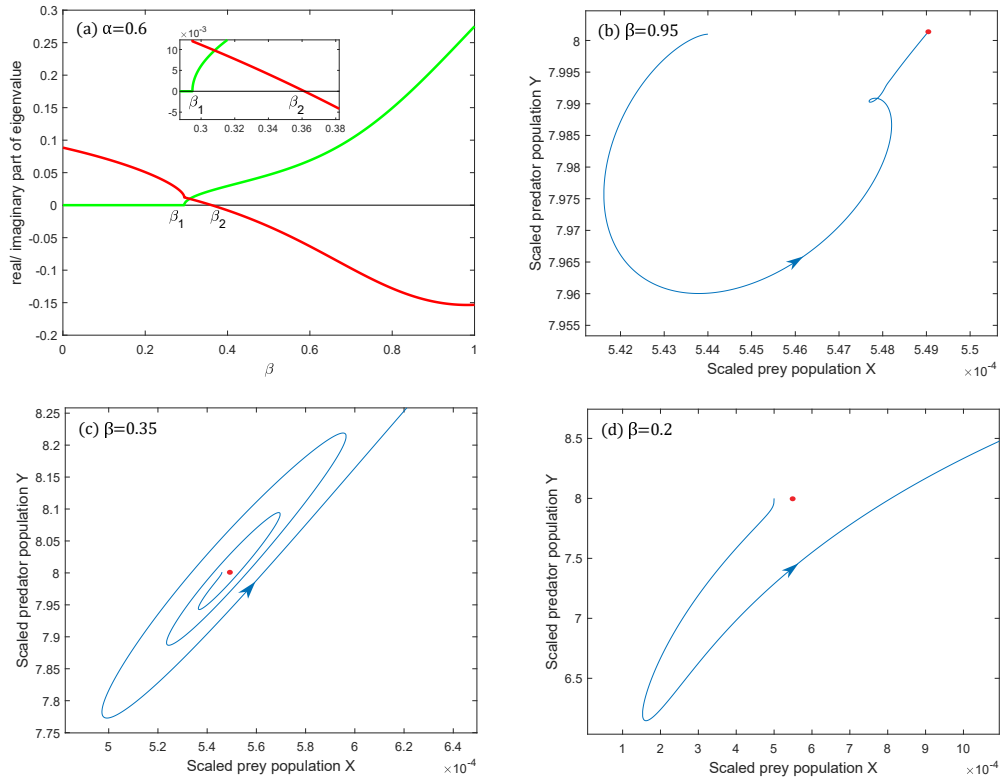

Figure 4.4: The behaviour of the incommensurate system, (4.25) and (4.26), when $\alpha = 0.6 < \alpha^*$. (a) One of the complex conjugate solutions (eigenvalues) to the characteristic equation (4.1) at the equilibrium point P_{32}. The real parts (red line) and the imaginary parts (green line). (b), (c) and (d) illustrate the phase plane trajectories when $\beta = 0.95$, $\beta = 0.35$ and $\beta = 0.2$, respectively, where the red point is P_{32}.

To confirm that the approximation analytical solution for the line $\beta(\alpha)$, the boundary between stable and unstable regions, in Figure 4.2, we plot the two approximation solutions (4.23) and (4.24) with the numerical solution in Figure 4.5. In this figure, we see that $\beta = \beta_1(\alpha)$ (red curve) and $\beta = \beta_2(\alpha)$ (blue dashed curve) are good approximation to the stability boundary found numerically, particularly close to $\alpha = \beta = \alpha^*$, as to be expected.

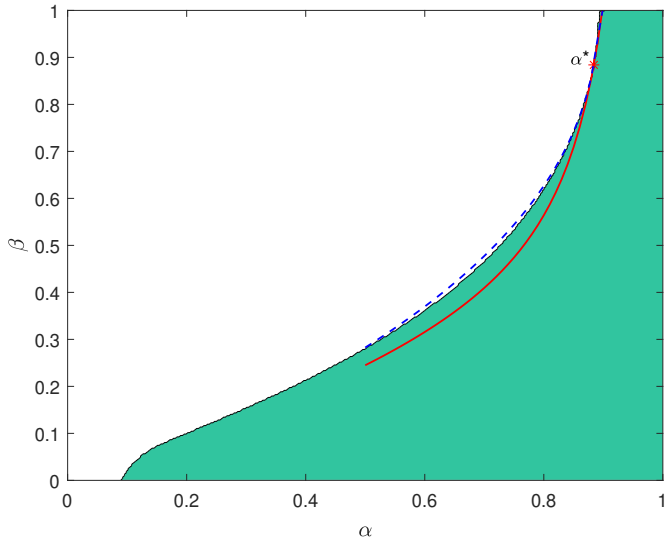

Figure 4.5: The curves $\beta = \beta_1(\alpha)$ (red curve) and $\beta = \beta_2(\alpha)$ (blue dashed curve) and the numerically determined stability boundary from Figure 4.2.

To summarise, we have shown both numerically and analytically that, in the incommensurate system (4.25) and (4.26), decreasing the predator fractional order β, can change a stable equilibrium point to an unstable point. This can not happen in the equivalent commensurate system, where decreasing the fractional order will only ever stabilise an unstable point. In order to examine if this is a more general result, it will be interesting to consider another incommensurate system, as we will do in the following section.

4.2.2 Plant-Herbivore Incommensurate System

Models of plant–herbivore interactions are often based on predator–prey models [74, 75] with the plants taking the role of prey and the herbivores taking the role of predator. In this section we will study a plant-herbivore model that includes a Holling type III predation rate, which has been used to study the effect of limited nutrients in a plant-herbivore system. Specifically, we used the model derived by Saha et al. [108]

$$\frac{dx}{dt} = rx\left(1 - \frac{x}{k}\right) - \frac{mx^2y}{n + x^2}, \tag{4.27}$$

$$\frac{dy}{dt} = \frac{emx^2y}{n + x^2} - hy, \tag{4.28}$$

where $x(t)$ represents the plant biomass (the "prey") and $y(t)$ represents the number of herbivores (the "predator") at time t. The per capita birth rate of plants

is $r\left(1-\frac{x}{k}\right)$ where r is a positive constant, the linear birth rate, and k is a positive constant representing the carrying capacity of the environment. In (4.27) and (4.28), the amount of plants eaten by the herbivore follows a Holling type III function, representing a system where the number of prey is low, and therefore harder to find. This type of interaction is suitable for some plant-herbivore systems and has been shown to be successful at describing interactions in these types of systems [108]. In this Holling type III function, m is the maximum uptake rate for herbivores, n is related to the half saturation plant density and e is the conversion factor that satisfies the condition $0 < e < 1$. The term hy in (4.28) represents the loss of herbivores through natural death or harvesting of the herbivore at a rate h. Saha et al. nondimensionalised (4.27) and (4.28) leading to

$$\frac{dX}{dT} = qX\left(1-\frac{X}{q}\right) - \frac{aX^2Y}{1+X^2} \tag{4.29}$$

$$\frac{dY}{dT} = \frac{bX^2Y}{1+X^2} - \gamma Y, \tag{4.30}$$

with the initial conditions $X(0) = X_0$ and $Y(0) = Y_0$, and where $X = x/\sqrt{n}$, $Y = y/\sqrt{n}$ and $T = r\sqrt{n}t/k$. The parameters in (4.29) and (4.30) have the following expressions $q = k/\sqrt{n}$, $a = mk/(r\sqrt{n})$, $b = emk/(r\sqrt{n})$ and $\gamma = hk/(r\sqrt{n})$, and are all real positive constants since k, m, e and r are positive and $e < 1$. The equilibrium points of (4.29) and (4.30), that are found in [108], are $E_0 = (0,0)$, the trivial equilibrium, $E_1 = (q,0)$ the herbivore-free state and $E_2 = (X^*, Y^*) = \left(\sqrt{\frac{\gamma}{b-\gamma}}, \frac{(q-X^*)(1+X^{*2})}{aX^*}\right)$, the coexisting plant-herbivore state.

The existence and the stability of the three equilibrium points were also found in [108]. The two equilibrium points E_0 and E_1 always exist. However, E_2 exists only when $b > \gamma$ and $X^* < q$. E_0 is always an unstable equilibrium point and E_1 is stable when E_2 does not exist. Thus, if E_2 exists, then E_1 is unstable.

In terms of investigating the stability around E_2, the characteristic equation is

$$\lambda^2 + \left(\frac{q - qX^{*2} + 2X^{*3}}{1+X^{*2}}\right)\lambda + \frac{2bX^{*2}(q-X^*)}{(1+X^{*2})^2} = 0,$$

and the condition for having complex eigenvalues, which we are interested in is $q_1 < q < q_2$, where

$$q_1 = \frac{2\left(2b(X^*)^2 - (X^*)^3 + (X^*)^5\right) - 2\sqrt{2}\sqrt{b(X^*)^7 + 2b^2(X^*)^4 - b(X^*)^3}}{(1-(X^*)^2)^2},$$

and

$$q_2 = \frac{2\left(2b(X^*)^2 - (X^*)^3 + (X^*)^5\right) + 2\sqrt{2}\sqrt{b(X^*)^7 + 2b^2(X^*)^4 - b(X^*)^3}}{(1-(X^*)^2)^2}.$$

The real part of the complex eigenvalues is positive when $q - qX^{*2} + 2X^{*3} < 0$. This condition has two possibilities which are $q < q_0$ when $X^* < 1$ $(b > 2\gamma)$ or $q > q_0$ when $X^* > 1$ $(b < 2\gamma)$, where $q_0 = \dfrac{2\gamma}{2\gamma - b}\sqrt{\dfrac{\gamma}{b-\gamma}}$.

For the values of parameters in Table 4.2, the two eigenvalues for E_2 are shown in Figure 4.6. The system has complex eigenvalues when $q_1 < q < q_2$, $q_1 = 3.58$ and $q_2 = 10.59$, and since $b = 1.2 < 2\gamma = 2$, the real part of the eigenvalues is positive when $q > q_0 = 5.59$.

Table 4.2: Parameter values used in our numerical simulations where they are the same values of the parameters in [35, 108].

Parameter	Value	Unit
a	1.25	Dimensionless
b	1.2	Dimensionless
γ	1	Dimensionless

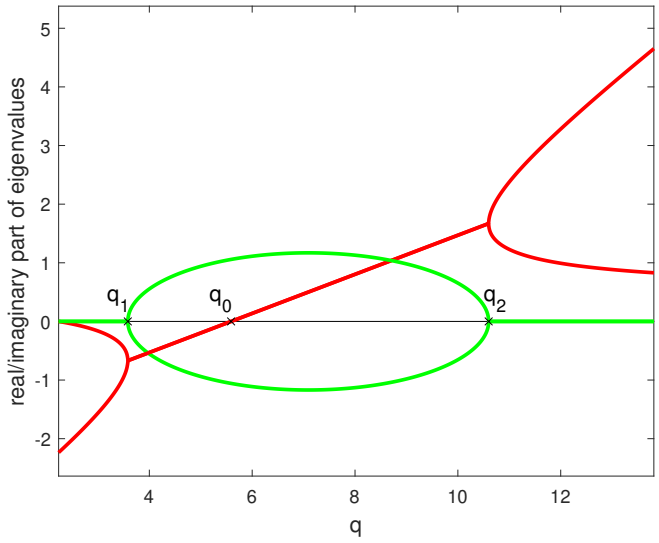

Figure 4.6: Real (red line) and imaginary (green line) part of eigenvalues of the integer system of the second equilibrium point E_2. Complex eigenvalues exist when $q_1 < q < q_2$ and the real parts of the complex eigenvalues is positive when $q > q_0$, where $q_1 = 10.59, q_2 = 3.58$ and $q_0 = 5.59$ for the parameters we have used.

As in the previous section, we will now assume that the memories of the two species are different. The effect on the stability of the E_2 equilibrium point of having these two fractional orders will then be explored. In this case, the plant-

herbivore interactions are described by the following incommensurate system:

$$
\begin{aligned}
{}^{c}D_{T}^{\alpha}X &= qX\left(1-\frac{X}{q}\right)-\frac{aX^{2}Y}{1+X^{2}}, && (4.31)\\
{}^{c}D_{T}^{\beta}Y &= \frac{bX^{2}Y}{1+X^{2}}-\gamma Y, && (4.32)
\end{aligned}
$$

with the initial conditions $X(0) = X_0$ and $Y(0) = Y_0$ and where $0 < \alpha < 1$ and $0 < \beta < 1$.

The fractional commensurate system based on (4.29) and (4.30) was introduced by El-Shahed et al. [35] where they found that E_2 is a stable equilibrium point if $\alpha \in (0, \alpha^*)$, where $\alpha^* = 0.606$. In this section, we will investigate how the critical fractional order changes as β is allowed to be different from α.

Using the command fsolve in Matlab, we consider changes in the unstable eigenvalue, $\lambda_0 = 0.8032 + 1.1296i$, in the integer system at E_2 when $a = 1.25, b = 1.2, \gamma = 1$ and $q = 8$, as α and β change. Two example situations, for when only one of α and β change, are given below, after which we consider a more general case.

If we retain integer order prey dynamics but allow fractional order predator dynamics, so that $\alpha = 1$ and $0 < \beta < 1$, then the complex eigenvalue of the system (see Figure 4.7(a, b)) swaps from having positive real part to negative real part as β decreases. The system (4.31) and (4.32), can therefore be stable when $\alpha = 1$ if we reduce β sufficiently. If we retain integer order predator dynamics but allow fractional order prey dynamics, so that $\beta = 1$ and $0 < \alpha < 1$, then the complex eigenvalue of the system is shown in Figure 4.7(c, d). The real part of the eigenvalue is always positive and so the system, (4.31) and (4.32), will never be stable around E_2 for any value of α when $\beta = 1$.

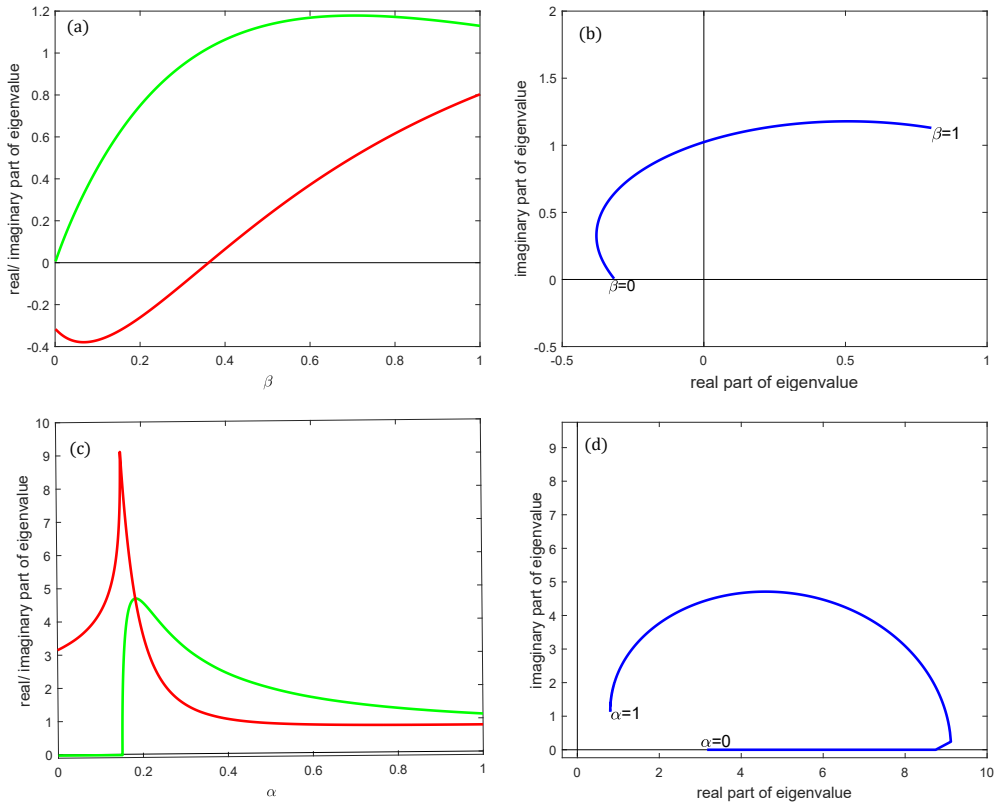

Figure 4.7: One of the complex conjugate solutions (eigenvalues) to the characteristic equation (4.1) for the incommensurate system, (4.31) and (4.32) at the equilibrium point E_2. In (a) and (c) the real parts (red line) and the imaginary parts (green line) while (b) and (d) show the Argand diagram.

From these example variations in α and β we see that, although reducing β can lead to the stabilisation of the E_2 equilibrium point, when $\beta = 1$ reducing α does not have a similar effect. The more general situation, when both α and β vary is shown in Figure 4.8, where the green region indicates that E_2 is unstable, i.e. there is an eigenvalue with positive real part, and the white region indicates that E_2 is stable, i.e. there are only eigenvalues with negative real part. The dashed line in Figure 4.8 shows that the unstable region (green) can be separated into two regions depending on the kind of instability the incommensurate system exhibits around E_2. For (α, β) on the right side of the dashed line, the unstable eigenvalues have nonzero imaginary part and the trajectories will spiral around the equilibrium point as they evolve away from E_2, and when (α, β) is on the left side of the dashed line the imaginary part of the eigenvalue is zero, thus the trajectories will not spiral around the equilibrium point as they evolve away from E_2.

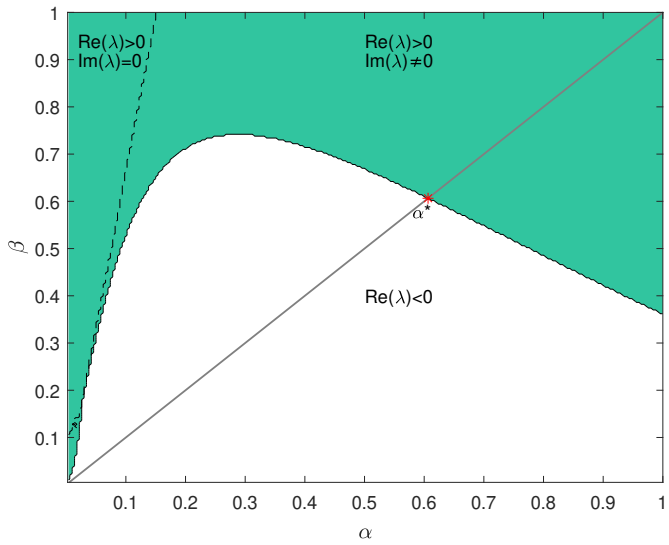

Figure 4.8: The regions of stability for various values of the fractional derivative order. For fractional orders chosen from the white region, the system will be stable around the equilibrium point E_2. For fractional orders chosen from the green region, the system will be unstable around the equilibrium point E_2. The line $\alpha = \beta$, i.e. the commensurate system, is shown as well as the point α^*, the critical value of the fractional order below which the commensurate system is stable.

El-Shahed et al. showed in [35] that for $\alpha > \alpha^*$ the commensurate system ($\alpha = \beta$) is unstable around the equilibrium point E_2. However, from Figure 4.8 we see that the incommensurate system may be stable when $\alpha > \alpha^*$ when (α, β) are chosen to be in the white region. Figure 4.9(a,b) illustrates this when $\alpha = 0.8 > \alpha^*$ and $\beta = 0.2$. In addition, in the commensurate system when $\alpha < \alpha^*$, the system is stable around the equilibrium point E_2. However, in the incommensurate system, if $\alpha < \alpha^*$, it is possible for the incommensurate system to be unstable if (α, β) are chosen to be in the green region. Figure 4.9(c,d) illustrates this when $\alpha = 0.2 < \alpha^*$ and $\beta = 0.80$.

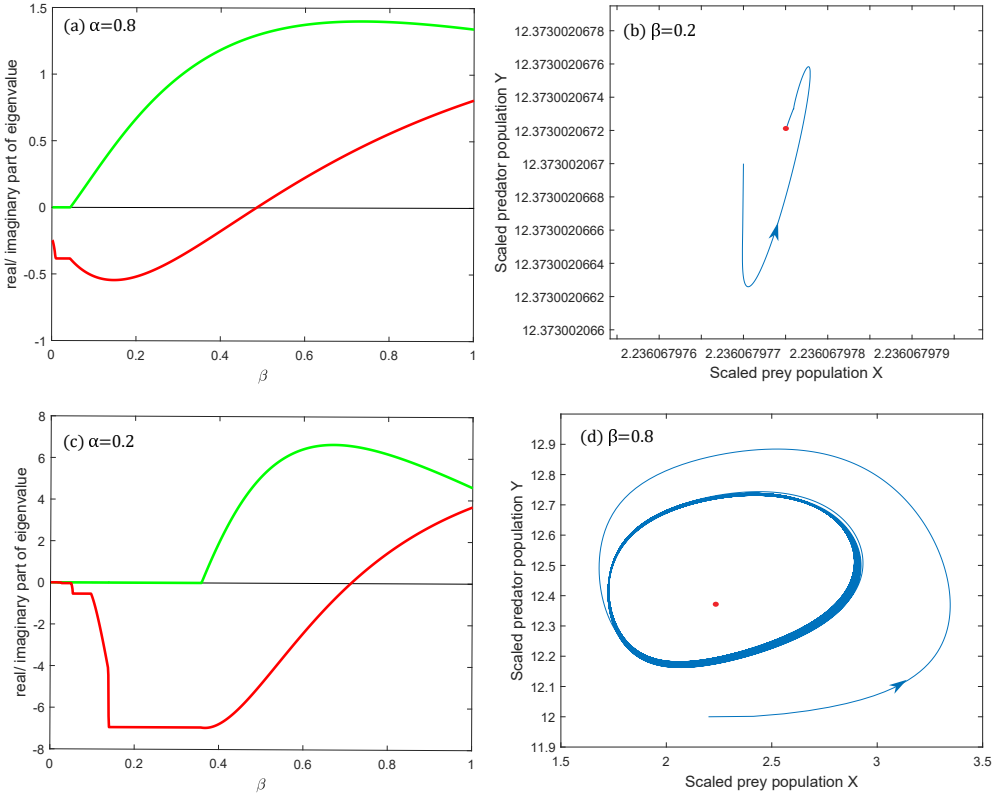

Figure 4.9: (a) and (c) One of the complex conjugate solutions (eigenvalues) to the characteristic equation (4.1) for the incommensurate system, (4.31) and (4.32), at the equilibrium point E_2 when $\alpha = 0.8 > \alpha^*$ and $\alpha = 0.2 < \alpha^*$, respectively, the real parts (red line) and the imaginary parts (green line). (b) and (d) The phase plane trajectories when $\beta = 0.2$ and $\beta = 0.8$, respectively, where the red point is the equilibrium point E_2.

As we see from Figure 4.8, there is a range of values of β, i.e. when $\beta = 0.65$, where there are two critical values of α. By increasing α for a fixed value of β, one of the eigenvalues will initially be complex with positive real part, then complex with negative real part and then again complex with positive real part. This behaviour is illustrated in Figure 4.10, when $\beta = 0.65$. In Figure 4.10 we see that the incommensurate system is unstable around the second equilibrium point E_2, when $\alpha = 0.1$ (Figure 4.10(b)), is asymptotically stable around E_2 when $\alpha = 0.3$ (Figure 4.10(c)), i.e. when (α, β) is in the white region, and unstable around E_2 when $\alpha = 0.95$ (Figure 4.10(d)). It should also be noted that the instability for $\alpha = 0.1$ and $\alpha = 0.95$ is different since these points lie on opposite sides of the dashed line in Figure 4.8. For $\alpha = 0.1$ the trajectory will not spiral out from E_2 but at $\alpha = 0.95$ it will.

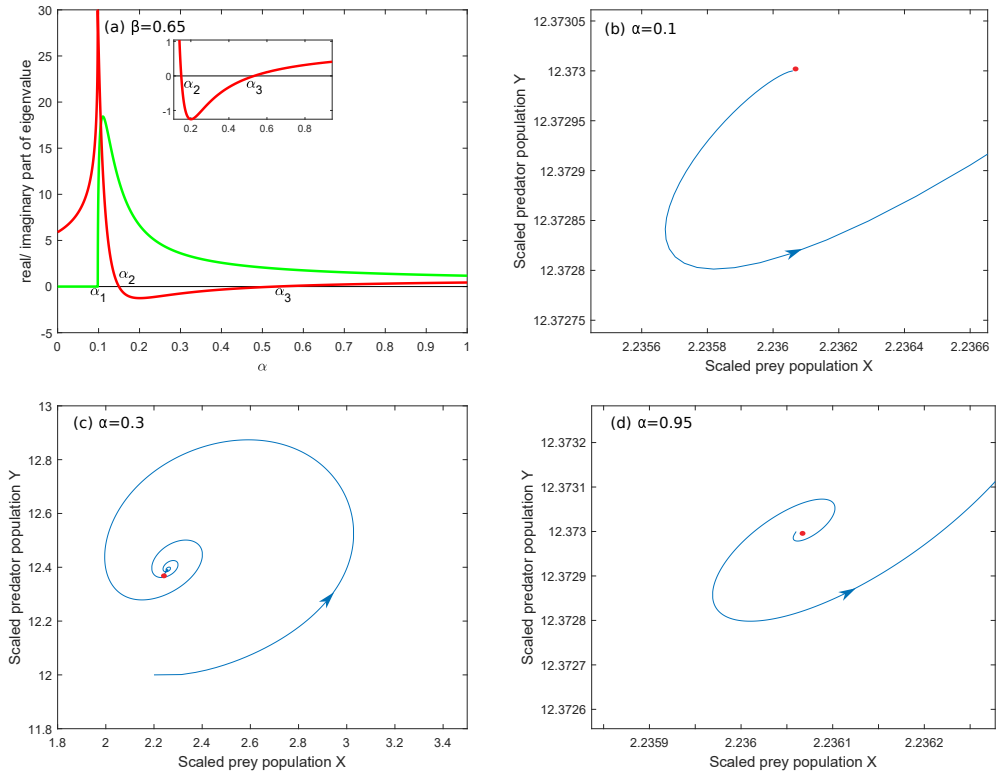

Figure 4.10: The behaviour of the incommensurate system, (4.31) and (4.32) when $\beta = 0.65$. (a) One of the solutions (eigenvalues) to the characteristic equation (4.1) at the equilibrium point E_2 as α varies, the real parts (red line) and the imaginary parts (green line). (b), (c) and (d) illustrate the phase plane trajectories when $\alpha = 0.1$, $\alpha = 0.3$ and $\alpha = 0.95$, respectively, where the red point is E_2.

To confirm that the approximate analytical solution for the boundary between stable and unstable regions, $\beta(\alpha)$, in Section 4.1.2, is close to the numerical solution, we plot the two approximation solutions (4.23) and (4.24) with the numerical solution, in Figure 4.11. In this Figure, we see that $\beta = \beta_1(\alpha)$ (red curve) and $\beta = \beta_2(\alpha)$ (blue dashed curve) are good approximation to the stability boundary found numerically, particularly near to $\alpha = \beta = \alpha^*$, as expected.

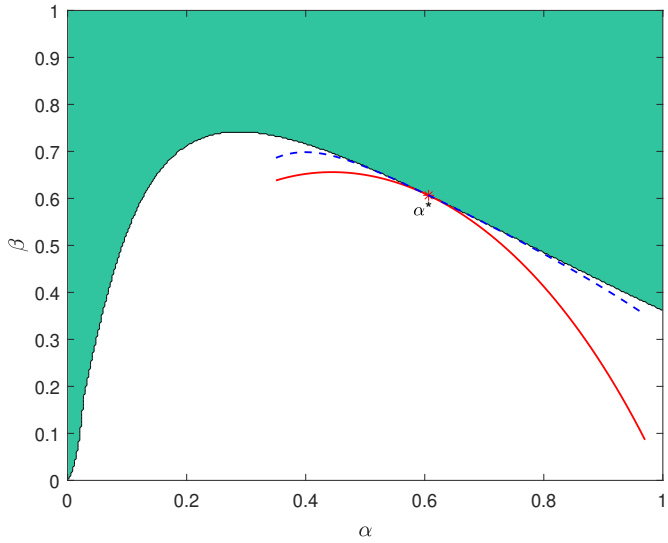

Figure 4.11: Confirmation that the analytical curves $\beta = \beta_1(\alpha)$ (red curve) and $\beta = \beta_2(\alpha)$ (blue dashed curve) are close to the contour that separates the stable region (coloured white) and unstable region (coloured green).

From the examples above we can say that the incommensurate system, (4.31) and (4.32), is an example showing that decreasing the fractional order β, may change unstable behaviour to stable behaviour. This is illustrated in Figure 4.8 if we choose any vertical line α = constant. The same behaviour happens in the commensurate system. However, in the commensurate system, decreasing the order α will never create an unstable system, while this behaviour can happen in the incommensurate system, as seen in Figure 4.8, if we choose any horizontal line β = constant below the value $\beta = 0.74$.

4.3 Conclusions

In this chapter, we have found approximate analytical solutions, using perturbation theory, for the eigenvalues of the characteristic equation of the incommensurate system for fractional orders that are close to commensurate. Then, we compared them to the numerical solutions showing that the approximate analytical solutions are good approximation to the general system when α and β are close to α^*. We can apply the approximate analytical solution that we found for the characteristic equation for the incommensurate system to any system which has two interacting species. For the incommensurate systems we have considered, we have found that it is possible to achieve stable incommensurate systems which would be unstable for a commensurate system. The two systems show us that reducing α can either have a stabilising or destabilising effect and similarly reducing β can lead to a stabilising or destabilising of the system.

Chapter 5

Models of Soil Water Uptake by Plant Roots

5.1 Introduction

Knowing how plants and water interact in desert environments has become more important as the global population continues to increase and land suitable for arable farming becomes scarcer. Producing crops while conserving water ensures that land continues to support human populations. In every environment, the amount of rainfall directly impacts the water that lies at the surface of the land, which we call surface water, and the water within the soil, which we call soil water, and which then affects the rate at which plants grow since they directly depend on the amount of water accessible to them, mainly through their root structures within the soil. Furthermore, understanding how much water is available to and then used by plants, in a particular period of time, is crucial to agricultural planning. As a result, mathematical models have emerged as an essential research tool in ecology to understand how plants, water and soil interact [100]. Many of these models are similar to the predator-prey models we have considered in previous chapters, with the plants playing the role of predators and the water the prey. For this reason, this chapter focuses on specific models that reflect this interaction between plants and water. Here we will focus attention on a particular set of models of plant, water, soil interactions and review the relevant papers below. There are many papers in the literature that consider plant-soil interactions and can be read for further information. Mathematical models of plant-soil interaction are reviewed in [105], soil, water and plant interactions are considered in [64, 128] and references therein.

The flow of water on slopes, the rates at which water is able to infiltrate the soil, erosion and salt deposited by the wind are among the different factors that have been researched. These factors have been investigated experimentally, observationally, and by building mathematical models [11, 76, 77, 101]. Some examples of how mathematical models have been used to investigate soil, plant and water

interactions will be explored further, and here we will briefly review the literature directly related to the model that is studied in this chapter. In 1997, Rietkerk and van de Koppel [101], studied stable states and threshold effects in a particular ecosystem by examining water, nutrients and levels of herbivory. In their study, the equilibria were highly dependent on herbivore consumption. When consumption was low, the system had two equilibria, one of which was stable and the other was unstable, whereas when it was higher, there were three, two of which were stable and one that was unstable. During this study, they particularly examined the water infiltration rate, which cannot exceed the rate of rainfall, and which increases as plant density increases until it reaches a maximum, which is the point at which the system has maximum plant biomass. Moreover, in 2000 Scott et al. [111] conducted extensive studies on where the plants in a specific area were getting their water. They concluded that an increase in the evaporation rates of certain plants was due to an increase in rainfall and concluded that a lack of water causes seasonal plant dormancy.

In terms of models that specifically incorporate the functions of roots, in 2001 HilleRisLambers et al. [53] developed a model to account for plant density, surface water and soil water as a function of time and space. In the same year, Roose et al. [104] studied the impact of root size and distribution, and soil water movement on nutrient uptake. Further, in 2004, Roose et al. [103] considered water uptake from plant roots in unsaturated soil by studying the flow of water both within the root and inside the soil using a mathematical model. In 2007, Gilad et al. [46] adapted a model to study plant biomass and water available to plants by considering how vegetation adapts to changing conditions, such as variations in water uptake by plant roots and increased water infiltration. In addition, in 2008, Roose et al. [105] reviewed mathematical models used to model water and nutrient uptake, presented the analytical results from these models, and explored how single root models can be expanded to encompass entire root systems. However, in all of these models the complex interaction and feedback between biomass, root growth and soil water dynamics were not fully incorporated.

One of the most significant variables in an ecosystem is water, and the primary source of water in many situations is usually rainfall. Of particular importance in many situations is temporal change in rainfall, over daily, monthly or yearly cycles. The importance of rainfall within an ecosystem cannot be understated since it crucially affects which plants grow, how much they grow [53, 66, 67, 82, 120, 126], and, over time, can actually lead to changes in climate that may further affect rainfall distributions [60]. Two examples of models that study how plant biomass is affected by rainfall are modelled by von Hardenberg et al. [126] and Rietkerk et al. [99]. Because little work had been done on the impact of rainfall on plant productivity [112, 124], Guttal et al. [50], filled an important gap by adapting a model to include the seasonal changes of rainfall and the biological productivity

of plants. Their study, on specific types of vegetation, showed that changes in rainfall had particular effects on the growth rate of plants as they adapted to wet and dry seasons, and that where plants grew, water is more easily absorbed than in areas bare of vegetation [107].

To continue this work on the interaction between rainfall and vegetation, models that consider characteristic vegetation patterns, such as the Dagbovie and Sherratt model [24], have been developed. In such work, the effect of varying rainfall patterns on vegetation on slopes was investigated. Their work highlights the importance of mathematical models by modeling certain landscape-scale patterns that can occur in particular environments, something that could not easily be done with either experimentation or fieldwork. Although Dagbovie and Sherratt study spatial vegetation patterns, which are not our focus, the model they use depends on the interaction between the three fundamentals we do consider in our work, i.e. surface water, plants and soil water. As such, their model provides the basis for the work in this chapter.

In this chapter, we consider two models of vegetation in a semi-arid environment. In Sections 5.2 and 5.3, we study the integer and fractional forms of Dagbovie and Sherratt's model, after excluding the spatial dimensions. Then, in Section 5.4, we introduce a new model that has similar biomass and surface water equations, with the Richards equation representing the soil water equation in this system. Then, the equilibrium solutions for this system are found in Section 5.5. After that, in Section 5.6 we find the dynamical solution for the Richards equation. We conclude by using a single mode form of solution to investigate the static and dynamic behaviour of this system. In Sections 5.8 to 5.10, we illustrate the numerical simulation for the critical value of rainfall, and we investigate two different situations for this system depending on the rainfall conditions, constant and time-dependent. Finally, in Section 5.11, we study the fractional derivative model for soil water uptake, concentrating on how the results of the previous sections are changed when we include a fractional derivative, modelling memory effect, in only the biomass evolution equation.

5.2 Biomass-Surface Water-Soil Water (BHW) Model

The model of Dagbovie and Sherratt [24] was used to describe the behaviour of vegetation in a semi-arid environment. In their paper, they considered the mechanism for banded vegetation to occur. Here we have adapted their model by excluding the spatial dimensions in order to concentrate on the interaction of plant biomass and water.

We will later build on this model, including a more accurate model of soil water. The model consists of a set of equations for the plant biomass $B(t)$ (kg m^{-2}), the surface water $H(t)$ (m) and the water in the soil $W(t)$ (m), all of which are functions of time,

$$\frac{dB}{dt} = cg\left(\frac{W}{W+k_1}\right)B - dB, \tag{5.1}$$

$$\frac{dH}{dt} = -IH\left(\frac{B+k\Omega}{B+k}\right) + r, \tag{5.2}$$

$$\frac{dW}{dt} = IH\left(\frac{B+k\Omega}{B+k}\right) - g\left(\frac{W}{W+k_1}\right)B - eW, \tag{5.3}$$

with the initial conditions $B(0) = B_0, H(0) = H_0$ and $W(0) = W_0$. We will term this model the BHW model. Figure 5.1 shows the basic elements in the biomass-surface water-soil water model with its flow diagram.

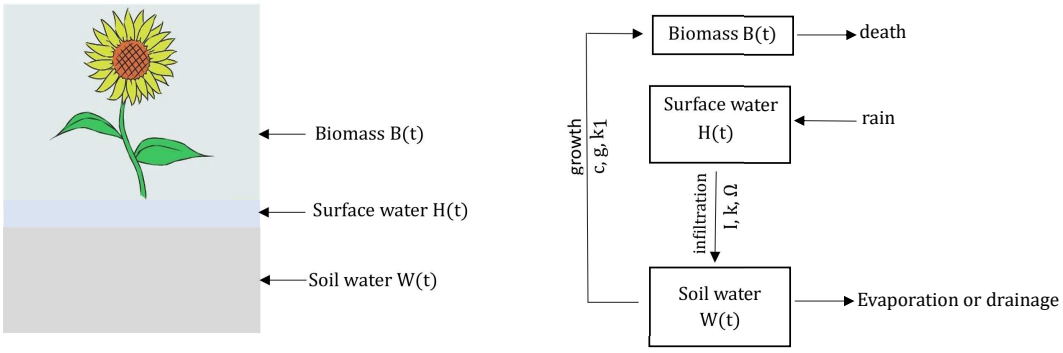

Figure 5.1: The basic elements in the BHW model with its flow diagram.

It should be noted that we are using different notation than the original paper by Dagbovie and Sherratt for consistency with later sections.

In the equation for plant biomass, (5.1), the term $cg\left(\frac{W}{W+k_1}\right)B$ indicates plant growth, where c is the conversion factor of water uptake into new biomass, g is the maximum water uptake per unit of biomass and k_1 is a half-saturation constant for water uptake $W(t)$. The second term in equation (5.1), $-dB$, models the death of plants, where d is the death rate.

The equation for surface water, (5.3), contains the removal of surface water by infiltration and rainfall, r, which we will here take to be constant (although we will allow time dependent rainfall in later sections).

In the last equation, (5.2), the term $-g\left(\frac{W}{W+k_1}\right)B$ models the water uptake by plants in order to grow and is associated with the first term in equation (5.1).

The term $IH\left(\frac{B+k\Omega}{B+k}\right)$ indicates the infiltration of surface water into the soil region. The parameter k is the saturation constant for water infiltration, I is the maximum infiltration rate and $I\Omega$ is the water infiltration rate without plants. The parameter e determines the specific rate of evaporation and drainage. In the following section we will introduce the possible equilibrium points of this model and investigate their existence.

5.2.1 Equilibrium Points

The equilibrium points of the system (5.1), (5.2) and (5.3) are the solutions to the following equations

$$\begin{aligned} 0 &= cg\left(\frac{W}{W+k_1}\right)B - dB, \\ 0 &= IH\left(\frac{B+k\Omega}{B+k}\right) - g\left(\frac{W}{W+k_1}\right)B - eW, \\ 0 &= -IH\left(\frac{B+k\Omega}{B+k}\right) + r. \end{aligned}$$

They are two equilibrium points, one in which there is no biomass present, which we term the desert state, and one with biomass present, which we term the vegetated state. These are, respectively

$$E_1 = (B_d, W_d, H_d) = \left(0, \frac{r}{e}, \frac{r}{\Omega I}\right), \tag{5.4}$$

$$E_2 = (B_v, W_v, H_v) = \left(\frac{r-eW_v}{gW_v}(W_v+k_1), W_v, \frac{r}{I}\frac{B_v+k}{B_v+k\Omega}\right), \tag{5.5}$$

where $W_v = \dfrac{dk_1}{cg-d}$.

Since $r, e, \Omega > 0$ then the desert state E_1 is always a possible state. If we also assume that the biomass growth factor are such that $cg > d$ then the vegetated state is possible if $r > eW_v$, i.e. the rainfall is greater than a critical value $r_0 = eW_v$. We will from now on assume that $cg > d$.

Notice that we can rewrite the components of vegetated state as functions of r. The first component is $B_v = \left(\frac{W_v+k_1}{gW_v}\right)r - \frac{e}{g}(W_v+k_1)$, so that biomass grows linearly with rainfall. The second component $W_v = \left(\frac{dk_1}{cg-d}\right)$ is a constant with respect to rainfall. The third component, H_v, is more complicated but can be written as

$$H_v = \frac{r((r-eW_v)(W_v+k_1)+kgW_v)}{I((r-eW_v)(W_v+k_1)+kgW_v\Omega)}, \tag{5.6}$$

from which we see that $H_v = 0$ when $r = 0$ or $r = r_0 - \dfrac{kgW_v}{W_v + k_1}$.

Considering the asymptotic form of H_v in equation (5.6) as $r \to \infty$ [114], we see that $H_v = \dfrac{r}{I} + \dfrac{kgW_v(1-\Omega)}{I(W_v+k_1)} + O\left(\dfrac{1}{r}\right)$, where $\Omega < 1$ (because the infiltration cannot be more than the amount of water that we have), so that the line $H = \dfrac{r}{I} + \dfrac{kgW_v(1-\Omega)}{I(W_v+k_1)}$ is an oblique asymptote. The function $H_v(r)$ also has a vertical asymptote, at $r = eW_v - \dfrac{kgW_v\Omega}{W_v+k_1}$.

In order to understand if the surface water goes up or down when rainfall increases, we consider the possibility of turning points in the graph $H_v(r)$ in equation (5.6). Using Maple, we found the first derivative of H_v, with respect to r, which equals zero at two values of r. Therefore, we see that the turning points occur at values of the rainfall,

$$r_1 = r_0 - \frac{dk\Omega}{c} + \frac{d}{c(cg-d)}\sqrt{k\left(\Omega-1\right)\left(cg-d\right)\left(k\left(cg-d\right)\Omega - ck_1\, e\right)},$$

and

$$r_2 = r_0 - \frac{dk\Omega}{c} - \frac{d}{c(cg-d)}\sqrt{k\left(\Omega-1\right)\left(cg-d\right)\left(k\left(cg-d\right)\Omega - ck_1\, e\right)} < r_0,$$

and these turning points only occur if $k\left(cg-d\right)\Omega - ck_1\, e < 0$. Calculation of the second derivative leads to

$$H_v''(r_1) = \frac{2c\left(cg-d\right)}{dI\sqrt{k\left(\Omega-1\right)\left(cg-d\right)\left(k\left(cg-d\right)\Omega - ck_1\, e\right)}} > 0,$$

and

$$H_v''(r_2) = \frac{-2c\left(cg-d\right)}{dI\sqrt{k\left(\Omega-1\right)\left(cg-d\right)\left(k\left(cg-d\right)\Omega - ck_1\, e\right)}} < 0.$$

So that, $(r_1, H_v(r_1))$ is a minimum and $(r_2, H_v(r_2))$ is a maximum. If the minimum in surface water is to the left of the critical rainfall for B_v, i. e. $r_0 > r_1$, then as the rainfall increases, the surface water always increases. However, if the minimum in surface water is to the right of the critical rainfall for B_v, i. e. $r_0 < r_1$, then the surface water initially decreases, before reaching a minimum and then increases.

5.2.2 Stability

As usual, determining whether an individual equilibrium point is stable is undertaken by considering the eigenvalues of the Jacobian matrix, $J(B, W, H)$ at an

equilibrium point (B, W, H). For the system (5.1), (5.2) and (5.3) the Jacobian matrix is:

$$J(B,W,H) = \begin{bmatrix} -d + \dfrac{cgW}{k_1+W} & \dfrac{cgk_1B}{(k_1+W)^2} & 0 \\ -\dfrac{gW}{k_1+W} + \dfrac{Ik(1-\Omega)H}{(k+B)^2} & -e - \dfrac{gk_1B}{(k_1+W)^2} & \dfrac{(k\Omega+B)I}{k+B} \\ -\dfrac{Ik(1-\Omega)H}{(k+B)^2} & 0 & -\dfrac{(k\Omega+B)I}{k+B} \end{bmatrix}.$$

The eigenvalues that correspond to E_1 are $\lambda_1 = -e$, $\lambda_2 = -\dfrac{dk_1e + dr - cgr}{k_1e + r}$ and $\lambda_3 = -\Omega I$. Thus, $\lambda_1, \lambda_3 < 0$ and $\lambda_2 < 0$ when $r < r_0$ and so if the system is asymptotically stable around E_1, then the second equilibrium point E_2 does not exist.

Now, if we assume that E_2 exists (so that E_1 is unstable), then the Jacobian matrix at E_2 will be

$$J(E_2) = \begin{bmatrix} 0 & G_1 & 0 \\ G_2 & G_3 & G_4 \\ G_5 & 0 & G_6 \end{bmatrix},$$

where

$$\begin{aligned}
G_1 &= \frac{k_1c(r - eW_v)}{W_v(W_v + k_1)} > 0, \\
G_2 &= \frac{-gW_v}{W_v + k_1} + \frac{r}{k\Omega + B_v} - \frac{r}{k + B_v} = \frac{-gW_v}{W_v + k_1} + \frac{rk(1-\Omega)}{(k\Omega + B_v)(k + B_v)}, \\
G_3 &= -e - \frac{r - eW_v}{W_v} + \frac{r - eW_v}{W_v + k_1} = -e - (r - eW_v)\left(\frac{k_1}{W_v(W_v + k_1)}\right) < 0, \\
G_4 &= \frac{(k\Omega + B_v)I}{k + B_v} > 0, \\
G_5 &= \frac{r}{k + B_v} - \frac{r}{k\Omega + B_v} = \frac{rk(\Omega - 1)}{(k + B_v)(k\Omega + B_v)} < 0, \\
G_6 &= -\frac{(k\Omega + B_v)I}{k + B_v} < 0.
\end{aligned}$$

The eigenvalues of $J(E_2)$ are the roots of the following characteristic equation

$$\lambda^3 + a_1\lambda^2 + a_2\lambda + a_3 = 0,$$

where $a_1 = -G_3 - G_6$, $a_2 = G_3G_6 - G_1G_2$, and $a_3 = G_1(G_2G_6 - G_4G_5)$. Since $cg - d > 0$ and $r > r_0$, we have $a_1 > 0$ and $a_3 > 0$. The Routh-Hurwitz criterion guarantees that the integer system will be locally asymptotically stable around E_2 if $a_1 > 0$ and $a_1a_2 > a_3$. We already have $a_1 > 0$, thus if $a_1a_2 > a_3$, the

system will be locally asymptotically stable around E_2. Therefore, it is possible for the system to be stable or unstable around E_2. The condition $a_1a_2 > a_3$, or equivalently $G_3(-G_3G_6 + G_1G_2 - G_6^2) + G_1G_4G_5 > 0$, could be rearranged for r, although this expression is complicated.

5.2.3 Numerical Simulation

Using the same parameters used in [24] except the value of g we now consider the numerical solution of the system. In [24] Dagbovie and Sherratt chose $g = 5.7870\times10^{-7}$m kg^{-1}m^2 s^{-1} but in our work we have used the values shown in Table 5.1 since this value leads to a change in the stability of E_2 at a realistic value of the rainfall r. The values of the components of E_1 and E_2 versus the rainfall r are illustrated in Figure 5.2. The values of the components of the equilibrium points E_1 and E_2 have positive values when $r > r_0$ where $r_0 = eW_v = 6.3047 \times 10^{-9}$ ms^{-1} is the critical value of r. For the rainfall parameter r, Rietkerk et al. [99] gave a range of values between 0 and 3.4722×10^{-8} ms^{-1}.

Table 5.1: Parameters values used in our numerical simulations of the system (5.1), (5.2) and (5.3).

Parameter	Value	Unit	Parameter	Value	Unit
B	plant biomass	kg m^{-2}	k_1	0.005	m
W	soil water	m	I	2.3148×10^{-6}	s^{-1}
H	surface water	m	k	0.03	kg m^{-2}
c	10	kg m^{-3}	Ω	0.2	no unit
g	3.4722×10^{-6}	m kg^{-1}m^2 s^{-1}	e	2.3148×10^{-6}	s^{-1}
r	varied	ms^{-1}	d	2.89×10^{-6}	s^{-1}

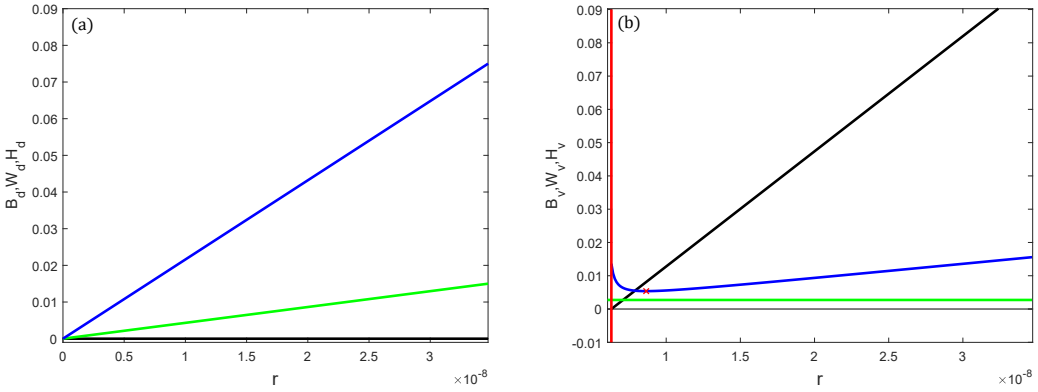

Figure 5.2: The equilibrium values for the system (5.1)-(5.3) as a function of rainfall r for the equilibrium points E_1 (a) and E_2 (b). The black lines indicate the value of plant biomass B, green lines indicate the soil water value W and blue lines indicate the surface water H. The red line in (b) indicates the critical value $r_0 = 6.3047 \times 10^{-9}$ ms^{-1} above which E_2 exists. The red point is the point $(r_1, H_v(r_1))$ for which the surface water has a minimum.

We will now investigate, numerically, the eigenvalues of the Jacobian matrix and the stability of system (5.1), (5.2) and (5.3) around the two equilibrium points for a range of values of r. The eigenvalues of the Jacobian matrix of system around E_1, for $0 < r < 3.4722 \times 10^{-8}$, are illustrated in Figure 5.3(a). We see that one of the eigenvalues is positive when $r > r_0$, so that the system will only be stable around E_1 when $r < r_0$. Figure 5.3(b) illustrates a trajectory, showing stability when $r = 4.9768 \times 10^{-10}$ ms^{-1}. However, the system will be unstable around E_1 when $r > r_0$, and Figure 5.3(c) illustrates the instability when $r = 2.5545 \times 10^{-8}$ ms^{-1}.

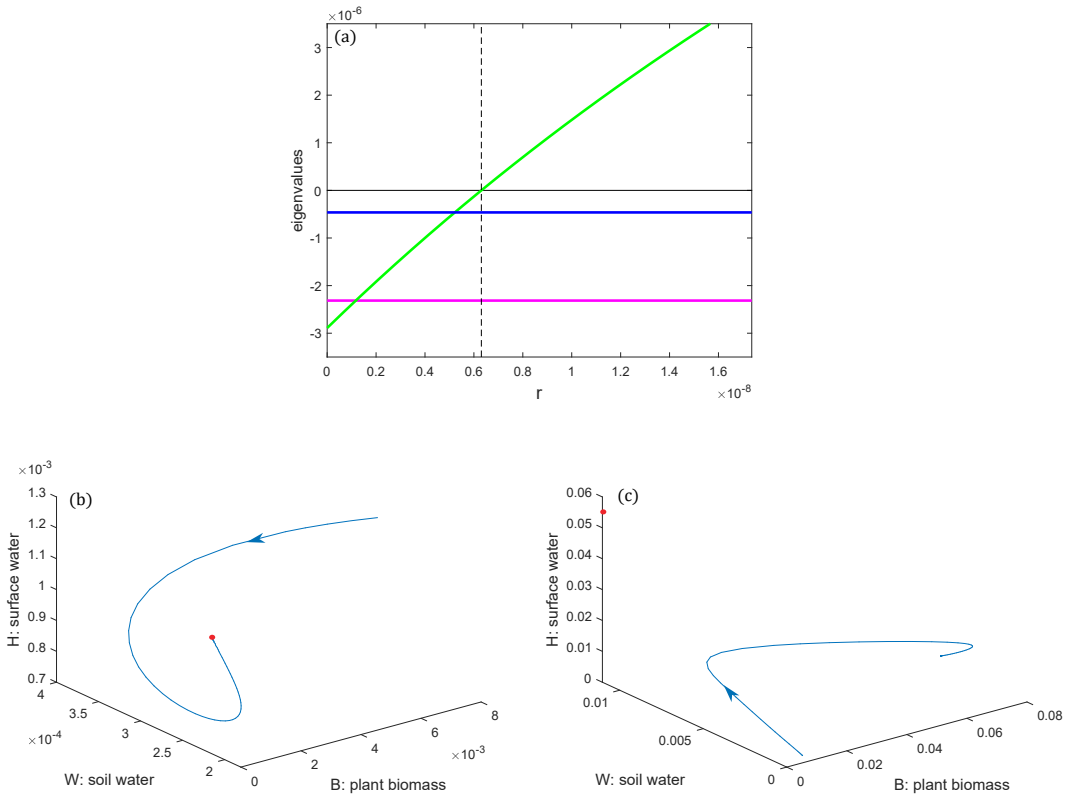

Figure 5.3: (a) The three eigenvalues of the Jacobian matrix of system (5.1)-(5.3) around E_1 when $0 < r < 1.7361 \times 10^{-8}$, represented by the pink, the blue and the green line. The vertical dashed line is $r_0 = 6.3047 \times 10^{-9}$ ms^{-1} at which one of the eigenvalues changes sign. (b) Trajectory of the system when $r = 4.9768 \times 10^{-10} < r_0$ showing asymptotic stability around the desert state $E_1 = (0, 0.0002, 0.001)$ (red point). (c) Trajectory of the system when $r = 2.5545 \times 10^{-8} > r_0$ showing the instability around the desert state $E_1 = (0, 0.011, 0551)$ (red point).

The eigenvalues of the Jacobian matrix of the system around E_2 for $r_0 < r < 7 \times 10^{-9}$ are illustrated in Figure 5.4(a-c). The first eigenvalue is negative for all values of r that are chosen, see Figure 5.4(a), while the second and third eigenvalues can be complex, with the sign of the real part being dependent on r, see Figure 5.4(b, c). Figure 5.4(d) shows the value of the conditions $a_1a_2 - a_3 > 0$ versus r showing that the classical Routh-Hurwitz condition is not satisfied for a range of the values of r. Thus, for $r > r_0$, it is possible for the system to be stable or unstable around E_2. As an example, Figure 5.5(a) shows that the system is asymptotically stable around E_2 when $r = 2.5545 \times 10^{-8}$ ms^{-1}, while Figure 5.5(b) shows that the system is unstable around E_2 when $r = 6.5277 \times 10^{-9}$ ms^{-1}.

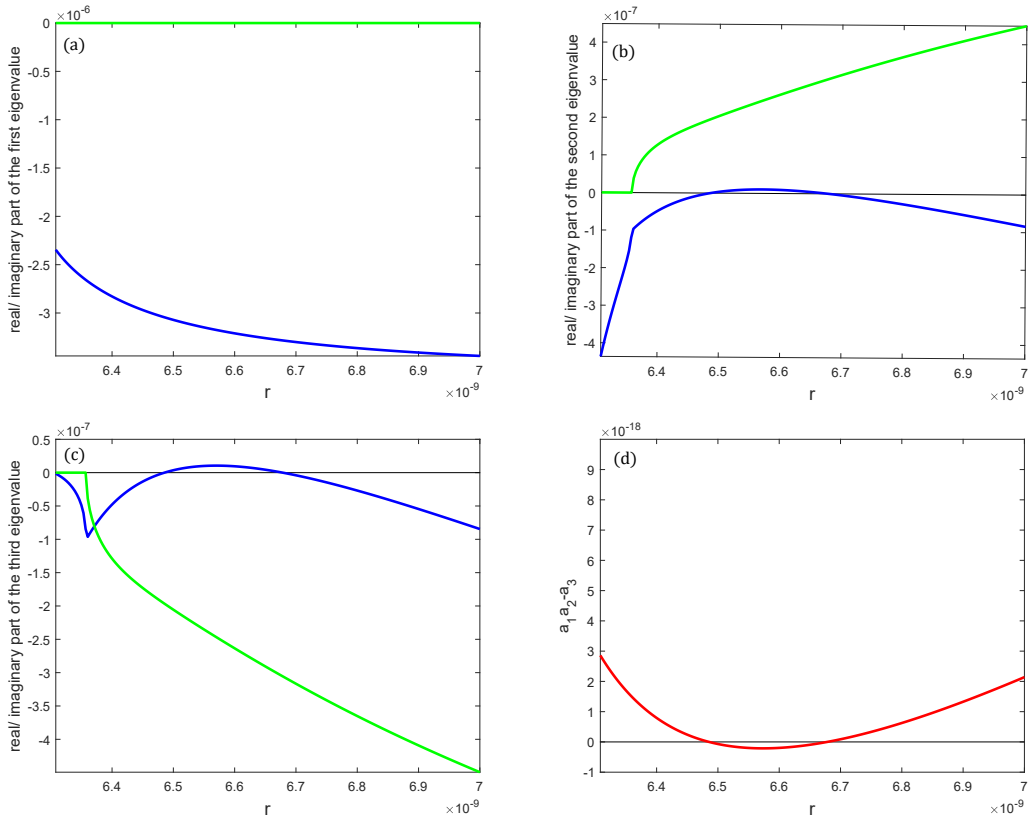

Figure 5.4: The real (blue) and imaginary (green) parts of the eigenvalues of the Jacobian of the system (5.1)-(5.3) at E_2. (a) The first eigenvalue is real and negative for all $r > r_0$. (b) and (c) The second and third eigenvalues, which can be complex with negative or positive real part. (d) The value of $a_1a_2 - a_3$ as a function of rainfall.

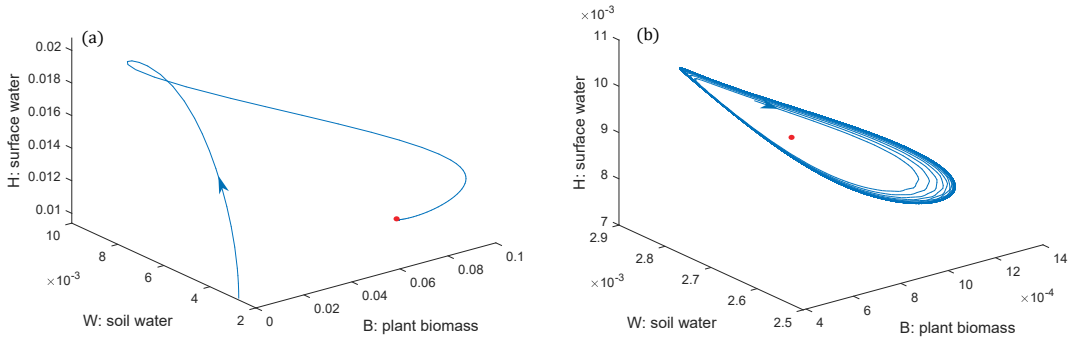

Figure 5.5: (a) The system (5.1)-(5.3) is asymptotically stable around $E_2 = (0.0665, 0.0027, 0.0116)$, when $r = 2.5545 \times 10^{-8}$ ms^{-1}. (b) The system (5.1)-(5.3) is unstable around $E_2 = (0.0007, 0.0027, 0.0091)$, when $r = 6.5277 \times 10^{-9}$ ms^{-1}.

In summary, from the discussions above, we see that the possibilities for the stability of the equilibrium points of the integer system are as follows:

1. If $r < r_0$, E_1 exists and is stable, and E_2 does not exist.

2. If $r > r_0$, E_1 exists and is unstable, and E_2 exists and it is possible for the system to be stable or unstable around E_2 depending on the value of r that is chosen.

In the next section we will consider the effect of introducing a fractional derivative to the stability of these equilibrium points.

5.3 Fractional BHW Model

The introduction of fractional derivatives cannot change the stability around E_1 because all the eigenvalues for this point are real. However, if E_2 is unstable, with an eigenvalue having positive real part, then, as we have seen in previous chapters, it may be possible for the fractional order system to induce stability around this point. In the following fractional system, we introduce a fractional derivative, of order ρ, only in the plant biomass equation because it is the only species that is biotic:

$$
\begin{aligned}
{}^{c}D_t^{\rho} B &= cg\frac{W}{W+k_1}B - dB, && (5.7)\\
\frac{dW}{dt} &= IH\frac{B+k\Omega}{B+k} - g\frac{W}{W+k_1}B - eW, && (5.8)\\
\frac{dH}{dt} &= -IH\frac{B+k\Omega}{B+k} + r. && (5.9)
\end{aligned}
$$

5.3.1 Numerical Simulation

For the values of the parameters used above, Figure 5.4 shows that there are some values of r that allow positive real parts for the complex roots of the characteristic equation at E_2 and here we take $r = 6.5277 \times 10^{-9}$ ms^{-1}. The effect of the fractional order on the stability of the system around E_2 is shown in Figure 5.6. In Figure 5.6(a) we see that for $\rho < 0.99931$, the system will become stable. For $\rho = 0.9975$, Figure 5.6(b) shows that the incommensurate system, (5.7), (5.8) and (5.9), will be asymptotically stable around E_2.

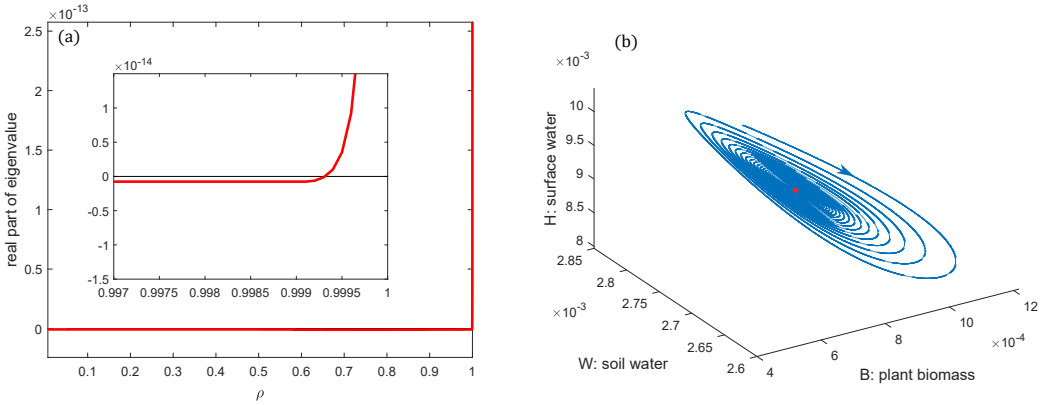

Figure 5.6: (a) Real part of the complex conjugate solutions (eigenvalues) to the characteristic equation for the incommensurate system, (5.7)-(5.9), at the equilibrium point E_2. (b) Trajectory of the incommensurate system (5.7)-(5.9) showing asymptotic stability around E_2 when $\rho = 0.9975$.

We have therefore shown that, for a relatively simple model of plant-water interaction, the fractional order, i.e. the memory effect, of the plants can have an effect on the stability of the system.

5.4 $BH\Phi$ Model

We will now look at a more complicated but more realistic model than that in the previous section. We now model the soil water through the depth of soil and consider water uptake by roots, modelled as a function of depth and root density. In later sections we then consider the growth of soil-rooted vegetation as being dependent on the flux of water from various sources (rain, surface water, soil water or groundwater) within the soil. In the next section we will illustrate how Richards' equation is linearized and coupled to the equation for the biomass of rooted vegetation.

5.4.1 Richards' Equation

The transport of water in soil has been studied for very many years, and is important for the transport of solutes in soil, rates of biological processes, water supply to organisms, the process of transpiration, the maintenance of soil water levels, and the amount of runoff and other environmental functions. The ability of plants to grow in soil is strongly affected by the status of water in any given area. In particular, how plant roots uptake water from the surrounding soil is an important variable in the water balance [94]. As a result, accurate simulations of soil water transport and flow at different scales are essential to various soil-related fields such as hydrology, plant science, and environmental protection [86, 94].

Ninety years ago, Richards published an equation based on a theory of the movement of water in unsaturated soils, and is still the basis of most physical soil water models [97, 98]. The classical form of Richards' equation is given as

$$\frac{\partial}{\partial z}\left(K(\Psi)\left(\frac{\partial \Psi}{\partial z}+1\right)\right)=\frac{\partial \theta}{\partial t},$$

where Ψ is the pressure head [m] (soil water content is then described in terms of Ψ) and it is negative in unsaturated soil, $K(\Psi)$ is the hydraulic conductivity [ms^{-1}], the variable z is the vertical coordinate throughout the soil profile, t is time [s], and θ is the volumetric water content. Note that Ψ is zero when the soil is fully saturated, and negative when it is partially saturated.

Richards' equation is an attempt to describe how water is distributed in unsaturated soil [94, 95], however, Pachepsky et al. demonstrated that Richards' equation is not general enough to explain the movement of water in all types of soil [86]. Attempts to generalise Richards' equation have been made by many authors, for instance by introducing an empirical dependence of the diffusivity on time or distance [49, 85]. Such generalisations of Richards' equation have been able to accurately describe the scaling of soil water content that was observed during experimentation [86]. One generalisation of Richards' equation is

$$\frac{\partial}{\partial z}\left(K(\Psi)\left(\frac{\partial \Psi}{\partial z}+1\right)\right)-S(z)=C(\Psi)\frac{\partial \Psi}{\partial t}, \tag{5.10}$$

where $S(z)$ is a root water uptake function [s^{-1}] and $C(\Psi)$ is the differential water capacity [m^{-1}], $C(\Psi)=\dfrac{\partial \theta}{\partial \Psi}$, where θ is the volumetric water content. Sirvastava and Yeh [113] assumed θ to be the form

$$\theta=\theta_r+(\theta_s-\theta_r)e^{(\alpha\Psi)}, \tag{5.11}$$

where θ_s is the water content at saturation (the maximum amount of the water within the soil space), θ_r is the residual water content (water that remains trapped

by the soil and the roots) and α is the soil pore size distribution parameter $[m^{-1}]$, which represents the reduction in the rate of the hydraulic conductivity as pore size changes.

Because of the nonlinear relationship between hydraulic conductivity and the pressure head, analytically solving Richards' equation in this form is difficult. To aid mathematical analysis, a transformation to a linear form is one of the methods often used. Since water uptake by roots is related to many variables such as root depth, water content and salinity, solving Richards' equation analytically with a sink term to describe root uptake is difficult. As a result, many analytical approaches assume that root water uptake is a specific function of root depth [10, 93, 106, 110]. For example, in 2005, Yuan and Lu linearized Richards' equation and used specific forms of $S(z)$, and then found the analytical solution [131]. For this work they used exponential water retention and hydraulic conductivity relationships to linearize Richards' equation.

5.4.2 Linearization of Richards' Equation

We assume that the pressure head has the initial condition

$$\Psi(z, 0) = \Psi_0(z), \tag{5.12}$$

and that the boundary conditions are

$$\Psi(-L, t) = \Psi_1, \tag{5.13}$$

and

$$\left[K(\Psi) \left(\frac{\partial \Psi}{\partial z} + 1 \right) \right]_{z=0} = i(t), \tag{5.14}$$

where Ψ_1 is the pressure head at the lower boundary $z = -L$ (i. e. at the water table) [m], $i(t)$ is the time dependent flux due to infiltration at the soil surface $[\text{ms}^{-1}]$ (so that positive flux means infiltration of water into the soil at $z = 0$).

For mathematical convenience, the hydraulic conductivity K is assumed to be an exponential function of the pressure head [131] so that

$$K(\Psi) = K_s e^{(\alpha \Psi)}, \tag{5.15}$$

where K_s $[\text{ms}^{-1}]$ is the hydraulic conductivity at saturation (when $\Psi = 0$). The matric potential [41] is then defined as the integral of the hydraulic conductivity, which can be simplified using (5.15),

$$\Phi(z, t) = \int_{-\infty}^{\Psi} K(\Psi) d\Psi = \frac{K_s}{\alpha} e^{(\alpha \Psi)}, \tag{5.16}$$

where Φ varies from K_s/α at full saturation to zero as $\Psi \to -\infty$. Richards' equation (5.10) may then be written in terms of the matric potential, using $\Psi = \left(\frac{1}{\alpha}\right) \ln\left(\frac{\alpha\Phi}{K_s}\right)$ from (5.16) and $C(\Psi) = \alpha^2(\theta_s - \theta_r)\frac{\Phi}{K_s}$ from (5.11), in the following form

$$\frac{\partial \Phi}{\partial t} = D\frac{\partial^2 \Phi}{\partial z^2} + D\alpha\frac{\partial \Phi}{\partial z} - DS, \tag{5.17}$$

where $D = \dfrac{K_s}{\alpha(\theta_s - \theta_r)}$ $[\mathrm{m}^{-2}\mathrm{s}^{-1}]$ is the diffusivity and is related to the hydraulic conductivity at saturation and the difference of soil water content.

In equation (5.17), which governs the soil water in our model, the first two terms on the right hand side relate to water diffusion. The last term in equation (5.17) models the removal of water by roots. We would expect that if the diffusivity is small, then the water cannot diffuse well in the soil and the actual uptake of water by roots would be reduced.

5.4.3 Model Formulation

In our model of biomass-water interaction we consider three variables: the plant biomass $B(t)$, the surface water depth $H(t)$ and the matric potential for the soil water $\Phi(z,t)$. The model will therefore be termed the $BH\Phi$ model. The three equations governing B, H and Φ are based on the biomass and surface water equations in (5.1) and (5.2), but with the soil water now being modelled by Richards' equation,

$$\frac{dB}{dt} = cV - dB, \tag{5.18}$$

$$\frac{dH}{dt} = -IH\left(\frac{B + k\Omega}{B + k}\right) + r(t). \tag{5.19}$$

$$\frac{\partial \Phi}{\partial t} = D\frac{\partial^2 \Phi}{\partial z^2} + D\alpha\frac{\partial \Phi}{\partial z} - DS, \tag{5.20}$$

The first equation, for the biomass, is similar to equation (5.1) but with the soil water dependence of biomass growth now being dependent on $V = \int_{-L}^{0} S(z,t)dz$ $[\mathrm{ms}^{-1}]$, the total water uptake rate by roots within the soil depth. In (5.18), c $[\mathrm{kgm}^{-3}]$ is the biomass that can be produced per volume of water. The parameter d $[\mathrm{s}^{-1}]$ in equation (5.18) is the natural rate of death of biomass. Equation (5.19) models the surface water H and is equivalent to the equation (5.2) except the rainfall here $r(t)$ is now taken as a function of time. The last equation, (5.20), is described in the previous section, where $-L < z < 0$.

5.4.4 Initial Conditions and Boundary Conditions

Equations (5.18), (5.19) and (5.20) will be solved subject to the initial conditions

$$B(0) = B_0, \quad H(0) = H_0, \tag{5.21}$$

and

$$\Phi(z, 0) = \Phi_0(z) = \frac{K_s}{\alpha} e^{\alpha \Psi_0(z)}. \tag{5.22}$$

The boundary conditions for (5.20) are

$$\Phi(-L, t) = \Phi_1 = \frac{K_s}{\alpha} e^{(\alpha \Psi_1)}, \tag{5.23}$$

$$\left[\frac{\partial \Phi}{\partial z} + \alpha \Phi \right]_{z=0} = IH \left(\frac{B + k\Omega}{B + k} \right), \tag{5.24}$$

so that we have the infiltration of water, $i(t)$, into the soil at the top of the surface due to surface water infiltration.

5.4.5 Models of Water Uptake

To complete the model in (5.18-5.20), we need to specify the rate of water uptake by roots, represented by the function $S = S(z, t)$. In previous work [131], S was taken to be independent of the matric potential Φ. However, this assumption can lead to root uptake of water even when no water is present. Therefore, we will now assume S to be a function of Φ, as well as z and t. The aim of studying this model is to assess the effect of changing the form of root water uptake on the growth of soil-rooted vegetation. Given that S will be non-negative, and reduce to zero when either there are no roots or when there is no water, we write the root uptake function as a simple linear function of the matric potential

$$S = S_0(z, t)\Phi(z, t),$$

where $S_0(z, t)$ is a function of the root density function $\chi(B, z)$, itself a function of depth and the amount of biomass,

$$S_0 = \frac{R_{\max}\alpha}{K_s} \chi(B). \tag{5.25}$$

In (5.25) $R_{\max}$ is the uptake value at saturation, when $\Phi = \dfrac{K_s}{\alpha}$. Although in this work we consider $S_0 \geq 0$, it should be noted that the case $S_0 < 0$, means that the amount of water in the soil increases, and $S_0\Phi$ will be a production term, a case that would model a form of irrigation.

We could consider three different simple models for $\chi(B)$: water uptake by roots being a constant function and independent of biomass,

$$\chi(B) = \chi_0, \tag{5.26}$$

where χ_0 is a constant root density; water uptake by roots being a linear function of the biomass:

$$\chi(B) = \chi_0 \frac{B}{B_0}, \tag{5.27}$$

where B_0 is a value of the biomass when the root density is χ_0 (a reference quantity); or water uptake by roots being a function of biomass that saturates at large values of B,

$$\chi(B) = \chi_0 \tanh \frac{B}{B_0}, \tag{5.28}$$

so that as $B \to 0$, $\chi \to \chi_0 \dfrac{B}{B_0}$ and as $B \to \infty$, $\chi \to \chi_0$.

Of the three possible forms of $\chi(B)$ described above, the first (5.26) results in a biomass-independent form of the root density. We do not believe this is biologically realistic since larger plant density will lead to larger root density. The third possibility (5.28) is perhaps the most realistic biologically, but leads to less analytically tractable equations in the analysis below. We therefore take a pragmatic approach and select the root density function given by equation (5.27), noting however, that in principle the framework below allows for any root density function to be used.

5.5 Equilibrium Solutions for the $BH\Phi$

The equilibrium points can be found by solving the following steady-state versions of (5.18)-(5.20),

$$\begin{aligned} 0 &= cV - dB, && (5.29)\\ 0 &= -IH\left(\frac{B + k\Omega}{B + k}\right) + r_0, && (5.30)\\ 0 &= \frac{d^2\Phi_s}{dz^2} + \alpha\frac{d\Phi_s}{dz} - S_0\Phi_s, && (5.31) \end{aligned}$$

where $V = \int_{-L}^{0} S_0\Phi_s dz$ and we have assumed a constant rainfall $r(t) = r_0$ in (5.19). The steady state versions of (5.29)-(5.31) lead to $B = cV/d$ and $H = \dfrac{r_0}{I}\left(\dfrac{B + k}{B + k\Omega}\right)$ and so B and H depend on the steady state matric potential Φ_s though V.

We will now find the steady-state solution of the matric potential Φ_s, that satisfies the ordinary differential equation (5.31), where S_0 is given by (5.25) and (5.27). Although S_0 depends on B, and thus on V, which in turn depends on Φ_s, it is a constant and thus we may solve equation (5.31) and later determine the value of S_0 implicitly. In this case the boundary conditions (5.23) and (5.24) will be

$$\Phi_s(-L) = \Phi_1 = \frac{K_s}{\alpha} e^{(\alpha \Psi_1)}, \tag{5.32}$$

and

$$\left[\frac{d\Phi_s}{dz} + \alpha \Phi_s\right]_{z=0} = IH\left(\frac{B + k\Omega}{B + k}\right) = r_0. \tag{5.33}$$

The solution of the steady-state equation (5.31) is

$$\Phi_s(z) = c_1 e^{\Lambda_1 z} + c_2 e^{\Lambda_2 z}, \tag{5.34}$$

where

$$\Lambda_1 = \frac{-\alpha + \sqrt{\delta}}{2} \quad \text{and } \Lambda_2 = \frac{-\alpha - \sqrt{\delta}}{2}, \tag{5.35}$$

and $\delta = \alpha^2 + 4S_0$. Using the boundary conditions in equations (5.32) and (5.33), we then find

$$c_2 = \frac{\alpha r_0 - (\Lambda_1 + \alpha) K_s e^{\alpha \Psi_1} e^{\Lambda_1 L}}{\alpha\left((\Lambda_2 + \alpha) - (\Lambda_1 + \alpha) e^{(\Lambda_1 - \Lambda_2)L}\right)}, \tag{5.36}$$

$$c_1 = \left(\frac{K_s}{\alpha} e^{\alpha \Psi_1} - \left(\frac{\alpha r_0 - (\Lambda_1 + \alpha) K_s e^{\alpha \Psi_1} e^{\Lambda_1 L}}{\alpha\left((\Lambda_2 + \alpha) - (\Lambda_1 + \alpha) e^{(\Lambda_1 - \Lambda_2)L}\right)}\right) e^{-L\Lambda_2}\right) e^{L\Lambda_1}. \tag{5.37}$$

Using this solution for Φ_s, we can find V thus

$$\begin{aligned} V &= \int_{-L}^{0} S_0 \left(c_1 e^{\Lambda_1 z} + c_2 e^{\Lambda_2 z}\right) dz, \\ &= S_0 \left[\frac{c_1}{\Lambda_1} e^{\Lambda_1 z} + \frac{c_2}{\Lambda_2} e^{\Lambda_2 z}\right]_{-L}^{0} \\ &= S_0 c_1 \left(\frac{1 - e^{-\Lambda_1 L}}{\Lambda_1}\right) + S_0 c_2 \left(\frac{1 - e^{-\Lambda_2 L}}{\Lambda_2}\right) \\ &= V_s(S_0) \end{aligned} \tag{5.38}$$

where Λ_1 and Λ_2 are given in (5.35), c_1 is given in (5.37), c_2 is given in (5.36) and which all depend on S_0 though δ. We may then calculate S_0 using one of the root density models. For instance, using (5.27), S_0 is determined by the implicit equation $S_0 = \dfrac{R_{\max}\alpha}{K_s} \chi_0 \dfrac{cV_s(S_0)}{dB_0}$.

Given the solution for Φ_s it is now possible to find the solutions for B from (5.29) by considering the function

$$F(B) = cV - dB, \tag{5.39}$$

with V given by (5.38). Before finding the roots of $F(B)$ analytically, we plot $F(B)$ to understand the behaviour of this function. Using the same values of the parameters that are shown in Table 5.1, together with the parameters given in Table 5.2, Figure 5.7 shows different possibilities for the function $F(B)$, for different values of r_0.

Table 5.2: Parameters used for the evaluation of critical rainfall expressions (5.18), (5.19) and (5.20). Both the water contents and root density are dimensionless quantities. However, we use $\mathrm{m^3 m^{-3}}$ for θ_s and θ_r because this indicates a volume of water per volume of soil and, similarly, the unit $\mathrm{m^2 m^{-2}}$ for χ_0 indicates surface area of roots per surface area of soil.

Parameter	Value	Unit	Reference
K_s	2.78×10^{-6}	$\mathrm{m\ s^{-1}}$	[131]
B_0	1×10^{-2}	$\mathrm{kg\ m^{-2}}$	[24]
θ_s	0.45	$\mathrm{m^3 m^{-3}}$	[131]
L	0.691	m	Estimated
θ_r	0.20	$\mathrm{m^3 m^{-3}}$	[131]
χ_0	0.05	$\mathrm{m^2 m^{-2}}$	Estimated
$R_{\max}$	1.1574×10^{-7}	$\mathrm{s^{-1}}$	Estimated
α	1	$\mathrm{m^{-1}}$	[131]
Ψ_1	0	m	[131]
q_n	changeable	no unit	roots of (5.58)

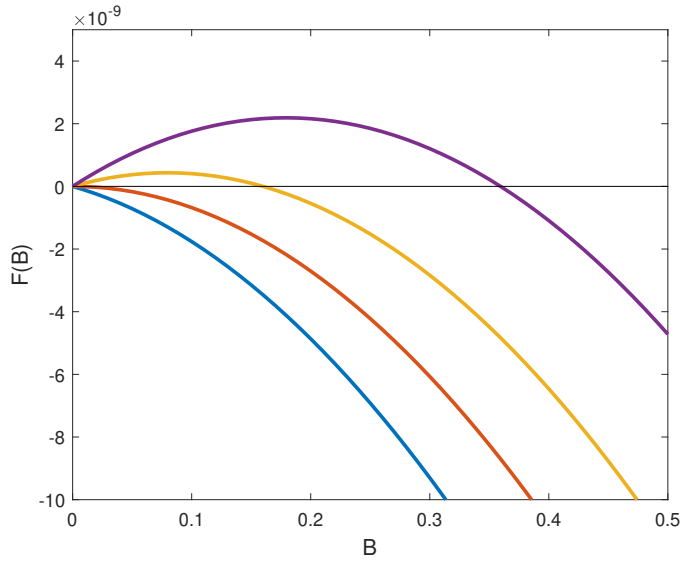

Figure 5.7: The function $F(B)$ for different values of r_0: $r_0 = -3r_c$ (blue curve), $r_0 = r_c$ (orange curve), $r_0 = 5r_c$ (yellow curve) and $r_0 = 10r_c$ (purple curve).

Figure 5.7 shows that as we increase r_0, $F(B)$ changes from having one solution $B_1 = 0$ to two solutions B_1 and $B_2 > 0$. The second solution B_2 emerges from $B_1 = 0$ at a critical value of the rainfall, which we will now determine. We consider the Taylor expansion of $F(B)$ about $B = 0$,

$$F(B) = F(0) + \frac{F'(0)}{1!}B + \frac{F''(0)}{2!}B^2 + O(B^3),$$

so that, since $F(0) = 0$, as well as the solution at $B = B_1 = 0$, we have an approximate solution of $F(B) = 0$ at $B = B_2 = -2F'(0)/F''(0)$.

The two equilibrium solutions are therefore

$$P_1 = (\Phi_{s1}(z), B_1, H_1) = (\Phi_{s1}(z), 0, r_0/I\Omega), \tag{5.40}$$

and

$$\begin{aligned} P_2 =&(\Phi_{s2}(z), B_2, H_2) \\ =&(\Phi_{s2}(z), -2F'(0)/F''(0), r_0(B_2 + k)/I(B_2 + k\Omega)), \end{aligned} \tag{5.41}$$

where $\Phi_{s1}(z)$ is given by (5.34) when $B = 0$, $\Phi_{s2}(z)$ is given by (5.34) when $B = B_2$,

$$F'(0) = c\frac{R_{max}\alpha\chi_0}{K_s B_0}\left(\left(\frac{L}{\alpha} + \frac{(1 - e^{\alpha L})}{\alpha^2 e^{\alpha L}}\right) r_0 - \frac{K_s e^{\alpha\Psi_1}(1 - e^{\alpha L})}{\alpha^2 e^{\alpha L}}\right) - d, \tag{5.42}$$

and

$$\begin{aligned} F''(0) = &- \frac{c(-4e^{\alpha(L+\Psi_1)}\alpha L + 2e^{\alpha(2L+\Psi_1)} - 2e^{\alpha\Psi_1})\chi_0^2 R_{max}^2 e^{-2\alpha L}}{\alpha^2 B_0^2 K_s} \\ &- \frac{c((\alpha^2 L^2 - 4)e^{2\alpha L} + (6\alpha L + 2)e^{L\alpha} + 2)\chi_0^2 R_{max}^2 e^{-2\alpha L} r_0}{\alpha^2 B_0^2 K_s^2}. \end{aligned} \tag{5.43}$$

We then find the critical value of r_0 to be the value when $F'(0) = 0$, namely

$$r_c = \left(\frac{K_s}{cR_{\max}\chi_0}\right)\left(\frac{cR_{\max}\chi_0 e^{(\alpha\Psi_1)}(e^{-\alpha L} - 1) + d\alpha B_0}{L\alpha + e^{-\alpha L} - 1}\right). \tag{5.44}$$

For the values of parameters used previously, $r_c = 6.8016 \times 10^{-9}\text{ms}^{-1}$. Therefore, there is one solution when $r_0 \leq r_c$ (for instance the blue curve, when $r_0 = -3r_c$, or the orange curve, when $r_0 = r_c$, in Figure 5.7) and two solutions when $r_0 > r_c$ (for instance the yellow curve, when $r_0 = 5r_c$ or the purple curve, when $r_0 = 10r_c$, in Figure 5.7).

For parameter values which give $r_c < 0$, this means that even with no rain a solution with positive biomass is possible, because the plants get sufficient water from the water table. The situation of having negative rainfall $r_0 < 0$ could be interpreted as the system losing water to the atmosphere i.e. evaporation from the surface water.

5.5.1 Depth Dependence of the Critical Value of Rainfall

In this section, we analytically investigate how the critical rainfall found in the previous section, equation (5.44), varies with the depth of the water table, L, which can vary significantly in different parts of the world.

From (5.44) we first see that $\lim_{L\to\infty} r_c = 0$ and $\lim_{L\to 0} r_c = \infty$. We can interpret these results in terms of the soil water draining into the water table at $z = -L$ and not being available to root uptake. When $L \to 0$, the roots are limited to a shallow soil layer and soil water enters and quickly drains into the water table. Alternatively, with $L \to \infty$ roots can spread within a large area of soil and thus the total amount of soil water available for the roots is large.

The series expansion for r_c around $L = 0$ (i.e. when the water table is shallow), using (5.44) is found to be

$$\begin{aligned} r_c(L) = &\frac{2dB_0K_s}{cR_{\max}\chi_0\alpha}\frac{1}{L^2} + 2\left(\frac{dB_0\alpha - 3K_se^{(\alpha\Psi_1)}cR_{\max}\chi_0}{3cR_{\max}\chi_0\alpha}\right)\frac{K_s}{L} \\ &+ \frac{6K_se^{(\alpha\Psi_1)}cR_{\max}\chi_0 + \alpha K_sdB_0}{18cR_{\max}\chi_0} + O(L), \end{aligned} \tag{5.45}$$

Therefore, for shallow water tables, we predict that the critical rainfall, above which plant biomass can be sustained, is to first order similar to $1/L^2$. Equation (5.45) also shows the dependence of r_c on various other parameters. For instance, r_c is proportional to $\dfrac{K_sB_0}{cR_{\max}\chi_0\alpha}$ which is related to the effectiveness of roots to take up water and convert it to biomass through equations (5.25) and (5.27). The critical rainfall is also directly proportional to the death rate of biomass, so that, as expected, a higher death rate leads to a higher critical rainfall for biomass to be sustained.

Figure 5.8 illustrates the critical rainfall, r_c, and the first three terms for the series expansion of r_c around zero from equation (5.45). These terms are good approximations for r_c around zero. As explained above, when there are more roots as L increases, more water can be contained in the soil and used to support growth, and therefore the required rainfall to support biomass growth increases when L is close to zero.

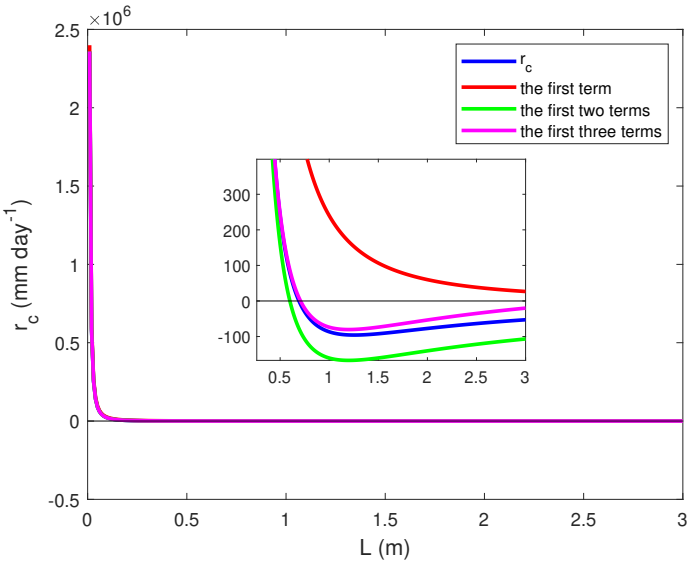

Figure 5.8: The critical value of rainfall r_c as a function of L, given by (5.44), and approximation using terms from the series expansion of r_c, (5.45).

We now consider the series expansion for r_c around $L = \infty$. Rearranging (5.44), we obtain

$$r_c = \left(\frac{K_s}{cR_{\max}\chi_0}\right)\left(\frac{cR_{\max}\chi_0 e^{(\alpha\Psi_1)}(e^{-\alpha L}-1)+d\alpha B_0}{L\alpha\left(1+\dfrac{e^{-\alpha L}-1}{L\alpha}\right)}\right), \tag{5.46}$$

and if we set $\delta = -(e^{-\alpha L}-1)/\alpha L$, (5.46) can be expanded in power of δ,

$$\begin{aligned} r_c &= \left(-K_s e^{(\alpha\Psi_1)}\delta + \frac{K_s d\alpha B_0}{cR_{\max}\chi_0(\alpha L)}\right)\left(1+\delta+\delta^2+\delta^3+...\right) \\ &= \left(-K_s e^{(\alpha\Psi_1)}\left(\frac{1-e^{-\alpha L}}{\alpha L}\right)+\frac{K_s d\alpha B_0}{cR_{\max}\chi_0(\alpha L)}\right)\left(1+\left(\frac{1-e^{-\alpha L}}{\alpha L}\right)\right. \\ &\left.+\left(\frac{1-e^{-\alpha L}}{\alpha L}\right)^2+...\right). \end{aligned}$$

Therefore, the expansion is equivalent to

$$\begin{aligned} r_c(L) = &\left[\left(-K_s e^{(\alpha\Psi_1)} + \frac{\alpha K_s}{cR_{\max}\chi_0} dB_0 \right) \left(\frac{1}{\alpha L} + \frac{1}{(\alpha L)^2} + \frac{1}{(\alpha L)^3} + ... \right) \right] \\ &+ \left[K_s e^{(\alpha\Psi_1)} \frac{1}{\alpha L} + \left(2K_s e^{(\alpha\Psi_1)} - \frac{\alpha K_s}{cR_{\max}\chi_0} dB_0 \right) \frac{1}{(\alpha L)^2} \right. \\ &\quad \left. + \left(3K_s e^{(\alpha\Psi_1)} - \frac{2\alpha K_s}{cR_{\max}\chi_0} dB_0 \right) \frac{1}{(\alpha L)^3} + ... \right] e^{-(\alpha L)} \\ &+ \left[-K_s e^{(\alpha\Psi_1)} \frac{1}{(\alpha L)^2} + \left(-3K_s e^{(\alpha\Psi_1)} + \frac{\alpha K_s}{cR_{\max}\chi_0} dB_0 \right) \frac{1}{(\alpha L)^3} + ... \right] e^{-2(\alpha L)} \\ &+ ... \end{aligned} \tag{5.47}$$

The largest term in equation (5.47) is $\left(-K_s e^{(\alpha\Psi_1)} + \frac{\alpha K_s}{cR_{\max}\chi_0} dB_0 \right) \frac{1}{\alpha L}$ and so we find

$$r_c(L) = \frac{K_s}{\alpha} \left(\frac{\alpha dB_0}{cR_{\max}\chi_0} - e^{(\alpha\Psi_1)} \right) \frac{1}{L} + O(L^{-2}).$$

Figure 5.9 shows plots of r_c from (5.44), the blue curve, and the various approximations of r_c from (5.47), i.e. the series expansion when $L \to \infty$. The red curve in Figure 5.9 is the first term, the green curve is the first two terms, and the purple curve is the first three terms in (5.47). All three are good approximations of the exact $r_c = r_c(L)$ when $L \to \infty$.

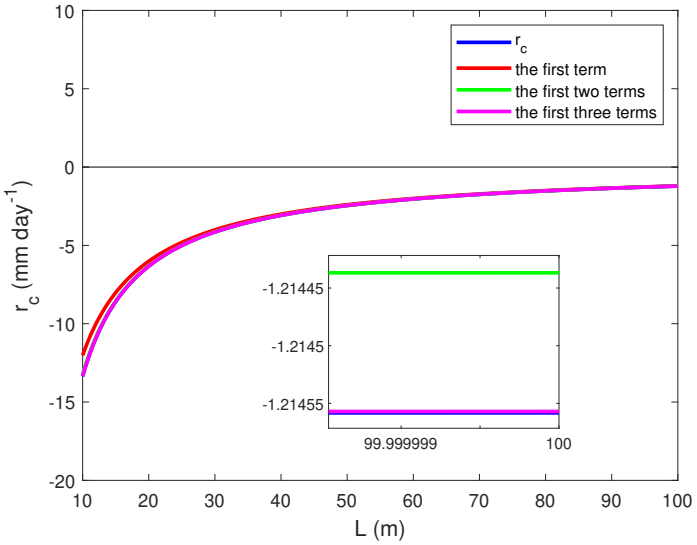

Figure 5.9: The critical value of rainfall r_c as a function of L, given by (5.44), and approximation using terms from the series expansion of r_c, (5.47). Note that the, blue, purple and green lines lie virtually on top of one another.

5.6 Dynamical Solutions for the $BH\Phi$ Model

We now consider the dynamic Richards' equation, first forming the equation with homogeneous boundary conditions, and then considering an approximate Fourier series solution. To simplify the boundary conditions we take

$$\Phi = \phi + M_1 z + M_2, \tag{5.48}$$

and assuming that $\phi(z,t)$ satisfies the boundary conditions $\phi(-L,t) = 0$ and $\left[\dfrac{\partial \phi}{\partial z} + \alpha\phi\right]_{z=0} = 0$, we find that using equations (5.23) and (5.24), the coefficients M_1 and M_2 are

$$M_1 = \frac{\sigma(B,H) - \alpha\Phi_1}{1+\alpha L}, \tag{5.49}$$

and

$$M_2 = \frac{\Phi_1 + L\sigma(B,H)}{1+\alpha L}, \tag{5.50}$$

where $\sigma(B,H) = IH\left(\dfrac{B+k\Omega}{B+k}\right)$. Therefore,

$$\Phi = \phi + \left(\frac{\sigma(B,H) - \alpha\Phi_1}{1+\alpha L}\right) z + \frac{\Phi_1 + L\sigma(B,H)}{1+\alpha L}. \tag{5.51}$$

It is then straightforward to show, using (5.20), that $\phi(z,t)$ satisfies

$$\frac{\partial \phi}{\partial t} - D\frac{\partial^2 \phi}{\partial z^2} - D\alpha\frac{\partial \phi}{\partial z} + DMB\phi = g(z,t), \tag{5.52}$$

where $M = \dfrac{R_{\max}\alpha\chi_0}{K_s B_0}$, and

$$g(z,t) = D\alpha M_1(t) - DMM_1(t)B(t)z - DMM_2(t)B(t) - M_3(t)(z+L), \tag{5.53}$$

and $M_3(t) = \dfrac{\dot{\sigma}(B,H)}{1+\alpha L}$, where $\dot{\sigma} = \dfrac{d\sigma}{dt}$ and remembering that $B(t)$, $H(t)$ are to be determined using equations (5.18) and (5.19), respectively. This equation will be solved with the initial conditions $\phi_0(z) = \Phi_0(z) - M_{1r_0}z - M_{2r_0}$ where

$$M_{1r_0} = \frac{r_0 - \alpha\Phi_1}{1+\alpha L}, \tag{5.54a}$$

$$M_{2r_0} = \frac{\Phi_1 + Lr_0}{1+\alpha L}, \tag{5.54b}$$

and $r_0 = r(0) = \sigma(B(0),H(0)) = IH(0)\left(\dfrac{B(0)+k\Omega}{B(0)+k}\right)$. The boundary conditions for $\phi(z,t)$ are then

$$\phi(-L,t) = 0 \tag{5.55}$$

and

$$\left[\frac{\partial \phi}{\partial z} + \alpha\phi\right]_{z=0} = 0. \tag{5.56}$$

The total water uptake rate V in (5.18) is then given by

$$V = \int_{-L}^{0} MB(t)\phi(z,t)\ dz - MB(t)M_1(t)\frac{L^2}{2} + MB(t)M_2(t)L. \tag{5.57}$$

We now consider the approximation to the solution of (5.52) using a Fourier series form, namely

$$\phi(z,t) = \sum_{n=-\infty}^{\infty} A_n(t)\sin(q_n z) + B_n(t)\cos(q_n z).$$

From the boundary conditions (5.55) and (5.56), we obtain $-A_n(t)\sin(q_nL) + B_n(t)\cos(q_nL) = 0$ and $B_n(t) = -q_nA_n(t)/\alpha$, which lead to the condition on the wave numbers

$$q_n = -\alpha\tan(q_nL), \quad n \in \mathbb{Z}. \tag{5.58}$$

Since $q_0 = 0$, the first term in the simulation will be zero since $\sin q_0 = 0$ and $B_0 = 0$. Therefore, using $B_n = -q_nA_n/\alpha$, we have

$$\phi(z,t) = \sum_{n=1}^{\infty} A_n(t)\left(\sin(q_n z) - \frac{q_n}{\alpha}\cos(q_n z)\right).$$

For simplicity, we will use only the first mode

$$\phi(z,t) = A_1(t)\left(\sin(q_1 z) - \frac{q_1}{\alpha}\cos(q_1 z)\right), \tag{5.59}$$

and we will later investigate if this is a good approximation by comparing the results with the full model in the steady state.

Using (5.59) in (5.52), gives

$$\begin{aligned}\left(\dot{A}_1 + Dq_1^2 A_1 + DMB(t)A_1\right)&\left(\sin(q_1 z) - \frac{q_1}{\alpha}\cos(q_1 z)\right)\\ &-D\alpha q_1 A_1\left(\cos(q_1 z) + \frac{q_1}{\alpha}\sin(q_1 z)\right)\\ &= (D\alpha M_1 - DMM_2 B - M_3 L)\\ &\quad - (DMM_1 B + M_3)\, z.\end{aligned} \tag{5.60}$$

As is standard in determining mode dynamics, we now multiply (5.60) by

$$\left(\sin(q_1 z) - \frac{q_1}{\alpha}\cos(q_1 z)\right),$$

and integrate all terms, we obtain

$$\begin{aligned}&\left(\dot{A}_1 + Dq_1^2 A_1 + DMBA_1\right)\int_{-L}^{0}\left(\sin(q_1 z) - \frac{q_1}{\alpha}\cos(q_1 z)\right)^2 dz\\ &-D\alpha q_1 A_1\int_{-L}^{0}\left(\cos(q_1 z) + \frac{q_1}{\alpha}\sin(q_1 z)\right)\left(\sin(q_1 z) - \frac{q_1}{\alpha}\cos(q_1 z)\right)dz\\ &= (D\alpha M_1 - DMM_2 B - M_3 L)\int_{-L}^{0}\left(\sin(q_1 z) - \frac{q_1}{\alpha}\cos(q_1 z)\right)dz\\ &\quad - (DMM_1 B + M_3)\int_{-L}^{0} z\left(\sin(q_1 z) - \frac{q_1}{\alpha}\cos(q_1 z)\right)dz.\end{aligned} \tag{5.61}$$

By directly finding all the integrals in (5.61), we get an equation for the first mode amplitude A_1,

$$\begin{aligned}G_{11}\dot{A}_1 + \left(Dq_1^2 G_{11} + DMBG_{11} - D\alpha q_1 G_{12}\right)A_1 &= \left(-DMM_1 G_{14} - DMM_2 G_{13}\right)B(t)\\ &\quad + \left(-M_3 G_{14} + (D\alpha M_1 - M_3 L)\, G_{13}\right),\end{aligned} \tag{5.62}$$

where G_{11}, G_{12}, G_{13} and G_{14} are given in (B.5), (B.6), (B.7) and (B.8) in Appendix B.2, respectively. For simplicity of notation, we set

$$U_{11} = \frac{Dq_1^2 G_{11} - D\alpha q_1 G_{12}}{G_{11}}, \tag{5.63}$$

$$U_{12} = DM, \tag{5.64}$$

$$R_{11} = \frac{-DMM_1 G_{14} - DMM_2 G_{13}}{G_{11}}, \tag{5.65}$$

and

$$R_{12} = \frac{-M_3 G_{14} + (D\alpha M_1 - M_3 L)\, G_{13}}{G_{11}}. \tag{5.66}$$

Then, (5.62) can be written as

$$\dot{A}_1 = -\left(U_{11} + U_{12} B\right) A_1 + R_{11} B + R_{12}. \tag{5.67}$$

The form of V in (5.18) is given now by (5.57), where ϕ is given by the first mode of the Fourier series

$$\begin{aligned} V =& M \frac{A_1(t)}{q_1} \left(-1 + \cos(Lq_1) - \frac{q_1}{\alpha} \sin(Lq_1)\right) B(t) \\ &+ \left(-\frac{L^2}{2} M M_1(t) + L M M_2(t)\right) B(t). \end{aligned}$$

Therefore,

$$V = \zeta B + \gamma_1 \frac{A_1}{q_1} B, \tag{5.68}$$

where $\zeta = M\left(-\frac{L^2}{2} M_1 + L M_2\right)$ and $\gamma_1 = M\left(-1 + \cos(Lq_1) - \frac{q_1}{\alpha}\sin(Lq_1)\right)$.
The initial conditions for the mode amplitudes $A_1(t)$ can be found by using (5.22)

$$A_1(0)\left(\sin(q_1 z) - \frac{q_1}{\alpha}\cos(q_1 z)\right) = \phi_0(z, 0), \tag{5.69}$$

multiplying by the mode $\left(\sin(q_1 z) - \frac{q_1}{\alpha}\cos(q_1 z)\right)$, and then integrating to obtain

$$A_1(0) G_{11} = \int_{-L}^{0} \left(\sin(q_1 z) - \frac{q_1}{\alpha}\cos(q_1 z)\right) \phi_0(z, 0) dz.$$

Therefore, the initial conditions for the single mode will be

$$A_1(0) = \frac{1}{G_{11}} \int_{-L}^{0} \left(\sin(q_1 z) - \frac{q_1}{\alpha}\cos(q_1 z)\right) \Phi_0(z) dz - \frac{r_0 - \alpha\Phi_1}{1 + \alpha L} \frac{G_{14}}{G_{11}} - \frac{\Phi_1 + L r_0}{1 + \alpha L} \frac{G_{13}}{G_{11}}. \tag{5.70}$$

We now have three equations in our model for the first mode amplitude $A_1(t)$, $B(t)$ and $H(t)$, in equations (5.18), (5.19) and (5.67), respectively, with the initial conditions (5.21) and (5.70), where V is given by (5.68).

5.7 Equilibrium Solution for the Single Mode $BH\Phi$ Model

The equilibrium points can be found by solving the steady-state situation for (5.18), (5.19) and (5.67)

$$0 = c\left(\zeta B + \gamma_1 \frac{A_1}{q_1} B\right) - dB, \tag{5.71}$$

$$0 = -IH\left(\frac{B + k\Omega}{B + k}\right) + r_0, \tag{5.72}$$

$$0 = -\left(U_{11} + U_{12}B\right) A_1 + R_{11}B + R_{12}, \tag{5.73}$$

where

$$\zeta = M\left(-\frac{L^2}{2} M_{1r_0} + L M_{2r_0}\right), \tag{5.74}$$

$$R_{11} = \frac{-DMM_{1r_0}G_{14} - DMM_{2r_0}G_{13}}{G_{11}}, \tag{5.75}$$

$$R_{12} = \frac{D\alpha M_{1r_0} G_{13}}{G_{11}}, \tag{5.76}$$

and M_{1r_0} and M_{2r_0} are given by (5.54a) and (5.54b). From (5.73), we obtain

$$A_1 = \frac{R_{11}B + R_{12}}{U_{11} + U_{12}B}. \tag{5.77}$$

and then from (5.71) we obtain

$$0 = c\left(\zeta B + \frac{\gamma_1}{q_1}\left(\frac{R_{11}B + R_{12}}{U_{11} + U_{12}B}\right) B\right) - dB.$$

Therefore, $B = B_1 = 0$ or $B = B_2 = \dfrac{q_1 U_{11}(d - c\zeta) - c\gamma_1 R_{12}}{c\gamma_1 R_{11} - q_1 U_{12}(d - c\zeta)}$, and substituting B_1 and B_2 into (5.72) and (5.77), we have two equilibrium points

$$P_1 = (A_{11}, B_1, H_1) = \left(\frac{R_{12}}{U_{11}}, 0, \frac{r_0}{I\Omega}\right), \tag{5.78}$$

$$P_2 = (A_{12}, B_2, H_2) = \left(\frac{q_1(d - c\zeta)}{c\gamma_1}, B_2, \frac{r_0(B_2 + k)}{I(B_2 + k\Omega)}\right). \tag{5.79}$$

From (5.59) we have at P_1

$$\phi_{s_{11}} = A_{11}\left(\sin(q_1 z) - \frac{q_1}{\alpha}\cos(q_1 z)\right),$$

and at P_2,

$$\phi_{s_{12}} = A_{12}\left(\sin(q_1 z) - \frac{q_1}{\alpha}\cos(q_1 z)\right).$$

Thus, from (5.51) we have two steady state solutions for the PDE (5.20), namely

$$\Phi_{s_{11}} = \phi_{s_{11}} + M_{1r_0} z + M_{2r_0}, \tag{5.80}$$

and

$$\Phi_{s_{12}} = \phi_{s_{12}} + M_{1r_0} z + M_{2r_0}. \tag{5.81}$$

As in the previous section we consider the existence of the equilibrium point using the function

$$F_1(B) = c\left(\zeta B + \gamma_1 \frac{A_1}{q_1} B\right) - dB. \tag{5.82}$$

Using the same values of the parameters shown in Table 5.1 and Table 5.2, we plot the function $F_1(B)$ for different values of r_0, see Figure 5.10.

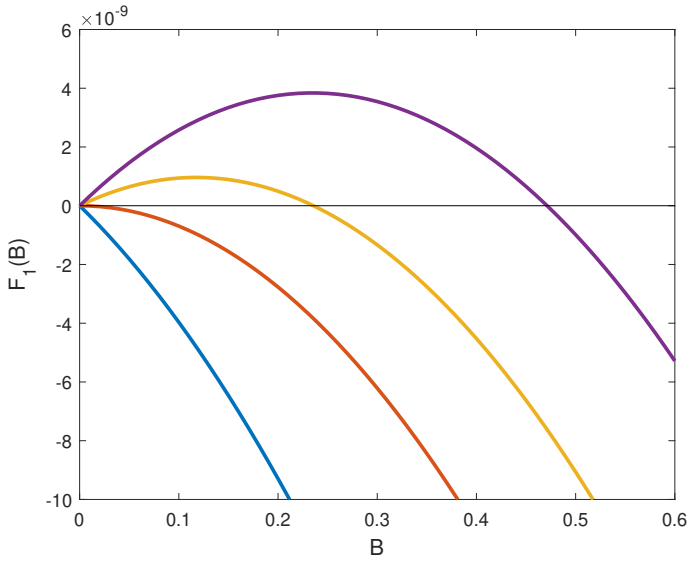

Figure 5.10: The function $F_1(B)$ for different values of r_0: $r_0 = -3r_{c1}$ (blue curve), $r_0 = r_{c1}$ (orange curve), $r_0 = 5r_{c1}$ (yellow curve) and $r_0 = 10r_{c1}$ (purple curve).

The critical value of rainfall when Φ depends only on the first mode can be found by using (5.82) where A_1 is given by (5.77). The same process for finding the only critical rainfall in the full model leads to the value when the solution depends on one mode,

$$\begin{aligned} r_{c1} =& \frac{-cK_s(G_{11}L^2MU_{11}\alpha q_1 - 2DG_{13}\alpha^2\gamma_1 + 2G_{11}LMU_{11}q_1)e^{(\alpha\Psi_1)}}{\alpha c(G_{11}L^2MU_{11}q_1 + 2DG_{13}\alpha\gamma_1)} \\ &+ \frac{2d\alpha(1+\alpha L)q_1 G_{11}U_{11}}{\alpha c(G_{11}L^2MU_{11}q_1 + 2DG_{13}\alpha\gamma_1)}. \end{aligned} \tag{5.83}$$

For the values of parameters used above, $r_{c1} = 2.0431 \times 10^{-8}\text{ms}^{-1}$, and $F_1(B)$ has one solution when $r_0 \leq r_{c1}$ (for instance the blue curve, when $r_0 = -3r_{c1}$, or

the orange curve, when $r_0 = r_{c1}$, in Figure 5.10) and two solutions when $r_0 > r_{c1}$ (for instance the yellow curve, when $r_0 = 5r_{c1}$ or the purple curve, when $r_0 = 10r_{c1}$, in Figure 5.10).

5.8 Numerical Simulation of the $BH\Phi$ Model

In order to investigate the approximation to only one mode for Φ, we will consider the equilibrium and dynamical solution of (5.18), (5.19) and (5.67). We first compare numerically the full steady state solution, Φ_s and the solution contains only the first mode, Φ_{s1}. We choose the same values of the parameters that are shown in Table 5.1 and Table 5.2 and, using (5.58), we obtain $q_1 = 2.7739$.

If $r_0 = 2r_{c1} > r_c, r_{c1}$, then we will have two equilibrium points P_1 which has zero biomass and P_2 which has nonzero biomass. Figure 5.11(a), shows the equivalent solutions Φ_s, from (5.34) with zero biomass, and Φ_{s11}, from (5.80). Figure 5.11(b), shows the solution for nonzero biomass. It should be noted that for the parameter value, $r_0 = 2r_{c1}$, the biomass is relatively small and the plots (a) and (b) in Figure 5.11 are therefore similar. The agreement between these steady states is a good approximation and suggests that the single mode approximation may be sufficient.

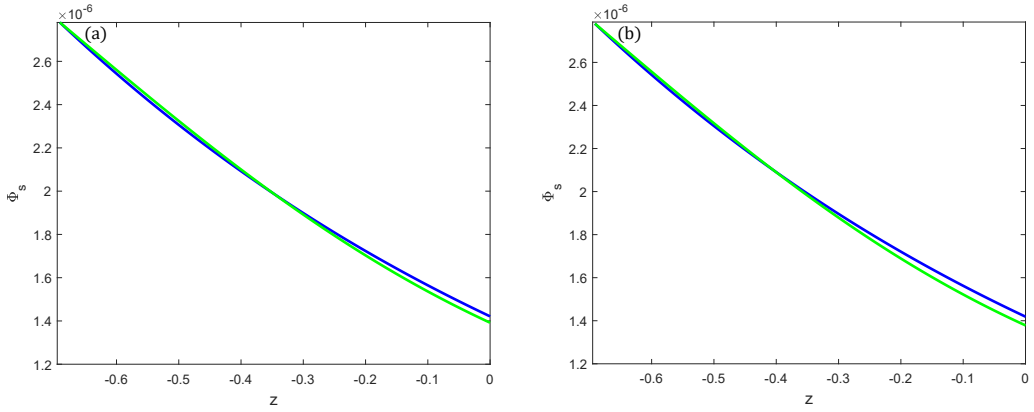

Figure 5.11: The steady state solution Φ_s (blue curve) and the approximate single mode steady state solution (green curve) for (a) the zero biomass state P_1, and (b) the nonzero biomass state P_2.

We now compare the values of the nonzero biomass equilibrium points, B_2 for the full and single mode solutions. Figure 5.12 shows that as the value of r_0 increases, the value of B_2 also increases, as expected, and that the two models show good agreement.

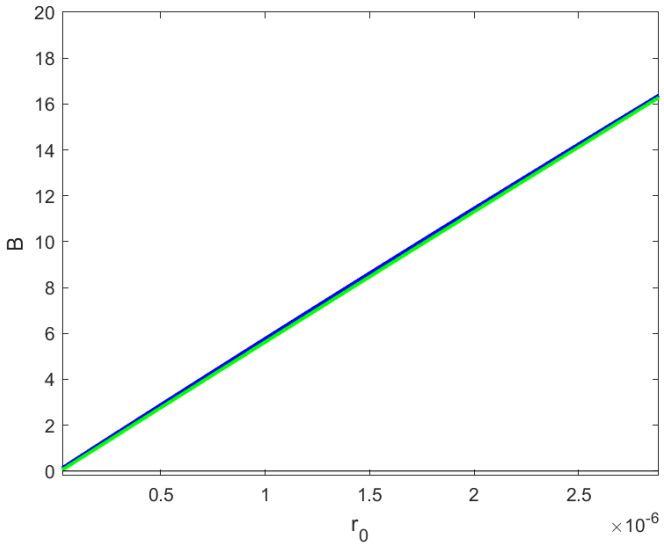

Figure 5.12: The value of B_2 as a function of rainfall. The blue and green lines are the values of B_2 for the full solution and the single mode solution, respectively.

The close agreement between the full solution and the single mode solution suggests that further modes are not necessary for an accurate model.

5.9 Dependence of r_c on Soil Parameters

The numerical calculation of the critical rainfall uses the same values of the parameters that are shown in Table 5.1, and Table 5.2. Figure 5.13 shows the values of critical rainfall when $0.3 < L < 10$. We see that for $L > L_c = 0.6919$ the critical value of rainfall is negative, i.e. biomass is supported by the soil even when there is water being removed from the system (i.e. by evaporation). For $L > L_c$ the amount of soil water taken into the plants by the roots is sufficient for growth even without rainfall, and for $L < L_c$ the reduced amount of roots, and therefore water from roots, means biomass cannot be supported for $r < r_c$.

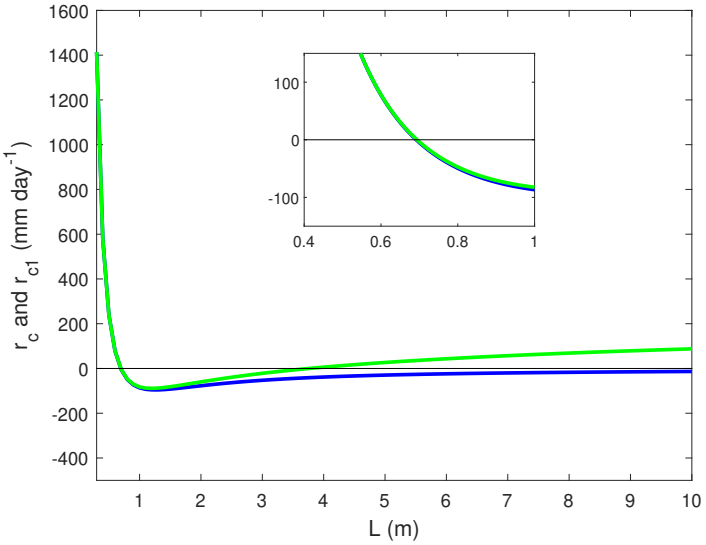

Figure 5.13: Critical values of rainfall as a function of L: r_c (blue curve) for the full solution of Φ, and r_{c1} (green curve) for a single mode.

Also, Figure 5.14(a) shows the values of the critical rainfall as a function of the soil pore-size distribution parameter α. When α is greater than a critical value, the critical value of the rainfall is positive. Figure 5.14(b) shows the values of critical rainfall as a function of the reference root density χ_0, where now below a critical value of χ_0 the critical rainfall is positive as similarly chosen to ensure positive critical rainfall values.

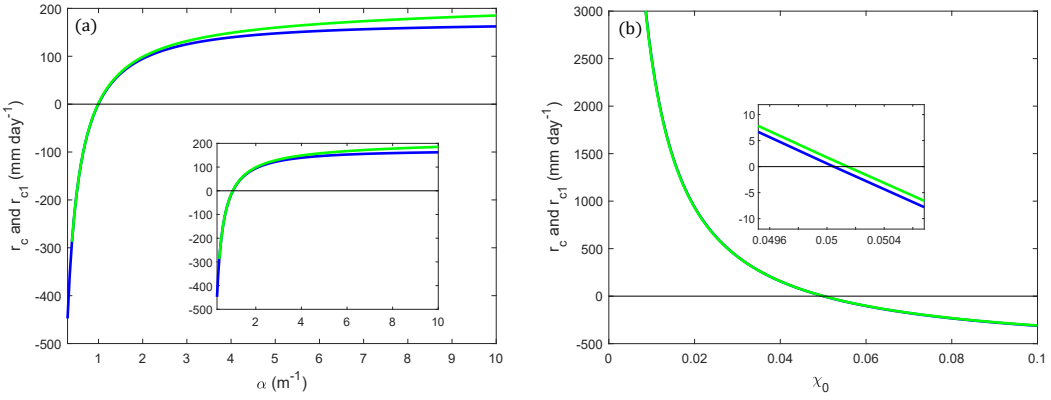

Figure 5.14: Critical values of rainfall as a function of (a) α and (b) χ_0. r_c (blue curve) for the full solution of Φ, and r_{c1} (green curve) for a single mode.

Both of these results are to be expected. For large values of α the soil water can be easily drained into the water table and so higher rainfall is needed to sustain

biomass. However, large values of root density allow more efficient uptake of water to sustain biomass.

5.10 The Dynamical Solution for the Single Mode $BH\Phi$ Model

From the previous sections, we have seen that a single mode solution is a good approximation for the equilibrium solution to the problem. We now consider the dynamical solution of (5.67), although care must be taken as there are time derivatives hidden in R_{12}, and (5.67) is in fact equivalent to the following equation,

$$\frac{dA_1}{dt} = -\left(U_{11} + U_{12}B\right)A_1 + R_{11}B + R_{13} + R_{14}\frac{dB}{dt} + R_{15}\frac{dH}{dt}, \tag{5.84}$$

where

$$R_{13} = \frac{D\alpha G_{13}M_1}{G_{11}}, \tag{5.85}$$

$$R_{14} = -\frac{G_{14} + LG_{13}}{G_{11}(1+\alpha L)}\left(-\frac{IHk(1-\Omega)}{(B+k)^2}\right), \tag{5.86}$$

and

$$R_{15} = -\frac{G_{14} + LG_{13}}{G_{11}(1+\alpha L)}\left(\frac{I(B+k\Omega)}{B+k}\right). \tag{5.87}$$

Using (5.18) and (5.19), we then obtain the following equation for A_1 which we consider in the numerical simulations, together with the two equations (5.18) and (5.19)

$$\begin{aligned}\frac{dA_1}{dt} =& -\left(U_{11} + U_{12}B\right)A_1 + R_{11}B + R_{13} \\ &+ R_{14}\left(c\left(\zeta B + \gamma_1\frac{A_1}{q_1}B\right) - dB\right) \\ &+ R_{15}\left(-IH\left(\frac{B+k\Omega}{B+k}\right) + r(t)\right),\end{aligned} \tag{5.88}$$

where U_{11}, U_{12}, R_{11}, R_{13}, R_{14} and R_{15} are given by (5.63), (5.64), (5.65), (5.85), (5.86) and (5.87) respectively. The amplitude A_1 is, perhaps, not the most physically relevant or experimentally measurable measure of the soil water, and so we will consider the total water content in the soil. By using (5.16), (5.51) and (5.59) in (5.11), and assuming the soil water depends on a single mode A_1, we obtain the

total water content in the soil Θ, the integral of θ through the soil,

$$\begin{aligned}\Theta &= \int_{-L}^{0} \left(\theta_r + (\theta_s - \theta_r)\frac{\alpha}{K_s}\Big(A_1(t)(\sin(q_1 z) - \frac{q_1}{\alpha}\cos(q_1 z)) + M_1 z + M_2\Big)\right) dz \\ &= \theta_r L + (\theta_s - \theta_r)\frac{\alpha}{K_s}\left[- \frac{A_1(t)}{q_1}(1 - \cos(q_1 L) + \frac{q_1}{\alpha}\sin(q_1 L)) - M_1\frac{L^2}{2} + M_2 L\right].\end{aligned} \tag{5.89}$$

We will now look at various rainfall scenarios, when $r(t)$ is a constant, and when $r(t)$ changes over time.

5.10.1 Instantaneous Change in Constant Rainfall

Rather than consider the equilibrium state that could result from constant rainfall, we now investigate the transient dynamics as the rainfall changes from one constant value to another. In our study we consider two examples of such a scenario. In the first scenario, we consider the constant rainfall value r_0 going from a low value to a high value and passing through the critical value r_{c1}. The idea here is to investigate the behaviour of the system going from a drought situation with low biomass to a high rainfall situation and we will investigate how much initial biomass B_0 must be planted, to obtain a high level of biomass in a short time.

In this numerical simulation we use the values of the parameters in Table 5.1 and Table 5.2, and $q_1 = 2.7739$. The behaviour of the system is investigated for an abrupt increase in rainfall, so that for $t \leq 0$ the rainfall is constant at a low value $r_0 = 0.5r_{c1} = 1.0215 \times 10^{-8}\, ms^{-1}$ and for $t > 0$ the rainfall is at a high value of $r_0 = 2r_{c1} = 4.0862 \times 10^{-8}\, ms^{-1}$. We choose the initial condition as the equilibrium point $Y_0 = P_1 = (A_{11}, B_0, H_1) = (1.0086 \times 10^{-7}, B_0, 0.0220)$, the value of A_1 and H_1 obtained from the state when $r_0 = 0.5r_{c1}$. The value of the initial biomass B_0 has values which are $0 \leq B_0 \leq B_2$, where B_2 here is the biomass for the second equilibrium point P_2 when $r_0 = 2r_{c1}$, i.e. $B_2 = 0.1178$.

For $t > 0$, when $r_0 = 2r_{c1}$, as shown in previous sections, there are two equilibrium points which are $P_1 = (A_{11}, B_1, H_1) = (9.9753 \times 10^{-8}, 0, 0.0882)$ and $P_2 = (A_{12}, B_2, H_2) = (1.0252 \times 10^{-7}, 0.1178, 0.0182)$. The numerical simulation, described in detail below, shows that the equilibrium point P_1 is unstable while P_2 is stable point.

Figure 5.15 describes the dynamic response of the system as rainfall increases, and for three different initial biomass values $B_0 = 0, 0.25B_2, 0.75B_2$. If the initial value of biomass is zero, the biomass does not become nonzero even with increased rainfall. Since plant growth depends on the presence of existing plants for propagation. The values of surface water and soil water content adapt due to the

increased rainfall and the system equilibrates to the new zero biomass state P_1, as seen in Figure 5.15(a, b) where in this figure, the simulation stopped when the surface water reached 95% of H_1, which is around 65 days. The black dashed line in (a) is $H = H_1$. The steady state of total water content Θ is 0.26340, the black dashed line in (b), which is the value of Θ when A_1 is the component of the first equilibrium point when $r_0 = 2r_{c1}$.

By increasing only the initial biomass value B_0, the system now starts with existing plants and eventually approaches the nonzero biomass equilibrium P_2. Figure 5.15(c, e) shows that the system stabilises around P_2 for $B_0 = 0.25B_2$ and $B_0 = 0.75B_2$, respectively. Figure 5.15(c, e) shows that the biomass takes around 15 years and 7 years, respectively, to get 95% of B_2.

From Figure 5.15(c, e) we see, in comparison to Figure 5.15(a), the surface water H is rapidly absorbed by the soil and, as the plants start to use this water to grow, the soil water content goes down, see Figure 5.15(d, f). The inset in Figure 5.15(d) shows that the soil water content initially increases because of the rapid infiltration of the surface water, before eventually decreasing as it is used by the plants. When there is initially more biomass, this increase in soil water content is not present, as shown in Figure 5.15(f).

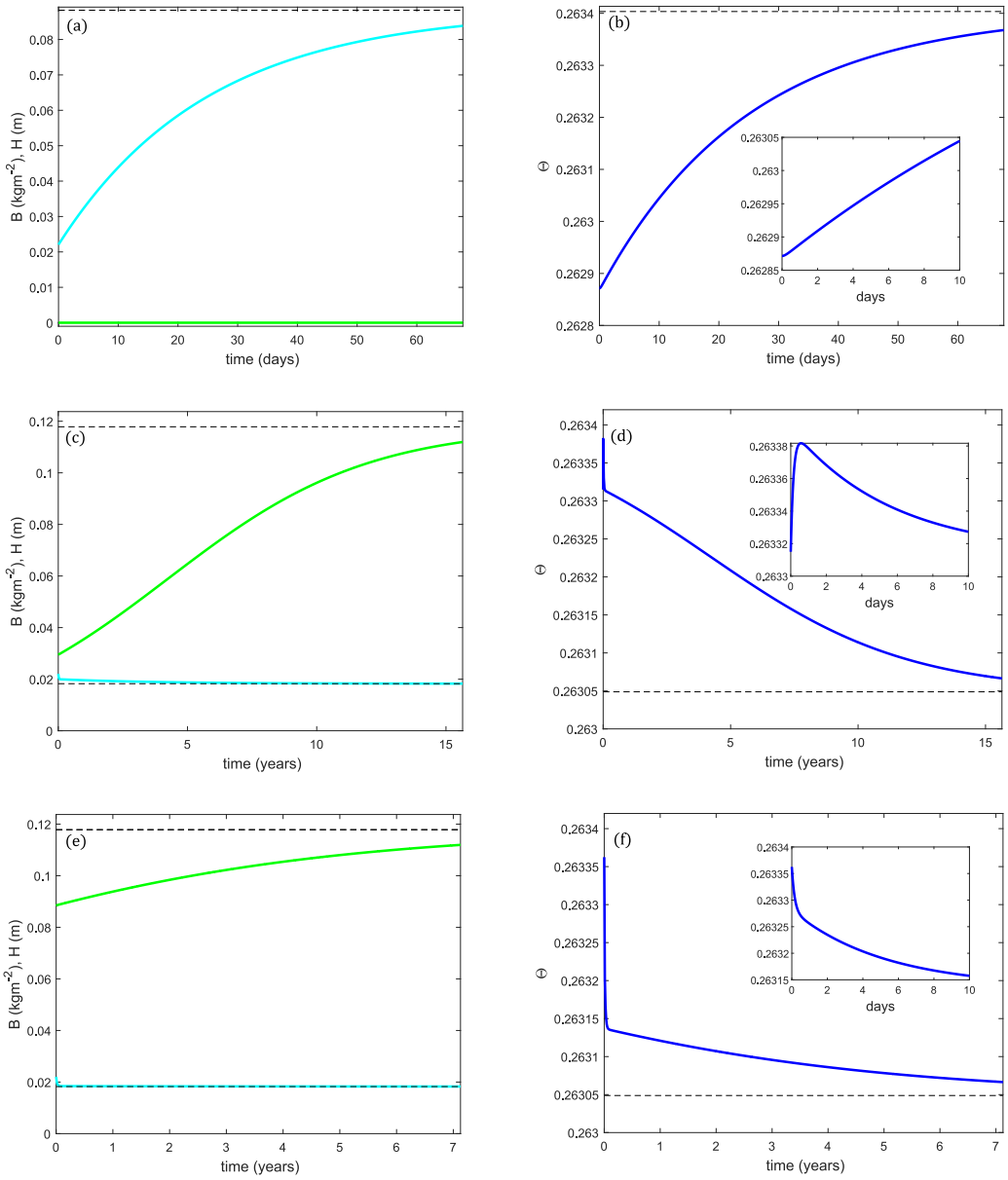

Figure 5.15: The dynamic behaviour of the system for $r_0 = 2r_{c1}$ where the biomass (green curve), the surface water (cyan curve) and the soil water content are plotted as functions of time and the black dashed lines are the equilibrium value of B, H and Θ. In (a) and (b) $B_0 = 0$, in (c) and (d) $B_0 = 0.25B_2$, and in (e) and (f) $B_0 = 0.75B_2$.

Figure 5.16(a) shows the time, in years, to approach B_2 as we change B_0. We see that the period of time to reach B_2 decreases as B_0 increases. For example, if the system is started with $B_0 = 25\%$ of B_2, it will reach 95% of the equilibrium biomass after approximately 15 years. While if the system is started with $B_0 = 75\%$ of

B_2, it will reach 95% of the equilibrium biomass in approximately 7 years. Figure 5.16(b) shows the contour plot of biomass for different initial values of biomass, and time. As is to be expected, this figure shows that increasing biomass after a drought by planting a large amount of biomass would be a successful strategy.

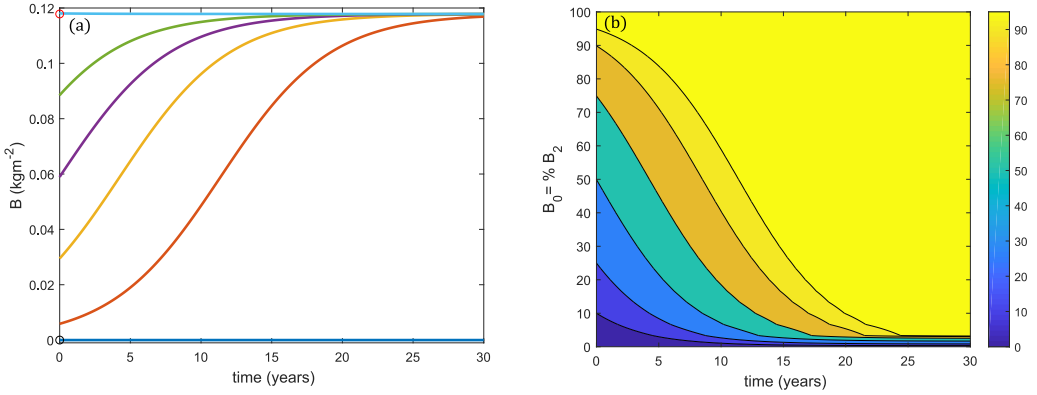

Figure 5.16: The dynamic behaviour of the system for $r_0 = 2r_{c1}$. (a) The trajectories of the biomass for different initial values of biomass, where the black circle is $B_0 = 0$ and the red circle is B_2. (b) The biomass contour (as a percentage of B_2) as a function of time and initial biomass.

In the second scenario, we consider the constant rainfall value r_0 from a high value to a low value and passing through the critical value r_{c1}. This case is the opposite of the previous one, where, for the time before $t = 0$, we have a period of rainy weather, and there is a lot of biomass. If the rain then suddenly stops, the behaviour of the system will change and we expect the level of biomass to reduce. The idea here is to investigate the behaviour of the system where it goes from a high rainfall situation to a drought situation and we will investigate how long the biomass takes to reach a very low level. These results may be useful to those designing an irrigation system for periods of drought.

The behaviour of the system is investigated for an abrupt decrease in rainfall, so that for $t \leq 0$ the rainfall is constant at a high value $r_0 = 2r_{c1} = 4.0862 \times 10^{-8}\, ms^{-1}$ and for $t > 0$ the rainfall is at a low value of $r_0 = 0.5r_{c1} = 1.0215 \times 10^{-8}\, ms^{-1}$. We choose the initial condition as $Y_0 = (A_{12}, B_0, H_2) = (1.0252 \times 10^{-7}, B_0, 0.0182)$, where the values of A_{12}, H_2 are obtained from the equilibrium state when $r_0 = 2r_{c1}$ (the equilibrium point when $B \neq 0$), and the value of the initial biomass B_0 has values varying from 0 to $2B_2$, where B_2 here is the biomass for the equilibrium state when $r_0 = 2r_{c1}$, i.e. $B_2 = 0.1178$. For $t > 0$, when $r_0 = 0.5r_{c1}$, as shown in the previous sections, there is one equilibrium point, the state with no biomass, which is $P_1 = (A_{11}, 0, H_1) = (1.0086 \times 10^{-7}, 0, 0.0220)$, the numerical simulation, described in detail below, confirms that this is the only stable equilibrium point.

Figures 5.17 and 5.18 show the biomass, surface water and soil water content as a function of time for the various values of initial biomass. We see that when the drought arrives, at $t = 0$, the values of the biomass and the surface water decrease, except in the case $B_0 = 0$ where with no biomass the value of B stays at zero. In all other cases the soil water content increases as the surface water moves into the soil. We see that, for a short time after $t = 0$, and for $B_0 = 0, 0.5B_2$ and $0.75B_2$, the soil water content increases. This increase is due to the surface water infiltrating into the soil, increasing the soil water content. Even though the biomass will be taking water from the soil, the small amount of biomass and the inefficiency of root extraction in these cases mean that overall the soil water content increases, at least initially. For longer time periods the soil water content then goes down over a period of days as the biomass now acts to take water from the soil. Over a much longer period of years, the system recovers to have a higher soil water content and finds an equiliubrium value only over a period of tens of years.

For the cases $B_0 = B_2, 1.5B_2$ and $2B_2$ the process is almost the same except the initial period of increased soil water content in the first day or two is now not present, presumably because the increased levels of biomass lead to higher root extraction of water and an immediate decrease of the soil water content.

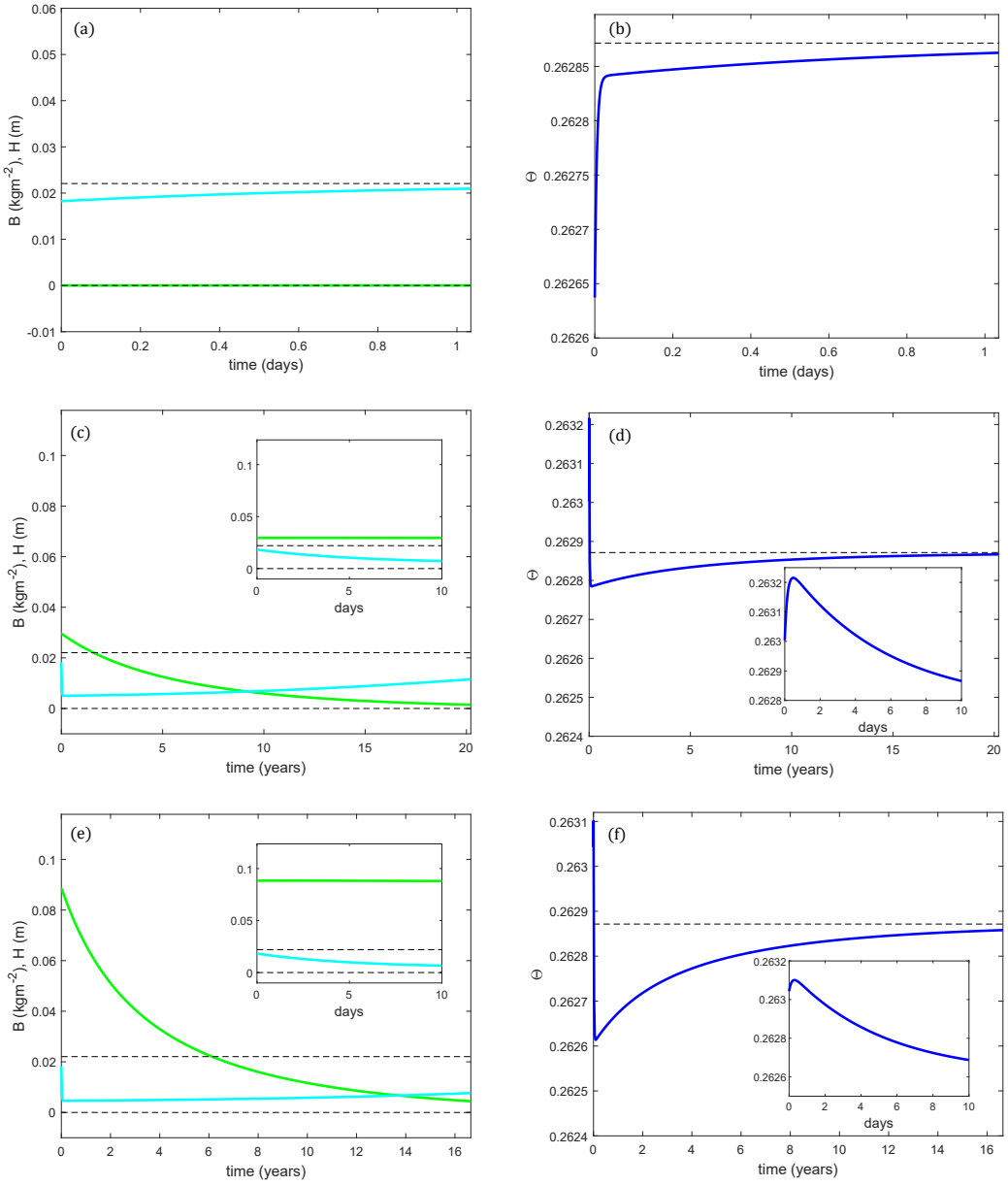

Figure 5.17: The dynamic behaviour of the system for $r_0 = 0.5r_{c1}$ where the biomass (green curve), the surface water (cyan curve) and the soil water content are plotted as functions of time and the black dashed lines are the equilibrium value of B, H and Θ. In (a) and (b) $B_0 = 0$, in (c) and (d) $B_0 = 0.25B_2$, and in (e) and (f) $B_0 = 0.75B_2$.

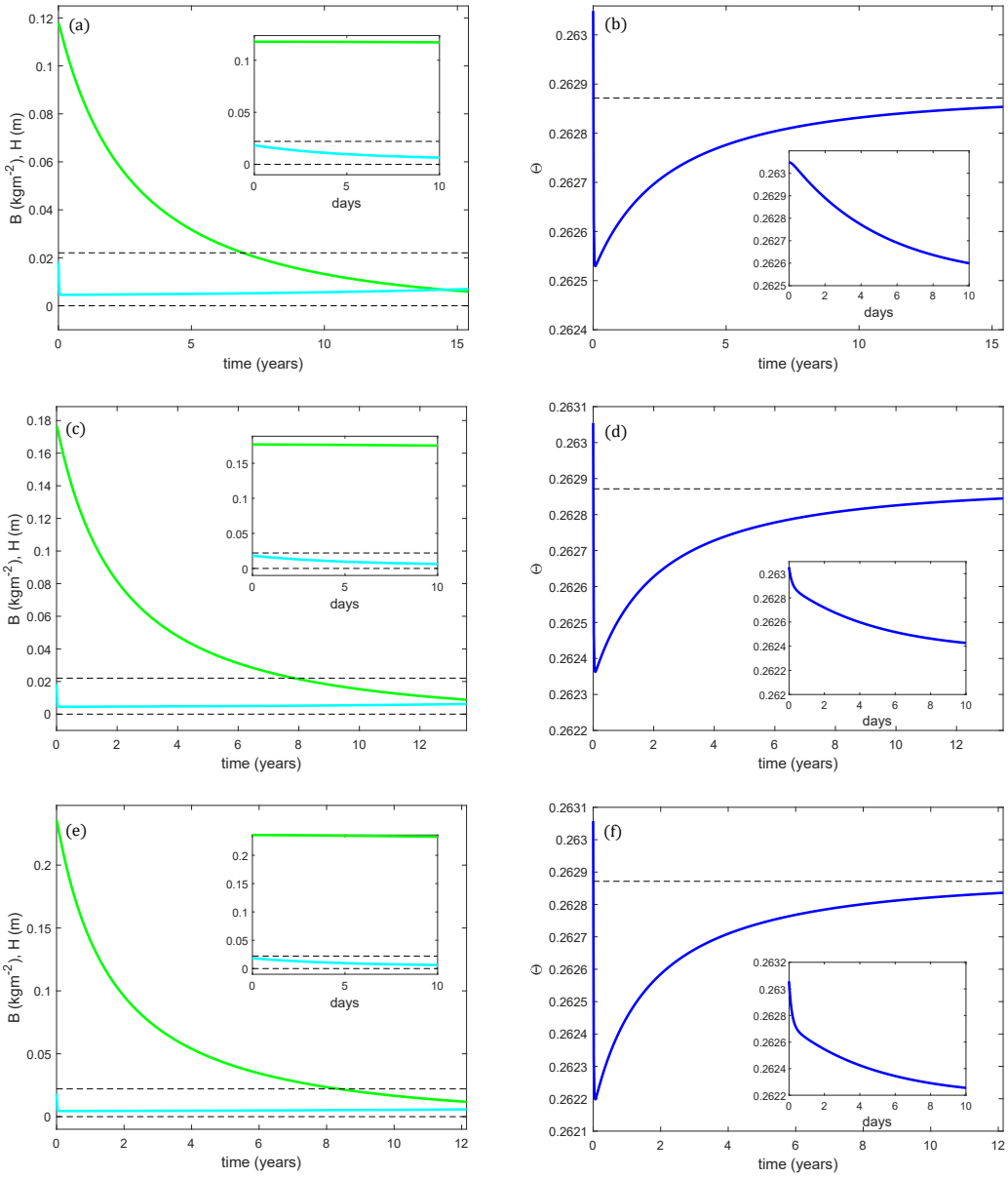

Figure 5.18: The dynamic behaviour of the system for $r_0 = 0.5r_{c1}$ where the biomass (green curve), the surface water (cyan curve) and the soil water content are plotted as functions of time and the black dashed lines are the equilibrium value of B, H and Θ. In (a) and (b) $B_0 = B_2$, in (c) and (d) $B_0 = 1.5B_2$, and in (e) and (f) $B_0 = 2B_2$.

Figure 5.19 summarises the long-term behaviour of the biomass for different values of the initial biomass conditions. Each trajectory of $B(t)$ takes a different amount of time to lose, say, 95% of the biomass. Figure 5.19(b) shows the contour plot of biomass for different initial values of biomass, and time. As is to be expected, this figure shows that the system collapses quickly to P_1, the zero biomass

state, when the initial values of the biomass are close to zero and more slowly when the initial values of B are bigger values.

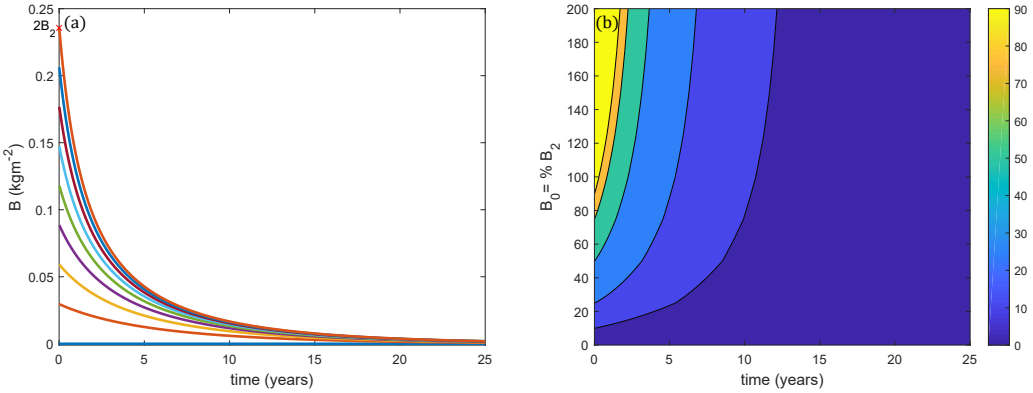

Figure 5.19: The dynamic behaviour of the system for $r_0 = 0.5r_{c1}$. (a) The trajectories of the biomass for different initial values of biomass. (b) The biomass contour (as a percentage of B_2) as a function of time and initial biomass.

5.10.2 Time Dependent Rainfall

In real life rainfall is not constant, and for this reason, we will also model the situation when $r = r(t)$. As an example of a time-dependent rainfall, we will consider $r(t) = \frac{r_m}{2}(1 + \cos \omega t)$, where r_m is the maximum value of the rain and ω is the frequency that determines the rainfall period $T = \pi/2\omega$. Figure 5.20 shows an example of this form of $r(t)$.

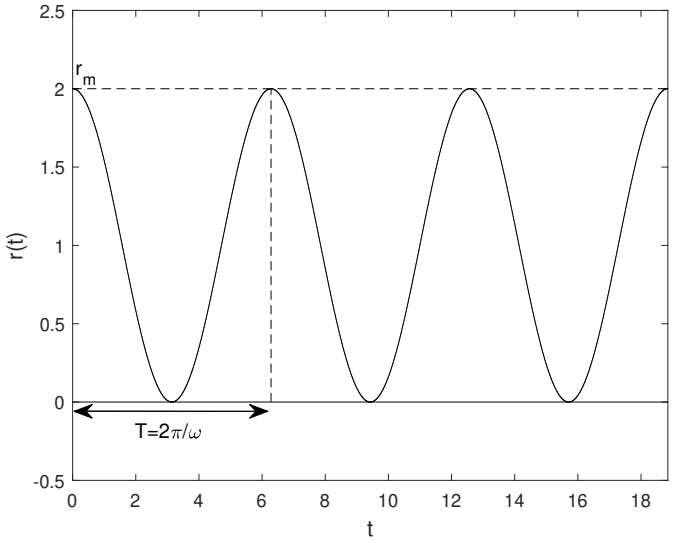

Figure 5.20: Rainfall function $r(t) = \dfrac{r_m}{2}(1+\cos\omega t)$, when $r_m = 2$ and $\omega = 1$. The minimum rainfall is $r = 0$ and the maximum is $r = r_m$.

We will now consider different values of ω, and therefore different periods T to understand the behaviour of the system under different rainfall forcing. In the following simulations, two possible cases for the value of r_m will be considered $r_m = 4r_{c1}$ and $r_m = 0.5r_{c1}$. The dynamic behaviour is then studied for different periods: $T = 1$ day, 1 week, 30 days and 6 months (the term month in the simulation is equal to 30 days). The maximum running time for the simulation is chosen to make sure the system settles down to a periodic state around the equilibrium point. In the following simulations one year is equal to 365 days.

Figure 5.21 shows the behaviour of the system when we set $r_m = 4r_{c1}$ and for periods $T = 1$ day, 1 week, 30 days and 6 months. From Figure 5.21(a, c, e, g) we see that the surface water reacts at a similar time scale as the rainfall, although the surface water is delayed if the rain water has a rapid frequency (1 day) and follows the rainfall more closely if the rainfall has a longer period. These figures also show that the biomass does not change over a short period of time. In Figure 5.21(b, d, f, h), we see that the biomass reaches a regular periodic state around the equilibrium point within 10 or 20 years, although the surface water already settles down in a much shorter period of time.

When $r_m = 0.5r_{c1}$, a rainfall below the critical value, which causes the surface water to decrease at the beginning of the simulation, Figure 5.22 shows the behaviour of the system for the periods $T = 1$ day, 1 week, 30 days and 6 months. From Figure 5.22(a), we see that for a short rainfall period, the surface water does not react on a similar time scale to the rainfall. However, when the rainfall occurs

over a longer period, i.e. in Figure 5.22(c, e, g), the surface water reacts at a similar time scale to the rainfall. These plots also show that the biomass changes over a relatively long period of time. In contrast to the case when $r_m = 4r_{c1}$, Figure 5.22(b, d, f, h) shows that the surface water changes significantly only over a long period time, i.e. 20 years. The plots also suggest that the system settles down to a periodic state around the equilibrium point that would occur in a constant rainfall situation.

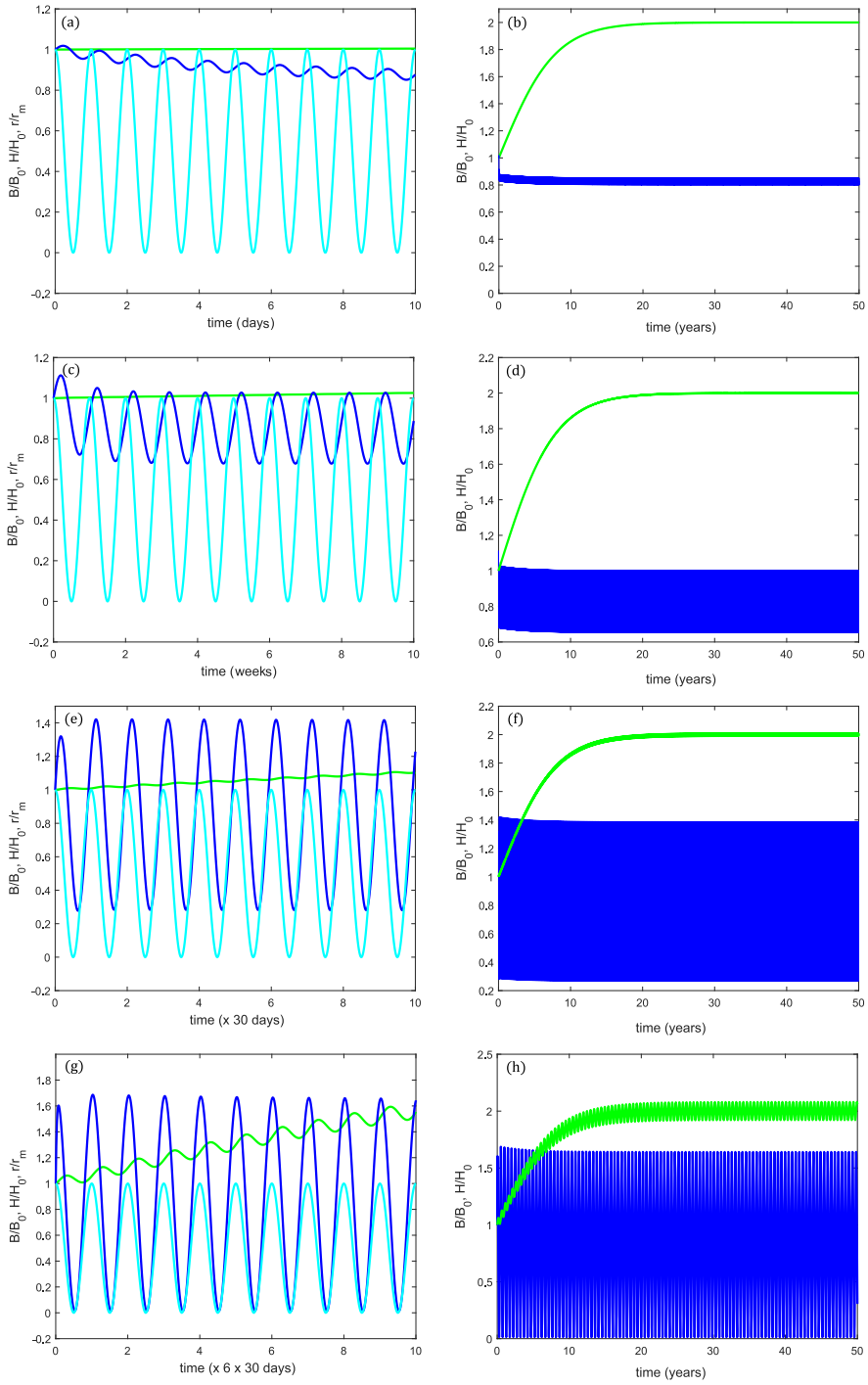

Figure 5.21: The dynamic behaviour of biomass (green curve), surface water (blue curve) and the rainfall (cyan curve) where $r_m = 4r_{c1}$. (a) and (b) $T = 1$ day. (c) and (d) $T = 1$ week. (e) and (f) $T = 30$ days. (g) and (h) $T = 6$ months. Note the plots on the left and right hand sides are for different timescales.

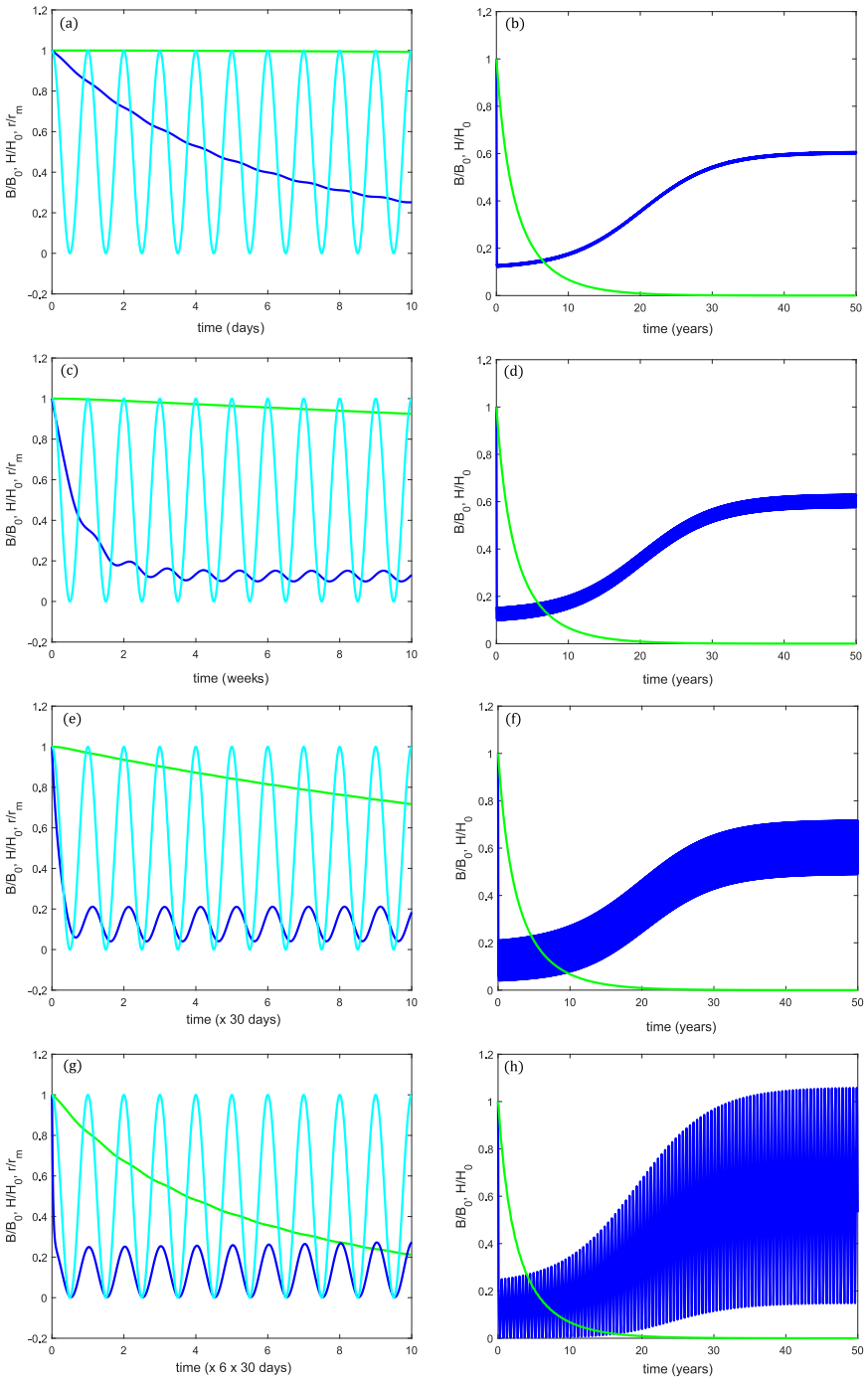

Figure 5.22: The dynamic behaviour of biomass (green curve), surface water (blue curve) and the rainfall (cyan curve) where $r_m = 0.5r_{c1}$. (a) and (b) $T = 1$ day. (c) and (d) $T = 1$ week. (e) and (f) $T = 30$ days. (g) and (h) $T = 6$ months. Note the plots on the left and right hand sides are for different timescales.

From the previous figures we see that the growth of biomass depends on the cycle period of the rainfall. For a short cycle, i.e. one day, the plants grow as the rainfall increases and then die again when it stops although there is no time for them to die completely because the rain returns the next day. Consequently, the oscillations in biomass are not large. However, for a larger cycle, i.e. 30 days, there are large oscillations in the biomass since the time scale for plant growth and death is closer to the period of rainfall. Therefore, for a short rain cycle and over a short period of time, the amount of plant matter stays almost constant. For a longer cycle, the biomass changes as the rainfall changes. This effect, where a rapid rain oscillation stabilises the biomass to be almost constant, is often termed high frequency stabilisation. Over a longer period (years) the average biomass does change and eventually the average biomass reaches an equilibrium.

We now compare the results of the model with constant rainfall to the model with periodic rainfall. To make this comparison we set $r_0 = r_m/2$ so that in both cases the average rainfall over time T is $r_m T/2$. Figure 5.23 shows the evolution of the biomass for constant and periodic rainfall models, for different values of r_m and for $T = 1$ day, 1 week, 30 days and 6 months. We see that, apart from the biomass oscillation, for large T described above, there is very little overall difference in the long time evolution of the biomass.

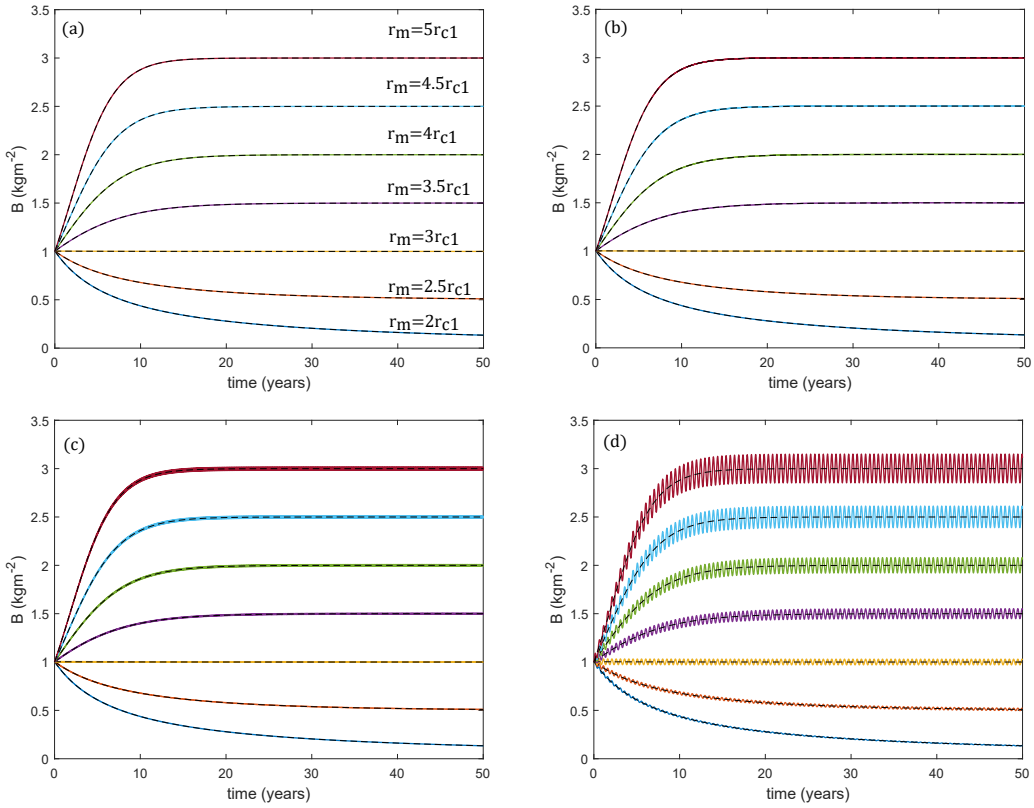

Figure 5.23: Biomass trajectory for different values of r_m, for both the periodic rainfall model (coloured lines) and the constant rainfall model (black dashed line) for (a) $T = 1$ day, (b) $T = 1$ week, (c) $T = 30$ days and (d) $T = 6$ months.

In the next section we will consider how the introduction of a fractional derivative in the evolution equation for biomass will change the system behaviour.

5.11 Fractional $BH\Phi$ Model

The aim of this section is to study the dynamical properties of a generalisation of the system described in (5.18), (5.19) and (5.20) through the introduction of the Caputo fractional derivative of order ρ, ${}^cD_t^\rho$. As fractional derivatives have been used to model memory, and only biotic components can have the form of memory we are considering, we will add the fractional order to the biomass but not to the water components. The incommensurate fractional model of the interaction of soil

water model can therefore be written as

$$
\begin{aligned}
{}^{c}D_t^{\rho} B &= cV - dB, && (5.90)\\
\frac{dH}{dt} &= -IH\left(\frac{B+k\Omega}{B+k}\right) + r(t), && (5.91)\\
\frac{\partial \Phi}{\partial t} &= D\frac{\partial^2 \Phi}{\partial z^2} + D\alpha\frac{\partial \Phi}{\partial z} - DS, && (5.92)
\end{aligned}
$$

where $V = \int_{-L}^{0} S(z)dz$, with the same initial conditions and the boundary conditions as the integer model. For the dynamic behaviour, we focus on the model with only single mode A_1, thus the fractional incommensurate system will include the equations (5.90), (5.91) and (5.88).
Or will be

$$
\begin{aligned}
{}^{c}D_t^{\rho} B &= cV - dB,\\
\frac{dH}{dt} &= -IH\left(\frac{B+k\Omega}{B+k}\right) + r(t),\\
\frac{dA_1}{dt} &= -\left(U_{11} + U_{12}B\right)A_1 + R_{11}B + R_{13}\\
&+ R_{14}\left(c\left(\zeta B + \gamma_1 \frac{A_1}{q_1}B\right) - dB\right)\\
&+ R_{15}\left(-IH\left(\frac{B+k\Omega}{B+k}\right) + r(t)\right),
\end{aligned}
$$

where U_{11}, U_{12}, R_{11}, R_{13}, R_{14} and R_{15} are given by (5.63), (5.64), (5.65), (5.85), (5.86) and (5.87) respectively. The equilibrium points for the fractional model are the same as the equilibrium points for the integer-order model, and are given by (5.78) and (5.79).

As we have seen in the integer model, the two possible equilibrium points (when $r_0 > r_{c1}$), are P_1, a saddle point, and P_2, which has real negative eigenvalues so it is a stable point. We have numerically determined that the eigenvalues in this situation are real, and so replacing the integer derivative with a fractional derivative does not affect the stability. The fractional system will always be stable around P_2. However, we will consider the transient, time dependent behaviour for various rainfall scenarios, when $r(t)$ is a constant and when $r(t)$ changes over time and consider how the fractional derivative affects the system.

5.11.1 Instantaneous Change in Constant Rainfall

Here we consider the same two cases discussed for the integer derivative system in the Section 5.10.1. We will use the same values of the parameters that are shown in Table 5.1 and Table 5.2, and the same value of the wave number, $q_1 = 2.7739$.

In the first situation we consider a value of r_0 greater than r_{c1} where the initial condition is the equilibrium state for a value of r_0 below r_{c1} while changing the initial value of the biomass. In this case the rainfall therefore switches from a low to a high value. The constant value of rainfall $r_0 = 2r_{c1}$ is chosen as the high value of rainfall, for which there are two equilibrium points, $P_1 = (A_{11}, B_1, H_1) = (9.9753 \times 10^{-8}, 0, 0.0882)$ and $P_2 = (A_{12}, B_2, H_2) = (1.0252 \times 10^{-7}, 0.1178, 0.0182)$. The equilibrium point P_1 is an unstable point (saddle point) while P_2 is a stable point for the system. The behaviour of the system is now investigated for a range of different initial conditions.

We first choose the initial condition to be the zero biomass equilibrium point for $r_0 = 0.5r_{c1}$, $(A_{11}, B_1, H_1) = (1.0086 \times 10^{-7}, 0, 0.0220)$. In this case and for all fractional orders we considered, the same results of the integer system are obtained since the biomass value remains at zero. Figure 5.24 shows the numerical solution for a range of values of ρ in this case.

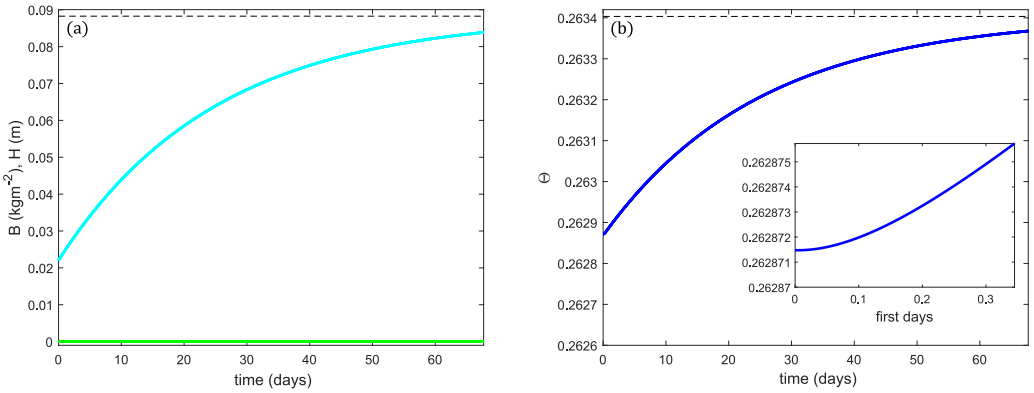

Figure 5.24: The dynamic behaviour of the fractional system where (a) the biomass B (green curve) and the surface water H (cyan curve), and (b) the soil water content Θ, for $r_0 = 2r_{c1}$, initial condition $I_0 = (1.0086 \times 10^{-7}, 0, 0.0220)$, and fractional orders $\rho = 0.5, 0.6, 0.7, 0.8, 0.9, 1$.

We now consider changing the initial biomass value B_0. We consider $B_0 = aB_2$ where $0 < a < 1$, and where B_2 is the equilibrium value for the higher value of rainfall. This system models the situation where, after a period of low rainfall, biomass is introduced as the rainfall increased to $r_0 > r_{c1}$. Figure 5.25 and Figure 5.26, show the cases when $a = 0.25$ and $a = 0.75$, respectively. We see a similar behaviour as the integer system. However, the time needed to approach the equilibrium point P_2 increases as the fractional order, ρ, decreases. This delay in reaching equilibrium for smaller values of ρ indicates that memory is acting in a similar way to inertia. There is an effective memory of the initial state that leads to prolonged effective drought behaviour.

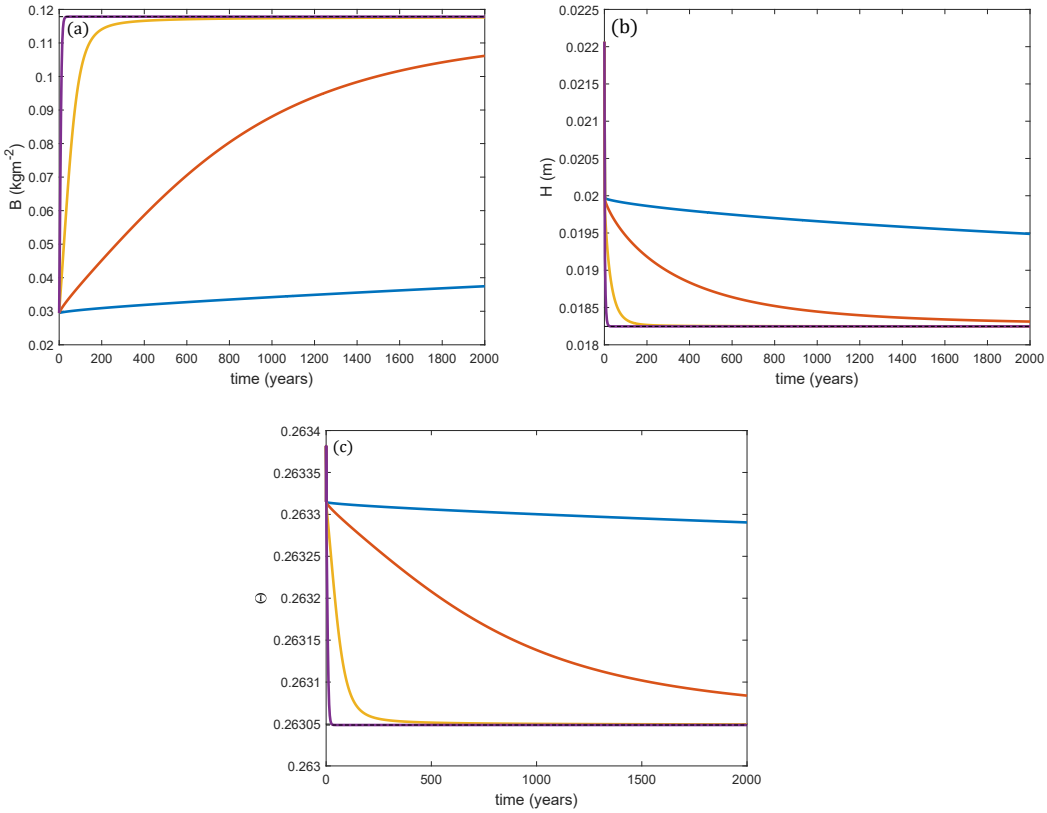

Figure 5.25: For initial condition $I_0 = (1.0086 \times 10^{-7}, 0.25 \times B_2, 0.0220)$, where $B_2 = 0.1178$, the dynamic behaviour of the fractional system where (a) the biomass B, (b) the surface water H and (c) the soil water content Θ, for $r_0 = 2r_{c1}$ and for fractional orders $\rho = 0.7$ (blue curves), $\rho = 0.8$ (orange curves), $\rho = 0.9$ (yellow curves) and $\rho = 1$ (purple curves).

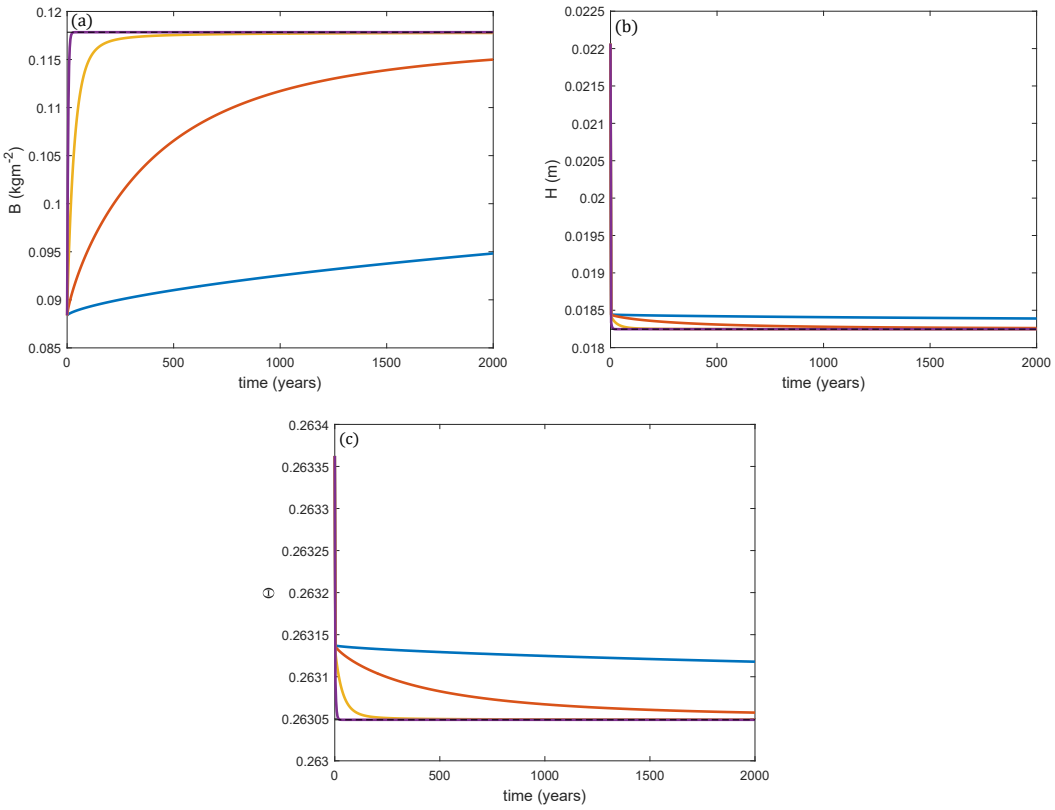

Figure 5.26: For initial condition $I_0 = (1.0086 \times 10^{-7}, 0.75 \times B_2, 0.0220)$, where $B_2 = 0.1178$, the dynamic behaviour of the fractional system where (a) the biomass B, (b) the surface water H and (c) the soil water content Θ, for $r_0 = 2r_{c1}$ and for fractional orders $\rho = 0.7$ (blue curves), $\rho = 0.8$ (orange curves), $\rho = 0.9$ (yellow curves) and $\rho = 1$ (purple curves).

The behaviour shown in Figures 5.25 and 5.26 can be seen for a range of initial biomass and this is summarised in Figure 5.27. In this figure, we show a contour plot of the biomass value, as a % of the long-time equilibrium biomass value, i.e. for the P_2 equilibrium point, as a function of initial biomass B_0, and time. As the fractional order decreases, the time taken to reach 90% of the equilibrium biomass value increases, i.e. the system is slower in its approach to equilibrium. The fractional derivative order is therefore acting as 'inertia' in the system.

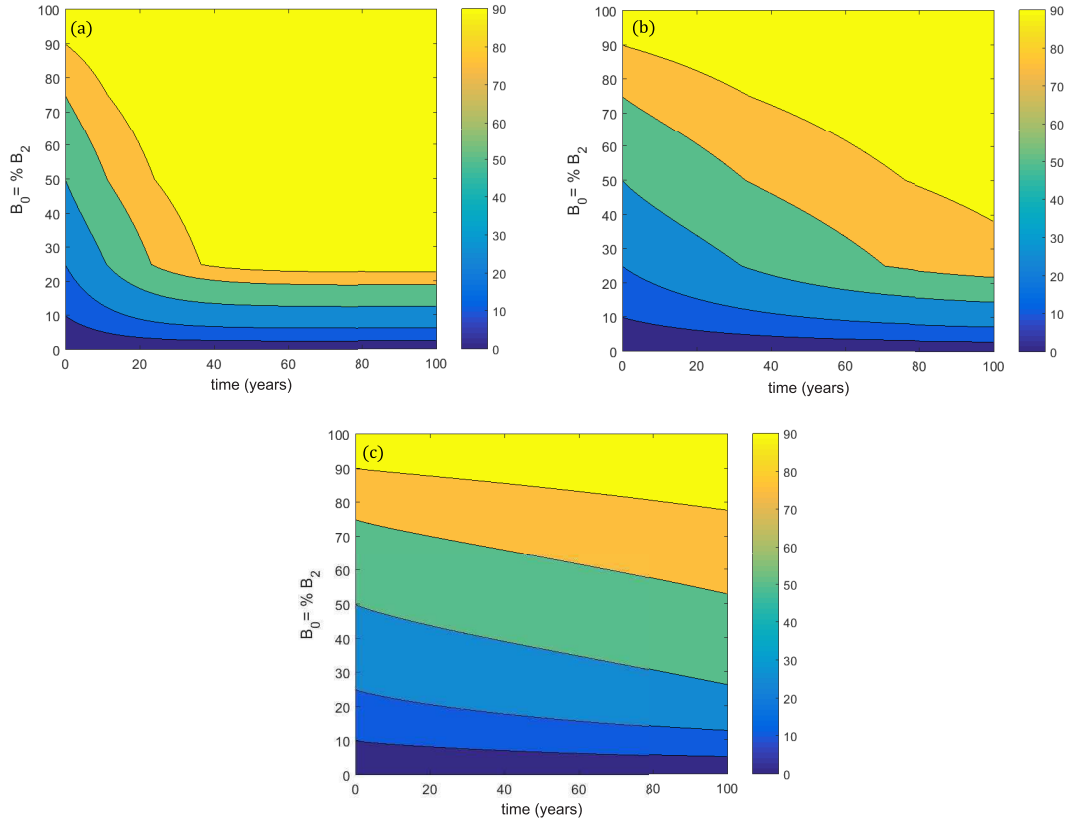

Figure 5.27: Contour plot of the biomass value, as a % of the equilibrium biomass value of P_2, as a function of initial biomass B_0, and time for fractional derivative orders (a) $\rho = 0.95$. (b) $\rho = 0.90$. (c) $\rho = 0.85$.

In the second situation we consider a value of r_0 less than r_{c1} and where the initial condition is the equilibrium state for value of r_0 above r_{c1} while changing the initial value of the biomass. In this case, the rainfall therefore switches from a high to a low value.

In the second case, the constant value of rainfall $r_0 = 0.5r_{c1}$ is chosen as the low value of rainfall, for which there is one equilibrium point, $P_1 = (A_{11}, 0, H_1) = (1.0086 \times 10^{-7}, 0, 0.0220)$, which is a stable point. The behaviour of the system is now investigated for a range of different initial conditions. In this case, we choose the initial condition to have the components, A_1 and H, for the nonzero biomass equilibrium point for $r_0 = 2r_{c1}$, i.e. $I_0 = (A_{12}, B_0, H_2) = (1.0252 \times 10^{-7}, B_0, 0.0182)$ where $B_0 = aB_2$, where $0 \leq B_0 \leq 2B_2$ with $B_2 = 0.1178$ is the equilibrium biomass for $r_0 = 2r_{c1}$.

We first choose the initial condition to be $I_0 = (1.0252 \times 10^{-7}, 0, 0.0182)$. In this case, and for all fractional orders, the results are the same as for the integer system. Since the biomass value remains at zero, the fractional order, which only

enters the biomass equation, does not change the system, and Figure 5.28 shows the numerical solution for a range of values of ρ in this case.

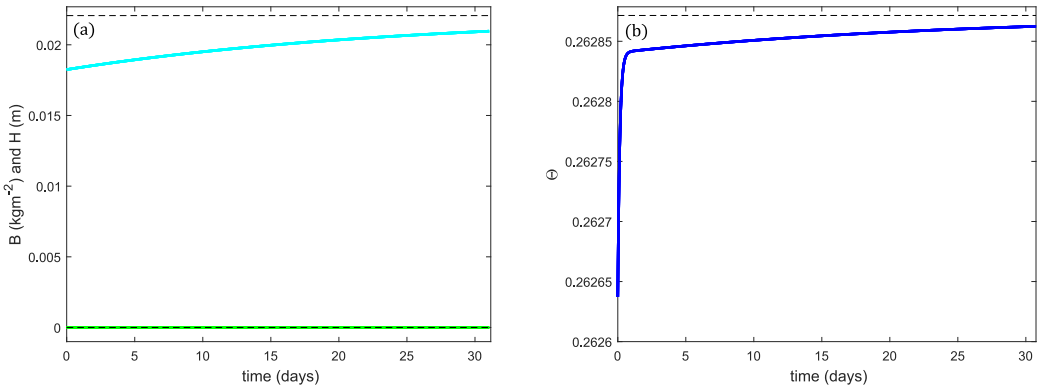

Figure 5.28: The dynamic behaviour of the fractional system where (a) the biomass B (green curve) and the surface water H (cyan curve), and (b) the soil water content Θ, for $r_0 = 0.5r_{c1}$, initial condition $I_0 = (1.0252 \times 10^{-7}, 0, 0.0182)$, and fractional orders $\rho = 0.5, 0.6, 0.7, 0.8, 0.9, 1$.

We now consider nonzero initial biomass values of B_0. This system models the situation where, after a period of high rainfall, the biomass is then reduced as the rainfall decreased to $r_0 < r_{c1}$. Figure 5.29 and Figure 5.30 show the cases when $B_0 = 0.5B_2$ and $1.5B_2$, respectively. In these figures, for all fractional orders, the value of the biomass decreases to the integer system equilibrium value. These figures also show that the surface water and water content in the soil decreased at the beginning of the simulation and then increased to approach the integer system equilibrium values. However, the time needed to approach the equilibrium point P_1 increases as the fractional order, ρ, decreases. This delay in reaching equilibrium for smaller values of ρ indicates that memory is acting in a similar way to inertia. This means that the loss of biomass is smaller for smaller α which again means the longer the memory is then the slower the loss of biomass.

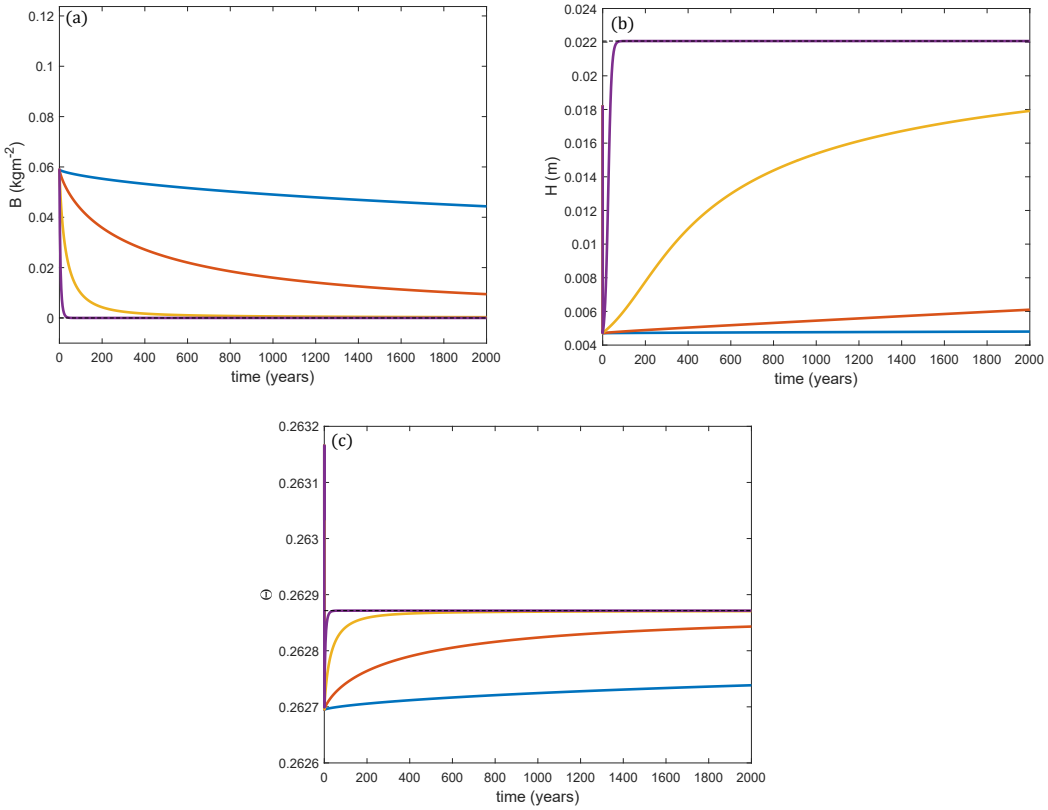

Figure 5.29: For initial condition $I_0 = (1.0252 \times 10^{-7}, 0.50 \times B_2, 0.01824)$, where $B_2 = 0.1178$, the dynamic behaviour of the fractional system where (a) biomass B, (b) surface water H, and (c) the soil water content Θ, for $r_0 = 0.5r_{c1}$ and for fractional orders $\rho = 0.7$ (blue curves), $\rho = 0.8$ (orange curves), $\rho = 0.9$ (yellow curves) and $\rho = 1$ (purple curves).

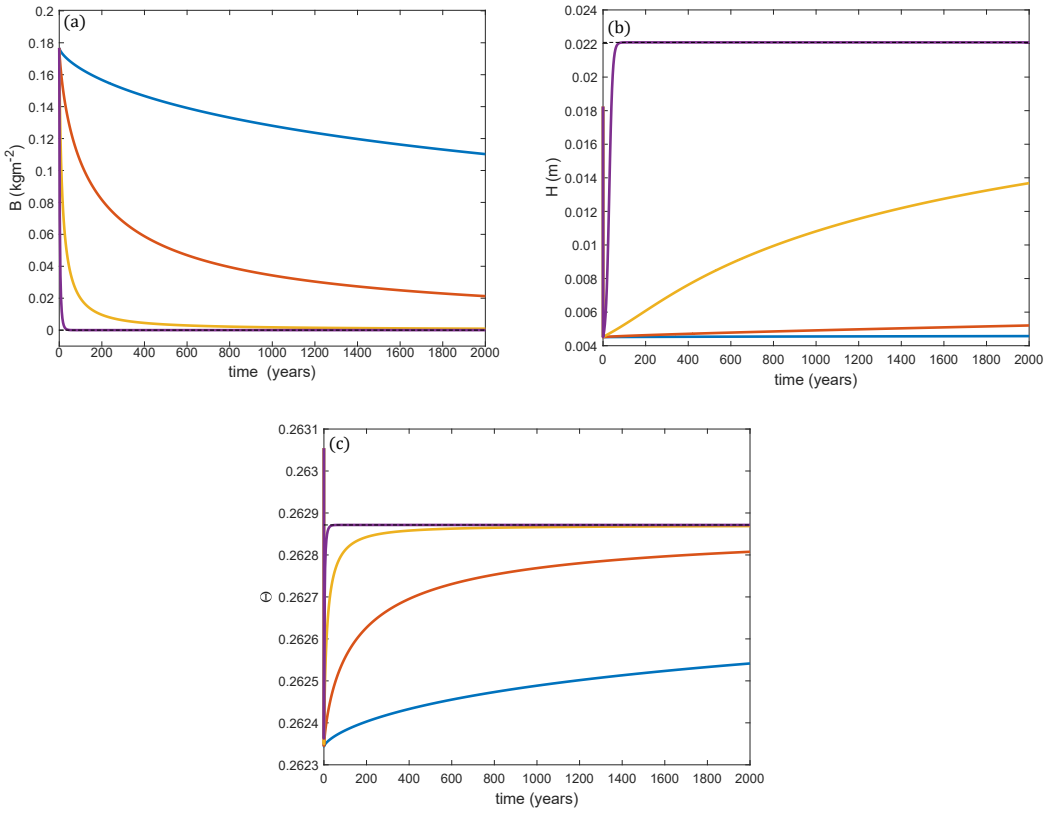

Figure 5.30: For initial condition $I_0 = (1.0252 \times 10^{-7}, 1.50 \times B_2, 0.01824)$, where $B_2 = 0.1178$, the dynamic behaviour of (a) biomass B, (b) surface water H, and (c) the water content Θ for $r_0 = 0.5r_{c1}$ and for fractional orders $\rho = 0.7$ (blue curves), $\rho = 0.8$ (orange curves), $\rho = 0.9$ (yellow curves) and $\rho = 1$ (purple curves).

The behaviour shown in Figures 5.28 to 5.30 is then summarised in Figure 5.31, where we show a contour plot of the biomass value, as a % of the long-time equilibrium biomass value, i.e. for the P_2 equilibrium point for the rainfall value for $t < 0$, as a function of initial biomass B_0, and time. As the fractional order decreases, the time taken to reach any particular level of the initial biomass value increases, i.e. the system is slower in its approach to equilibrium. Therefore, as in the previous case, the fractional order is acting as 'inertia' in the system.

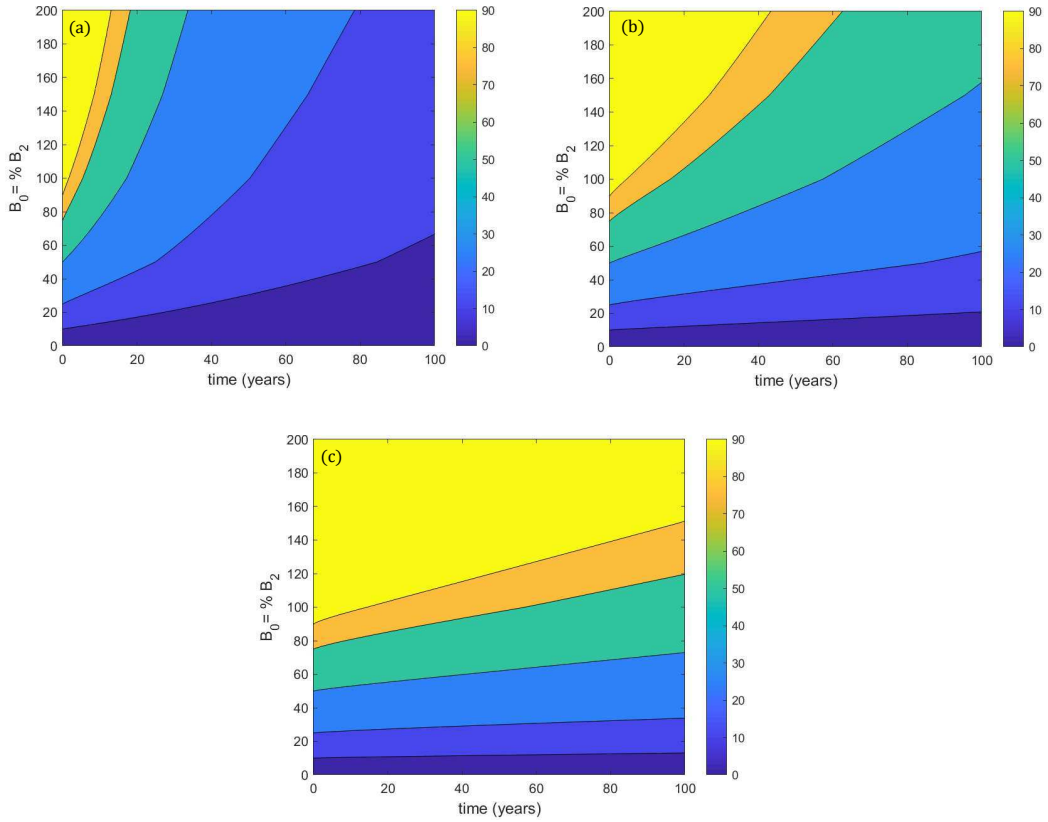

Figure 5.31: Contour plot of the biomass value, as a % of the initial equilibrium biomass value of P_2, as a function of initial biomass B_0, and time for fractional derivative orders (a) $\rho = 0.90$. (b) $\rho = 0.85$. (c) $\rho = 0.80$.

5.11.2 Time Dependent Rainfall

Consider now the effect of the fractional derivative on the model with periodic rainfall. As in the integer derivative case, we expect the important factors to be r_m and T. Therefore, in the simulations, we consider two values of r_m, $r_m > r_{c1}$ and $r_m < r_{c1}$. The dynamic behaviour is then studied for different periods of time, T, namely $T = 1$ day, 1 week, 30 days and 6 months. As in the integer system, the maximum values of the rainfall that are considered in the following simulations, are $r_m = 4r_{c1}$ and $r_m = 0.5r_{c1}$.

For $r_m = 4r_{c1}$ case, we choose the initial conditions for the soil and surface water as the equilibrium point when $r_0 = 0.5r_{c1}$. For the biomass, as in the integer case, we assume a level of biomass to be related to the biomass of the second component of the second equilibrium point when $r_0 = 2r_{c1}$, which is $B_2 = 0.1178$. This system investigates how, in a fractional system, after drought conditions a large amount of biomass initially grows when rain occurs. Figure 5.32 shows the behaviour of the fractional system in this model with the average biomass oscillating about the

equilibrium value when we run the system for long periods of time.

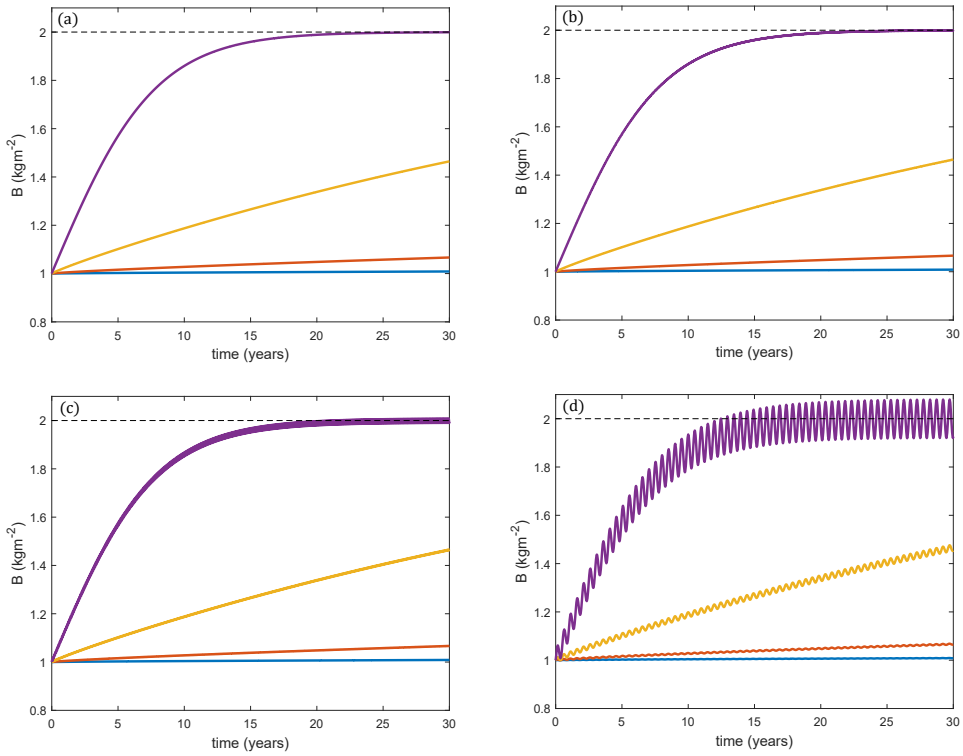

Figure 5.32: The dynamic behaviour of the biomass in the fractional system, for the fractional orders $\rho = 0.7$ (blue curves), $\rho = 0.8$ (orange curves), $\rho = 0.9$ (yellow curves) and $\rho = 1$ (purple curves) where $r_m = 4r_{c1}$. (a) $T = 1$ day. (b) $T = 1$ week. (c) $T = 30$ days. (d) $T = 6$ months.

For the $r_m = 0.5r_{c1}$ case, we choose the initial condition as the stable equilibrium point when $r_0 = 2r_{c1}$ in order to model a situation where a period of drought ($r_m < r_{c1}$) occurs after a period of rainfall ($r_m > r_{c1}$). Figure 5.33 shows the behaviour of the fractional system in this model with the average biomass oscillating about the equilibrium value when we run the system for long periods of time, the plot looks the same but at higher T a difference is seen.

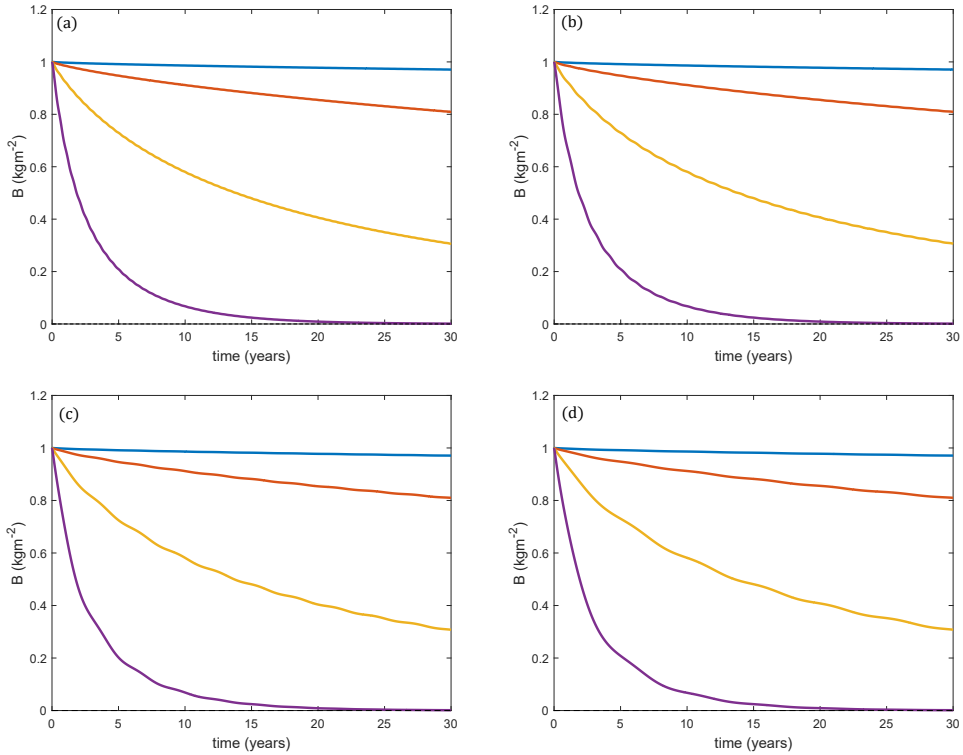

Figure 5.33: The dynamic behaviour of the biomass and the surface water in the fractional system, for the fractional orders $\rho = 0.7$ (blue curves), $\rho = 0.8$ (orange curves), $\rho = 0.9$ (yellow curves) and $\rho = 1$ (purple curves) where $r_m = 0.5r_{c1}$. (a) $T = 6$ months. (b) $T = 1$ year. (c) $T = 3$ years. (d) $T = 5$ years.

In the fractional system we have therefore seen similar behaviour to the integer system, with the biomass value stabilising to oscillate around the biomass value of the equilibrium point when the rainfall is a constant.

Figure 5.34 shows the long-term behaviour of the biomass for different values of r_m and fractional order, where we see that the average biomass when $r = r(t)$ is the same value of the biomass when rainfall is constant and $r_0 = r_m/2$. It is again clear that reducing ρ leads to a delay in B reaching its long-term behaviour, i.e. the fractional order is behaving as a type of inertia in the system.

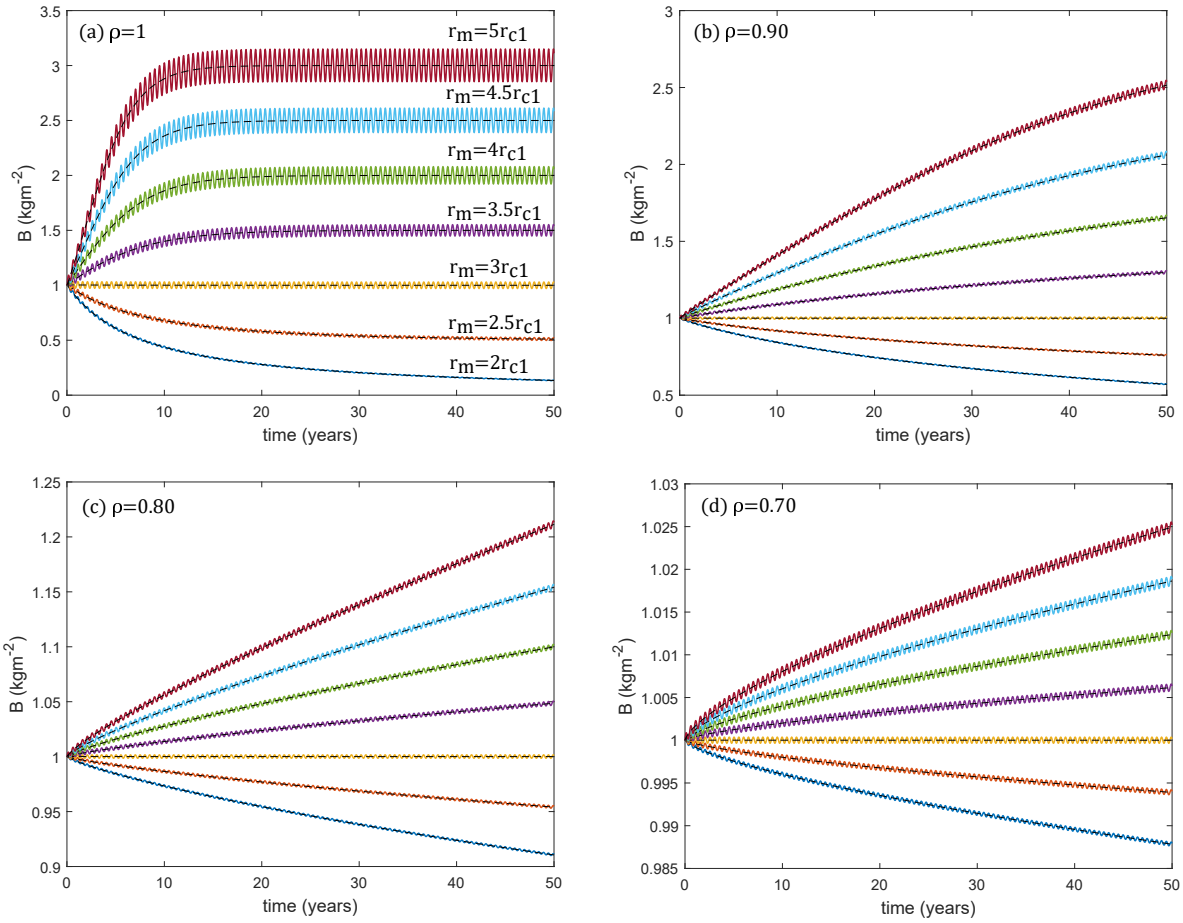

Figure 5.34: Biomass trajectory as a function of time for the time dependent for different values of r_m, for both the periodic rainfall model (coloured lines) and the constant rainfall model (black dashed line) when $T = 6$ months for different fractional orders. (a) $\rho = 1$. (b) $\rho = 0.9$. (c) $\rho = 0.8$. (d) $\rho = 0.7$.

5.12 Conclusion

In this chapter we have developed models of plant-water-soil interactions and considered effects of memory, modelled by a fractional derivative, in the plant biomass equation.

In the first model we considered, the interaction of the biomass, surface water and soil water were considered in a similar way to Dagbovie and Sherratt [24] but without spatial derivatives. The stability of the integer system was considered and it was found that in an incommensurate version of this model, one of the unstable equilibrium points could be stable in a fractional system.

The second model we considered includes a more accurate representation of the soil water and the uptake by plant roots of this soil water. In this system soil water was modelled through the Richards equation. We were able to analytically find the steady state solution and, in a simplified case, the transient solution for this model. We then numerically investigated two cases for time-dependent rainfall, the first one being when the rainfall is constant and the second being when it depends on time. We found that the long-term behaviour of the biomass can be related to the time-averaged rainfall value.

In the final section of this chapter, we studied the incommensurate form of the previous system, where a fractional order replaced the order one derivative in the only biotic component, the biomass, in order to model memory effects. In this model, since, when it existed, the only non-trivial state was always stable, the presence of a fractional derivative did not affect the stability of the system. The key differences between the fractional and integer model were therefore only observed in the long-term behaviour. When the fractional order is decreased the system takes longer to approach a regular periodic solution.

The main results in this chapter are in the development of new, integer and fractional, differential equation models of plant-water interaction. The single mode Richards equation model would certainly be interesting to consider in further work.

Chapter 6

Conclusion

6.1 Overall Conclusions

This thesis has shed light on the effects of fractional derivatives on the stability of various mathematical models. In particular, it has investigated commensurate and incommensurate predator-prey models to show these effects. In the beginning, we recalled that the Lotka-Volterra model can be viewed as the foundation of all subsequent predator-prey models. We formulated integer differential equation models into those using fractional derivatives. In general, the reformulated models are useful for considering distributed memory effects, in particular finding stable equilibrium points that are unstable in the integer model or investigating the fractional order dependence of the time taken to approach equilibrium point.

In Chapter 3, by studying a fractional order predator-prey model, we found that through the variation of the fractional order it is possible to transition from a monostable to a bistable system. By bistable system, we are referring to a system with two stable equilibrium points. The transient behaviour of this fractional system, in particular the dependence of trajectories on the initial states, was found. Moreover, we found the observed domains of attraction of the two stable points changed as the fractional order was changed [4].

Chapter 4 gives a more complete investigation of the predator-prey model studied in Chapter 3 by extending this model using an incommensurate fractional system. An incommensurate system is a more realistic situation where each of the species has different fractional orders. We have shown that in this incommensurate system, decreasing the predator fractional order can change a stable equilibrium point to an unstable point, which cannot happen with the commensurate system, where decreasing the fractional order will only ever stabilise an unstable point. In order to determine if this change in stability is a more general result, we decided to consider another system, a model of plant-herbivore interaction. Our findings demonstrated that decreasing the predator fractional order may change the sta-

bility in the same way as in the commensurate system. In contrast, we found that decreasing the prey fractional order in the incommensurate system would create an unstable system, which is not be true in a commensurate system. We found an approximate analytical solution for the characteristic equation of the incommensurate system when the two fractional orders α and β are similar and were able to find an approximate analytic form of the stability boundary.

In Chapter 5, we adapted two models that consider the interaction between surface water, soil water and biomass. First, we used Dagbovie and Sheratt's model, without spatial derivatives. Then, we studied the stability of an equivalent incommensurate system which showed that in a fractional system one of the unstable points would become stable, so that the fractional derivative affects the stability of this model. Second, we adapted another model, similar to the Dagbovie and Sherratt model except that the soil water equation was replaced with the Richards equation. This equation is a more accurate depiction of soil water dynamics. We found the steady state solution for the Richards equation and its dynamical solution by using the Fourier series. We also found that a single mode was a good approximation for this solution. As a result, we developed a model containing three equations, and subsequently, investigated the equilibrium points for this system. The dynamic behaviour of the whole system was investigated for two rainfall states, constant rainfall and time-dependent rainfall. After that, we replaced the integer derivative in the biomass equation with a Caputo fractional derivative which resulted in an incommensurate system. However, in this system the fractional derivative did not affect the stability of the equilibrium points because the unstable equilibrium does not have complex eigenvalues. The only effect which resulted from the fractional system is in the time for the system to approach equilibrium. It should be noted that the work in this chapter has not been an area of focus in any previous studies.

The transient behaviour in commensurate systems studied in Chapter 3 has many useful possible applications. For example, the study of two different breeds of animals with possibly different inherent memory, modeled as different values of α to determine which breed stabilizes at a certain equilibrium, could use our model to determine which one would be preferable. Similarly, the incommensurate systems discussed in Chapter 4 could have ecological applications in that understanding the differences in memory between two species (i.e. the values of α and β) provides greater insight and accuracy when studying the complexities of a particular ecosystem. Chapter 5, which focuses on interactions of biomass, surface water and soil water, can also prove useful in the study of rainfall in semi-arid regions, where the amount of surface and soil water is affected by many factors, but most of all rainfall. Our model could help determine the amount of biomass that is needed to protect an area that has been affected by drought so that the system is sustainable until the next occurrence of rain. It would also be useful in

agriculture and crop production to determine plant productivity under different rainfall conditions.

6.2 Future Work and Extensions

The work in this thesis can be extended in many ways. In our system, both our predator and prey were healthy, but a possible future area of focus is where diseases affect the predator–prey interaction. This would involve introducing new species into our equations, and the model would then be extended to an ecoepidemic model with healthy prey, infected prey, healthy predators, and infected predators. This addition to our models would be useful in the field of ecology because it would reflect a realistic ecosystem where predators might only catch infected prey or only avoid infected prey because these prey are in some way unacceptable. It would be possible to allow infected and healthy populations a different value of memory. More realistic models would mean that ecologists and wildlife biologists are better able to predict future occurrences of disease in ecosystems.

In terms of our work in Chapter 3, further investigation of the fine structure of the boundaries of the domain of attraction is necessary, although this will also depend on the value of t_{end} that is used. This investigation may, for instance, uncover fractal domains of attraction such as those found in systems of delay-differential equations [119]. Of course, without a satisfactory link between a model of memory function and the fractional derivative model of population dynamics this is only speculation, but an understanding of the changes in the domains of attraction as a function of α may prove useful for a comparison between experimental or field trial work and theoretical models.

In terms of the $BH\Phi$ model that is introduced in Chapter 5, we could add a spatial derivative as Dagbovie and Sherratt do in their model. We could also have used the fractional form of the Richards equation by adding the fractional spatial derivatives, which are often used to model the porous nature of soil. Further models of the root density dependence on B could also be considered.

In summary, although we have developed a deeper understanding of the effects of commensurate and incommensurate fractional predator-prey systems, there is much to be discovered in future work.

Appendix A

Appendix of Chapter 4

A.1 The Value of the Real and Imaginary Parts of λ^{α}

Let $Q = -{J_{11}}^2 + 2J_{11}J_{22} - 4J_{12}J_{21} - {J_{22}}^2$, then

$$x = -\frac{(J_{11}+J_{22})\left({J_{11}}^2 - 2J_{11}J_{22} + 4J_{12}J_{21} + {J_{22}}^2\right)}{2Q}, \tag{A.1}$$

$$y = -\frac{{J_{11}}^2 - 2J_{11}J_{22} + 4J_{12}J_{21} + {J_{22}}^2}{2\sqrt{Q}}, \tag{A.2}$$

also,

$$\begin{aligned} x_1 =& \frac{1}{2Q^{3/2}}\Bigg[\Bigg[\left(J_{11}/4 - J_{22}/4\right)Q^{3/2} + 1/4\left(J_{11}+J_{22}\right)\left({J_{11}}^2 - 2J_{11}J_{22}\right. \\ &\left. + 4J_{12}J_{21} + {J_{22}}^2\right)\sqrt{Q}\Bigg]\ln(J_{11}^2 + 2J_{11}J_{22} + J_{22}^2 + Q) + Q\big(J_{11}J_{22} \\ &- 2J_{12}J_{21} - {J_{22}}^2\big)\arctan\left(\sqrt{Q}, J_{11}+J_{22}\right) - \frac{1}{2}\Bigg(\left(J_{11}-J_{22}\right)Q^{3/2} \\ &+ \left(J_{11}+J_{22}\right)\left({J_{11}}^2 - 2J_{11}J_{22} + 4J_{12}J_{21} + {J_{22}}^2\right)\sqrt{Q}\Bigg)\ln(2)\Bigg], \end{aligned} \tag{A.3}$$

$$\begin{aligned} y_1 =& \frac{-1}{4Q^{3/2}}\Bigg[Q\left(J_{11}J_{22} - 2J_{12}J_{21} - {J_{22}}^2\right)\ln\left({J_{11}}^2 + 2J_{11}J_{22} + {J_{22}}^2 + Q\right) \\ &+ \Bigg(\left(-J_{11}+J_{22}\right)Q^{3/2} - \left({J_{11}}^2 - 2J_{11}J_{22} + 4J_{12}J_{21} + {J_{22}}^2\right)\sqrt{Q}\big(J_{11} \\ &+ J_{22}\big)\Bigg)\arctan\left(\sqrt{Q}, J_{11}+J_{22}\right) - 2\,Q\ln(2)\left(J_{11}J_{22} - 2J_{12}J_{21} - {J_{22}}^2\right)\Bigg] \end{aligned} \tag{A.4}$$

$$
\begin{aligned}
x_2 = \Bigg[& -1/2 J_{22}\sqrt{Q}\left({J_{11}}^2 - 2J_{11}J_{22} + 4J_{12}J_{21} + {J_{22}}^2\right)\Bigg(\ln\left({J_{11}}^2\right. \\
& \left. + 2J_{11}J_{22} + {J_{22}}^2 + Q\right)^2\Bigg) + \Bigg(\Big(-{J_{22}}^4 + 2J_{11}{J_{22}}^3 + \big(-6J_{12}J_{21} \\
& + Q\big){J_{22}}^2 - 2J_{11}\big({J_{11}}^2 + 2J_{12}J_{21} + Q\big)J_{22} + \left({J_{11}}^2 + 2\,J_{12}J_{21}\right)\left({J_{11}}^2\right. \\
& \left. + Q\right)\Big)\arctan\left(\sqrt{Q}, J_{11} + J_{22}\right) + \left(-J_{11} + J_{22}\right)Q^{3/2} - \Bigg(-2\,J_{22} \\
& \left({J_{11}}^2 - 2J_{11}J_{22} + 4J_{12}J_{21} + {J_{22}}^2\right)\ln(2) + \left(J_{11} + J_{22}\right)\left({J_{11}}^2\right. \\
& \left. - 2J_{11}J_{22} + 2J_{12}J_{21} + {J_{22}}^2\right)\Bigg)\sqrt{Q}\Bigg)\ln\left({J_{11}}^2 + 2J_{11}J_{22} + {J_{22}}^2\right. \\
& \left. + Q\right) + 2J_{22}\sqrt{Q}\big({J_{11}}^2 - 2J_{11}J_{22} + 4J_{12}J_{21} + {J_{22}}^2\big) \qquad \text{(A.5)} \\
& \left(\arctan\left(\sqrt{Q}, J_{11} + J_{22}\right)\right)^2 + \Bigg(\Big(2{J_{22}}^4 - 4J_{11}{J_{22}}^3 + \big(12J_{12}J_{21} \\
& - 2Q\big){J_{22}}^2 + 4J_{11}\left({J_{11}}^2 + 2J_{12}J_{21} + Q\right)J_{22} - 2\left({J_{11}}^2 + 2J_{12}J_{21}\right) \\
& \left({J_{11}}^2 + Q\right)\Big)\ln(2) - 4Q\left(J_{11}J_{22} - J_{12}J_{21} - {J_{22}}^2\right)\Bigg) \\
& \arctan\left(\sqrt{Q}, J_{11} + J_{22}\right) + 2\Bigg(\left(J_{11} - J_{22}\right)Q^{3/2} + 2\sqrt{Q}\Bigg(-J_{22} \\
& \left({J_{11}}^2 - 2J_{11}J_{22} + 4J_{12}J_{21} + {J_{22}}^2\right)\ln(2) + \left(J_{11} + J_{22}\right)\left({J_{11}}^2 - 2J_{11}J_{22}\right. \\
& \left. + 2J_{12}J_{21} + {J_{22}}^2\right)\Bigg)\Bigg)\ln(2)\Bigg]\left(\frac{1}{8Q^{3/2}}\right),
\end{aligned}
$$

$$
\begin{aligned}
y_2 = & \Bigg[\Bigg(1/4 {J_{22}}^4 - 1/2 J_{11} {J_{22}}^3 + \left(-Q/4 + 3/2 J_{12} J_{21}\right) {J_{22}}^2 + 1/2 J_{11} \big({J_{11}}^2 \\
& + 2 J_{12} J_{21} + Q \big) J_{22} - 1/4 \left({J_{11}}^2 + 2 J_{12} J_{21} \right) \left({J_{11}}^2 + Q \right) \Bigg) \\
& \ln \left({J_{11}}^2 + 2 J_{11} J_{22} + {J_{22}}^2 + Q \right)^2 + \Bigg(- 2 J_{22} \sqrt{Q} \big({J_{11}}^2 - 2 J_{11} J_{22} \\
& + 4 J_{12} J_{21} + {J_{22}}^2 \big) \arctan \left(\sqrt{Q}, J_{11} + J_{22} \right) + \Big(- {J_{22}}^4 + 2 J_{11} {J_{22}}^3 \\
& + \big(- 6 J_{12} J_{21} + Q \big) {J_{22}}^2 - 2 J_{11} \left({J_{11}}^2 + 2 J_{12} J_{21} + Q \right) J_{22} + \big({J_{11}}^2 \\
& + 2 J_{12} J_{21} \big) \left({J_{11}}^2 + Q \right) \Big) \ln (2) + 2 Q \left(J_{11} J_{22} - J_{12} J_{21} - {J_{22}}^2 \right) \Bigg) \\
& \ln \left({J_{11}}^2 + 2 J_{11} J_{22} + {J_{22}}^2 + Q \right) + \Big(- {J_{22}}^4 + 2 J_{11} {J_{22}}^3 + \big(- 6 J_{12} J_{21} \\
& + Q \big) {J_{22}}^2 - 2 J_{11} \left({J_{11}}^2 + 2\, J_{12} J_{21} + Q \right) J_{22} + \left({J_{11}}^2 + 2 J_{12} J_{21} \right) \left({J_{11}}^2 \right. \\
& \left. + Q \big) \Big) \arctan \left(\sqrt{Q}, J_{11} + J_{22} \right)^2 + \Bigg(\left(-2 J_{11} + 2 J_{22} \right) Q^{3/2} - 2 \Big(- 2 J_{22} \\
& \left({J_{11}}^2 - 2 J_{11} J_{22} + 4 J_{12} J_{21} + {J_{22}}^2 \right) \ln (2) + \left(J_{11} + J_{22} \right) \left({J_{11}}^2 - 2 J_{11} J_{22} \right. \\
& \left. + 2 J_{12} J_{21} + {J_{22}}^2 \right) \Big) \sqrt{Q} \Bigg) \arctan \left(\sqrt{Q}, J_{11} + J_{22} \right) - \Bigg(\Big(- {J_{22}}^4 \\
& + 2 J_{11} {J_{22}}^3 + \left(-6 J_{12} J_{21} + Q \right) {J_{22}}^2 - 2 J_{11} \left({J_{11}}^2 + 2 J_{12} J_{21} + Q \right) J_{22} \\
& + \left({J_{11}}^2 + 2 J_{12} J_{21} \right) \left({J_{11}}^2 + Q \right) \Big) \ln (2) + 4 Q \left(J_{11}\, J_{22} - J_{12} J_{21} - {J_{22}}^2 \right) \Bigg) \\
& \ln (2) \Bigg] \left(\frac{1}{8\, Q^{3/2}} \right).
\end{aligned}
\tag{A.6}
$$

Appendix B

Appendix of Chapter 5

B.1 Proving $F''(0)$ is Negative

We investigate the sign of $F''(0)$ to understand when B_2 is a physical solution. From (5.39), we have

$$\begin{aligned} F''(B) =& \frac{d}{dB}\left(c(S_0c_1)\frac{d}{dB}\left(\frac{1-e^{-\Lambda_1 L}}{\Lambda_1}\right)+c\left(S_0\frac{dc_1}{dB}+\frac{dS_0}{dB}c_1\right)\left(\frac{1-e^{-\Lambda_1 L}}{\Lambda_1}\right)\right) \\ &+\frac{d}{dB}\left(c(S_0c_2)\frac{d}{dB}\left(\frac{1-e^{-\Lambda_2 L}}{\Lambda_2}\right)+c\left(S_0\frac{dc_2}{dB}+\frac{dS_0}{dB}c_2\right)\left(\frac{1-e^{-\Lambda_2 L}}{\Lambda_2}\right)\right). \end{aligned} \tag{B.1}$$

Using (5.25) in (B.1), we obtain

$$\begin{aligned} F''(0) =& 2c\frac{dS_0}{dB}\Bigg[c_1\frac{d}{dB}\left(\frac{1-e^{-\Lambda_1 L}}{\Lambda_1}\right)+\frac{dc_1}{dB}\left(\frac{1-e^{-\Lambda_1 L}}{\Lambda_1}\right) \\ &+c_2\frac{d}{dB}\left(\frac{1-e^{-\Lambda_2 L}}{\Lambda_2}\right)+\frac{dc_2}{dB}\left(\frac{1-e^{-\Lambda_2 L}}{\Lambda_2}\right)\Bigg]_{B=0}. \end{aligned} \tag{B.2}$$

From (5.25), (5.35), (5.36) and (5.37), in (B.2) we then obtain

$$\begin{aligned} F''(0) =& -\frac{c(-4e^{\alpha(L+\Psi_1)}\alpha L+2e^{\alpha(2L+\Psi_1)}-2e^{\alpha\Psi_1})\chi_0^2R_{max}^2e^{-2\alpha L}}{\alpha^2B_0^2K_s} \\ &-\frac{c((\alpha^2L^2-4)e^{2\alpha L}+(6\alpha L+2)e^{L\alpha}+2)\chi_0^2R_{max}^2e^{-2\alpha L}r_0}{\alpha^2B_0^2K_s^2}. \end{aligned} \tag{B.3}$$

If we put $x=\alpha L$, then (B.3) can be written as

$$\begin{aligned} F''(0) =& -\frac{c(-4xe^x+2e^{2x}-2)e^{\alpha\Psi_1}\chi_0^2R_{max}^2e^{-2x}}{\alpha^2B_0^2K_s} \\ &-\frac{c((x^2-4)e^{2x}+(6x+2)e^x+2)\chi_0^2R_{max}^2e^{-2x}r_0}{\alpha^2B_0^2K_s^2}. \end{aligned} \tag{B.4}$$

If we set $Y_1 = -4xe^x + 2e^{2x} - 2$, the functional form of the first term in (B.4), then by using the series expansion for Y_1', we obtain

$$Y_1' = 4e^x \left(\frac{x^2}{2!} + \frac{x^3}{3!} + ... \right),$$

which shows that $Y_1' > 0$ for all $x > 0$. Therefore, Y_1 shown in Figure B.1(a) will always be positive. Setting $Y_2 = (x^2 - 4)e^{2x} + (6x + 2)e^x + 2$, the functional form of the second term in (B.4), then by using the series expansion for Y_2', we obtain

$$Y_2' = e^x \left(\frac{5}{3}x^3 + x^4 + \frac{7}{20}x^5 + ... \right),$$

which shows that $Y_2' > 0$ for all $x > 0$. Therefore, Y_2 shown in Figure B.1(b) will be always positive. Therefore, $F''(0) < 0$.

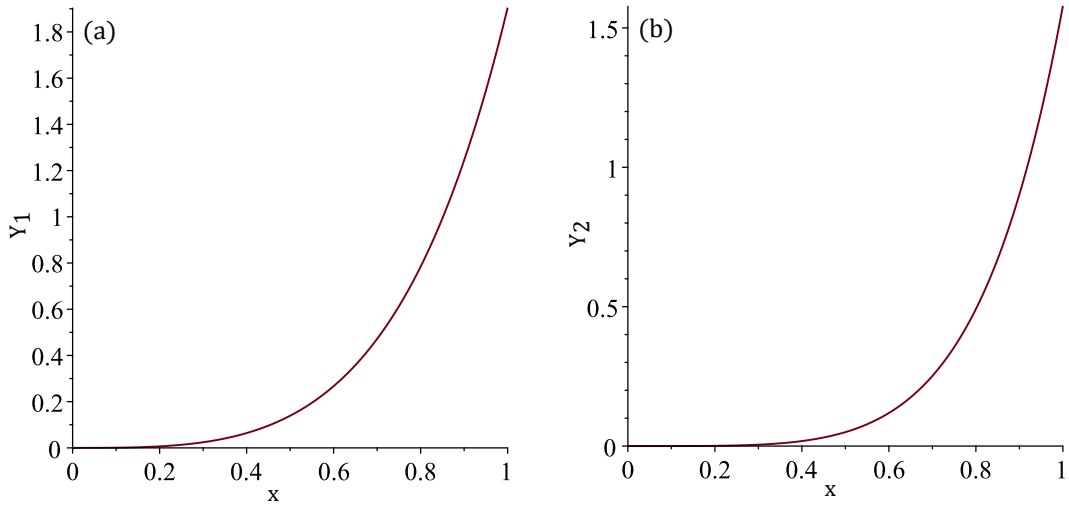

Figure B.1: Plots of Y_1 (a) and Y_2 (b) as functions of x.

B.2 The Value of G_{11}, G_{12}, G_{13} and G_{14}.

Here we will find the integrals in (5.61). The first integral is:

$$\begin{aligned}
\int_{-L}^{0}\left(\sin(q_1z)-\frac{q_1}{\alpha}\cos(q_1z)\right)^2dz &= \int_{-L}^{0}\left(\sin^2(q_1z)-\frac{q_1}{\alpha}\sin(2q_1z)+\frac{q_1^2}{\alpha^2}\cos^2(q_1z)\right)dz\\
&=\int_{-L}^{0}\frac{1}{2}(1-\cos 2q_1z)dz-\frac{q_1}{\alpha}\int_{-L}^{0}\sin(2q_1z)dz\\
&\quad+\frac{q_1^2}{\alpha^2}\int_{-L}^{0}\frac{1}{2}(1+\cos 2q_1z)dz\\
&=\frac{1}{2}\left(z-\frac{\sin(2q_1z)}{2q_1}\right)\Bigg|_{-L}^{0}+\frac{q_1}{\alpha}\frac{\cos(2q_1z)}{2q_1}\Bigg|_{-L}^{0}\\
&\quad+\frac{q_1^2}{2\alpha^2}\left(z+\frac{\sin(2q_1z)}{2q_1}\right)\Bigg|_{-L}^{0}\\
&=-\frac{1}{2}\left(-L-\frac{\sin(-2q_1L)}{2q_1}\right)+\frac{q_1}{\alpha}\left(\frac{1}{2q_1}\right.\\
&\quad\left.-\frac{1}{2q_1}\cos(-2q_1L)\right)-\frac{q_1^2}{2\alpha^2}\left(-L+\frac{\sin(-2q_1L)}{2q_1}\right)\\
&=\frac{1}{2}\left(L+\frac{\sin(-2q_1L)}{2q_1}\right)+\frac{q_1}{\alpha}\left(\frac{1}{2q_1}\right.\\
&\quad\left.-\frac{1}{2q_1}\cos(-2q_1L)\right)+\frac{q_1^2}{2\alpha^2}\left(L-\frac{\sin(-2q_1L)}{2q_1}\right)\\
&=\frac{1}{2}\left(L-\frac{\sin(2q_1L)}{2q_1}\right)+\frac{q_1}{\alpha}\left(\frac{1}{2q_1}-\frac{1}{2q_1}\cos(2q_1L)\right)\\
&\quad+\frac{q_1^2}{2\alpha^2}\left(L+\frac{\sin(2q_1L)}{2q_1}\right)\\
&=\frac{L}{2}-\frac{\sin(2q_1L)}{4q_1}+\frac{1}{2\alpha}-\frac{1}{2\alpha}\cos(2q_1L)\\
&\quad+\frac{q_1^2L}{2\alpha^2}+\frac{q_1^2\sin(2q_1L)}{4\alpha^2q_1},
\end{aligned}$$

therefore,

$$\begin{aligned}
G_{11} &= \int_{-L}^{0}\left(\sin(q_1z)-\frac{q_1}{\alpha}\cos(q_1z)\right)^2dz\\
&= \frac{L}{2}\left(1+\frac{q_1^2}{\alpha^2}\right)+\frac{1}{2\alpha}+\frac{\sin(2q_1L)}{4}\left(\frac{-1}{q_1}+\frac{q_1}{\alpha^2}\right)-\frac{1}{2\alpha}\cos(2q_1L).
\end{aligned}\tag{B.5}$$

The second integral is:

$$\begin{aligned}\int_{-L}^{0}\left(\cos(q_1z)+\frac{q_1}{\alpha}\sin(q_1z)\right)\left(\sin(q_1z)-\frac{q_1}{\alpha}\cos(q_1z)\right)dz &= \int_{-L}^{0}\Big[\sin(q_1z)\cos(q_1z)\\ &+\frac{q_1}{\alpha}\sin^2(q_1z)-\frac{q_1}{\alpha}\cos^2(q_1z)-\frac{q_1^2}{\alpha^2}\sin(q_1z)\cos(q_1z)\Big]dz\\ &=\int_{-L}^{0}(1-\frac{q_1^2}{\alpha^2})\sin(q_1z)\cos(q_1z)dz\\ &+\int_{-L}^{0}\frac{q_1}{\alpha}(\sin^2(q_1z)-\cos^2(q_1z))dz\\ &=\left(1-\frac{q_1^2}{\alpha^2}\right)\frac{(\sin(q_1z))^2}{2q_1}\Bigg|_{-L}^{0}+\frac{q_1}{2\alpha}\left(z-\frac{\sin(2q_1z)}{2q_1}\right)\Bigg|_{-L}^{0}\\ &-\frac{q_1}{2\alpha}\left(z+\frac{\sin(2q_1z)}{2q_1}\right)\Bigg|_{-L}^{0}\\ &=-\left(1-\frac{q_1^2}{\alpha^2}\right)\frac{(\sin(q_1L))^2}{2q_1}+\frac{q_1}{2\alpha}\left(L-\frac{\sin(2q_1L)}{2q_1}\right)\\ &+\frac{q_1}{2\alpha}\left(-L-\frac{\sin(2q_1L)}{2q_1}\right)\\ &=-\left(1-\frac{q_1^2}{\alpha^2}\right)\frac{(\sin(q_1L))^2}{2q_1}-\frac{q_1}{2\alpha}\frac{\sin(2q_1L)}{2q_1}\\ &-\frac{q_1}{2\alpha}\frac{\sin(2q_1L)}{2q_1}\end{aligned}$$

therefore,

$$\begin{aligned}G_{12}&=\int_{-L}^{0}\left(\cos(q_1z)+\frac{q_1}{\alpha}\sin(q_1z)\right)\left(\sin(q_1z)-\frac{q_1}{\alpha}\cos(q_1z)\right)dz\\ &=\left(\frac{q_1}{2\alpha^2}-\frac{1}{2q_1}\right)(\sin(q_1L))^2-\frac{1}{2\alpha}\sin(2q_1L).\end{aligned}\tag{B.6}$$

The third integral is:

$$\begin{aligned}\int_{-L}^{0}(\sin(q_1z)-\frac{q_1}{\alpha}\cos(q_1z))dz &=-\left(\frac{\cos(q_1z)}{q_1}\right)\Bigg|_{-L}^{0}-\frac{q_1}{\alpha}\left(\frac{\sin(q_1z)}{q_1}\right)\Bigg|_{-L}^{0}\\ &=-\left(\frac{1}{q_1}-\frac{\cos(-q_1L)}{q_1}\right)-\frac{1}{\alpha}\left(-\sin(-q_1L)\right),\end{aligned}$$

therefore,

$$G_{13}=\int_{-L}^{0}(\sin(q_1z)-\frac{q_1}{\alpha}\cos(q_1z))dz=-\frac{1}{q_1}+\frac{\cos(q_1L)}{q_1}-\frac{\sin(q_1L)}{\alpha}.\tag{B.7}$$

The fourth integral, which we found by using the integral by parts method, is

$$\begin{aligned}
\int_{-L}^{0} z\left(\sin(q_1 z) - \frac{q_1}{\alpha}\cos(q_1 z)\right) dz &= \int_{-L}^{0} z\sin(q_1 z)dz - \frac{q_1}{\alpha}\int_{-L}^{0} z\cos(q_1 z)dz \\
&= -\frac{z\cos(q_1 z)}{q_1}\bigg|_{-L}^{0} + \int_{-L}^{0}\frac{\cos(q_1 z)}{q_1}dz \\
&\quad - \frac{q_1}{\alpha}\left(\frac{z\sin(q_1 z)}{q_1}\bigg|_{-L}^{0} - \int_{-L}^{0}\frac{\sin(q_1 z)}{q_1}dz\right) \\
&= \left(-\frac{z\cos(q_1 z)}{q_1} + \frac{\sin(q_1 z)}{q_1^2}\right)\bigg|_{-L}^{0} \\
&\quad - \frac{q_1}{\alpha}\left(\frac{z\sin(q_1 z)}{q_1} + \frac{\cos(q_1 z)}{q_1^2}\right)\bigg|_{-L}^{0} \\
&= -\left(-\frac{-L\cos(-q_1 L)}{q_1} + \frac{\sin(-q_1 L)}{q_1^2}\right) \\
&\quad - \frac{q_1}{\alpha}\left(\frac{1}{q_1^2} - \left(\frac{-L\sin(-q_1 L)}{q_1} + \frac{\cos(-q_1 L)}{q_1^2}\right)\right) \\
&= -\left(\frac{L\cos(q_1 L)}{q_1} - \frac{\sin(q_1 L)}{q_1^2}\right) - \frac{q_1}{\alpha}\left(\frac{1}{q_1^2}\right. \\
&\quad \left. - \frac{L\sin(q_1 L)}{q_1} - \frac{\cos(q_1 L)}{q_1^2}\right) \\
&= -\frac{L\cos(q_1 L)}{q_1} + \frac{\sin(q_1 L)}{q_1^2} - \frac{1}{\alpha q_1} + \frac{L\sin(q_1 L)}{\alpha} \\
&\quad + \frac{\cos(q_1 L)}{\alpha q_1}
\end{aligned}$$

therefore,

$$\begin{aligned}
G_{14} = \int_{-L}^{0} z\left(\sin(q_1 z) - \frac{q_1}{\alpha}\cos(q_1 z)\right) dz &= \left(-L + \frac{1}{\alpha}\right)\frac{\cos(q_1 L)}{q_1} \\
&\quad + \left(\frac{L}{\alpha} + \frac{1}{q_1^2}\right)\sin(q_1 L) - \frac{1}{\alpha q_1}.
\end{aligned} \tag{B.8}$$

Bibliography

[1] E. Ahmed, A. El-Sayed, and H. El-Saka. Equilibrium points, stability and numerical solutions of fractional-order predator–prey and rabies models. *Journal of Mathematical Analysis and Applications*, 325:542–553, 2007.

[2] M. Akinlar, A. Secer, and M. Bayram. Stability, synchronization control and numerical solution of fractional Shimizu-Morioka dynamical system. *Applied Mathematics & Information Sciences*, 8:1699–1705, 2014.

[3] J. Alidousti, R. Ghaziani, and A. Eshkaftaki. Stability analysis of nonlinear fractional differential order systems with Caputo and Riemann–Liouville derivatives. *Turkish Journal of Mathematics*, 41:1260–1278, 2017.

[4] Z. Alqahtani, M. El-Shahed, and N. Mottram. Derivative-order-dependent stability and transient behaviour in a predator–prey system of fractional differential equations. *Letters in Biomathematics*, 6:32–49, 2019.

[5] B. Anderson, J. Jackson, and M. Sitharam. Descartes' rule of signs revisited. *The American Mathematical Monthly*, 105:447–451, 1998.

[6] R. Anderson and R. May. Regulation and stability of host-parasite population interactions: I. regulatory processes. *Journal of Animal Ecology*, 47:219–247, 1978.

[7] S. Arshad, D. Baleanu, J. Huang, Y. Tang, and M. Al Qurashi. Dynamical analysis of fractional order model of immunogenic tumors. *Advances in Mechanical Engineering*, 8:1–13, 2016.

[8] A. Atangana and A. Secer. A note on fractional order derivatives and table of fractional derivatives of some special functions. *Abstract and Applied Analysis*, 2013:1–8, 2013.

[9] S. Banerjee. *Mathematical Modeling: Models, analysis and Applications*. CRC Press, 2014.

[10] H. Basha. Multidimensional linearized nonsteady infiltration toward a shallow water table. *Water Resources Research*, 36:2567–2573, 2000.

[11] A. Belsky. Population and community processes in a mosaic grassland in the Serengeti, Tanzania. *The Journal of Ecology*, 74:841–856, 1986.

[12] L. Bolton, A. Cloot, S. Schoombie, and J. Slabbert. A proposed fractional-order Gompertz model and its application to tumour growth data. *Mathematical Medicine and Biology*, 32:187–209, 2015.

[13] J. Bonnar. *The Gamma Function*. Treasure Trove of Mathematics, 2017.

[14] O. Brandibur and E. Kaslik. Stability properties of a two-dimensional system involving one Caputo derivative and applications to the investigation of a fractional-order Morris-Lecar neuronal model. *Nonlinear Dynamics*, 90:2371–2386, 2017.

[15] O. Brandibur and E. Kaslik. Stability of two-component incommensurate fractional-order systems and applications to the investigation of a FitzHugh-Nagumo neuronal model. *Mathematical Methods in the Applied Sciences*, 41:7182–7194, 2018.

[16] M. Caputo. Linear models of dissipation whose q is almost frequency independent—II. *Geophysical Journal International*, 13:529–539, 1967.

[17] M. Caputo. The unknown set of memory constitutive equations of plastic media. *Progress in Fractional Differentiation and Applications*, 2:77–83, 2016.

[18] M. Caputo and C. Cametti. Diffusion with memory in two cases of biological interest. *Journal of Theoretical Biology*, 254:697–703, 2008.

[19] M. Caputo and C. Cametti. The memory formalism in the diffusion of drugs through skin membrane. *Journal of Physics D: Applied Physics*, 42:1–7, 2009.

[20] M. Caputo and J. Carcione. A memory model of sedimentation in water reservoirs. *Journal of Hydrology*, 476:426–432, 2013.

[21] M. Caputo and F. Mainardi. A new dissipation model based on memory mechanism. *Pure and Applied Geophysics*, 91:134–147, 1971.

[22] A. Carpinteri and F. Mainardi. *Fractals and Fractional Calculus in Continuum Mechanics*. Springer-Verlag Wien GmbH, 1997.

[23] J. Cresson and A. Szafrańska. Discrete and continuous fractional persistence problems-the positivity property and applications. *Communications in Nonlinear Science and Numerical Simulation*, 44:424–448, 2017.

[24] A. Dagbovie and J. Sherratt. Pattern selection and hysteresis in the Rietkerk model for banded vegetation in semi-arid environments. *Journal of The Royal Society Interface*, 11:1–13, 2014.

[25] B. Datsko and Y. Luchko. Complex oscillations and limit cycles in autonomous two-component incommensurate fractional dynamical systems. *Mathematica Balkanica*, 26:1–14, 2012.

[26] J. Dawes and M. Souza. A derivation of Holling's type I, II and III functional responses in predator–prey systems. *Journal of Theoretical Biology*, 327:11–22, 2013.

[27] W. Deng, C. Li, and J. Lü. Stability analysis of linear fractional differential system with multiple time delays. *Nonlinear Dynamics*, 48:409–416, 2007.

[28] K. Diethelm. *The Analysis of Fractional Differential Equations: An Application-Oriented Exposition Using Differential Operators of Caputo Type*. Springer, 2010.

[29] K. Diethelm and N. Ford. Analysis of fractional differential equations. *Journal of Mathematical Analysis and Applications*, 265:229–248, 2002.

[30] K. Diethelm, N. Ford, and A. Freed. A predictor-corrector approach for the numerical solution of fractional differential equations. *Nonlinear Dynamics*, 29:3–22, 2002.

[31] K. Diethelm, N. Ford, A. Freed, and Y. Luchko. Algorithms for the fractional calculus: a selection of numerical methods. *Computer Methods in Applied Mechanics and Engineering*, 194(6-8):743–773, 2005.

[32] K. Diethelm and A. Freed. The fracPECE subroutine for the numerical solution of differential equations of fractional order. *Forschung und wissenschaftliches Rechnen*, 1999:57–71, 1998.

[33] M. Du, Z. Wang, and H. Hu. Measuring memory with the order of fractional derivative. *Scientific Reports*, 3:1–3, 2013.

[34] H. El-Saka, S. Lee, and B. Jang. Dynamic analysis of fractional-order predator-prey biological economic system with Holling type II functional response. *Nonlinear Dynamics*, 96:407–416, 2019.

[35] M. El-Shahed, A. Ahmed, and I. Abdelstar. Dynamics of a plant-herbivore model with fractional order. *Progress in Fractional Differentiation and Applications*, 3:59–67, 2017.

[36] M. El-Shahed and A. Alsaedi. The fractional SIRC model and influenza A. *Mathematical Problems in Engineering*, 2011:1–10, 2011.

[37] M. Farkas. *Dynamical Models in Biology.* Academic Press, 2001.

[38] J. Forde. *Delay differential equation models in mathematical biology.* PhD thesis, University of Michigan, 2005.

[39] H. Freedman. *Deterministic Mathematical Models in Population Ecology.* Marcel Dekker Incorporated, 1980.

[40] H. Freedman and V. Rao. Stability criteria for a system involving two time delays. *SIAM Journal on Applied Mathematics*, 46:552–560, 1986.

[41] W. Gardner. Some steady-state solutions of the unsaturated moisture flow equation with application to evaporation from a water table. *Soil Science*, 85:228–232, 1958.

[42] R. Garrappa. On linear stability of predictor–corrector algorithms for fractional differential equations. *International Journal of Computer Mathematics*, 87:2281–2290, 2010.

[43] R. Garrappa. Short tutorial: solving fractional differential equations by Matlab codes, 2014, https://docplayer.net/42613994-Short-tutorial-solving-fractional-differential-equations-by-matlab-codes.html (accessed March 21, 2020).

[44] R. Garrappa. Trapezoidal methods for fractional differential equations: Theoretical and computational aspects. *Mathematics and Computers in Simulation*, 110:96–112, 2015.

[45] R. Garrappa. Numerical solution of fractional differential equations: A survey and a software tutorial. *Mathematics*, 6:16, 2018.

[46] E. Gilad, J. von Hardenberg, A. Provenzale, M. Shachak, and E. Meron. A mathematical model of plants as ecosystem engineers. *Journal of Theoretical Biology*, 244:680–691, 2007.

[47] A Golbabai and K. Sayevand. Analytical modelling of fractional advection–dispersion equation defined in a bounded space domain. *Mathematical and Computer Modelling*, 53:1708–1718, 2011.

[48] R. Gorenflo, A. Kilbas, F. Mainardi, and S. Rogosin. *Mittag-Leffler Functions, Related Topics and Applications.* Springer, 2014.

[49] I. Guerrini and D. Swartzendruber. Fractal characteristics of the horizontal movement of water in soils. *Fractals*, 2:465–468, 1994.

[50] V. Guttal and C. Jayaprakash. Self-organization and productivity in semi-arid ecosystems: Implications of seasonality in rainfall. *Journal of Theoretical Biology*, 248:490–500, 2007.

[51] K. Hadeler, M. Mackey, and A. Stevens. *Topics in Mathematical Biology*. Springer, 2017.

[52] G. Harrison. Comparing predator-prey models to Luckinbill's experiment with didinium and paramecium. *Ecology*, 76(2):357–374, 1995.

[53] R. HilleRisLambers, M. Rietkerk, F. van den Bosch, H. Prins, and H. De Kroon. Vegetation pattern formation in semi-arid grazing systems. *Ecology*, 82:50–61, 2001.

[54] C. Holling. The components of predation as revealed by a study of small-mammal predation of the European pine sawfly. *The Canadian Entomologist*, 91:293–320, 1959.

[55] C. Holling. Some characteristics of simple types of predation and parasitism. *The Canadian Entomologist*, 91:385–398, 1959.

[56] M. Iannelli and A. Pugliese. *An Introduction to Mathematical Population Dynamics: Along the Trail of Volterra and Lotka*, volume 79. Springer, 2015.

[57] M. Ishteva. *Properties and applications of the Caputo fractional operator*. Master thesis, Department of Mathematics, University of Karlsruhe, Karlsruhe, 2005.

[58] Y. Ji, J. Lu, and J. Qiu. Stability of equilibrium points for incommensurate fractional-order nonlinear systems. In *Proceedings of the 35th Chinese Control Conference*, pages 10453–10458, 2016.

[59] T. Kar, K. Chakraborty, and U. Pahari. A prey-predator model with alternative prey: Mathematical model and analysis. *Canadian Applied Mathematics Quarterly*, 18:137–167, 2010.

[60] R. Katz and B. Brown. Extreme events in a changing climate: variability is more important than averages. *Climatic Change*, 21:289–302, 1992.

[61] A. Khan and A. Tyagi. Disturbance observer-based adaptive sliding mode hybrid projective synchronisation of identical fractional-order financial systems. *Pramana-Journal of Physics*, 90:67, 2018.

[62] A. Kilbas, H. Srivastava, and J. Trujillo. *Theory and Applications of Fractional Differential Equations*. Elsevier, 2006.

[63] Y. Kuang. *Delay Differential Equations: With Applications in Population Dynamics*. Academic Press, 1993.

[64] R. Kumar, Vijay Shankar, and Mahesh Kumar Jat. Evaluation of root water uptake models–a review. *ISH Journal of Hydraulic Engineering*, 21:115–124, 2015.

[65] N. Leedle. *A new predictor-corrector method for solving nonlinear fractional differential equations with graded meshes*. PhD thesis, University of Chester, 2017.

[66] R. Lefever and O. Lejeune. On the origin of tiger bush. *Bulletin of Mathematical Biology*, 59:263–294, 1997.

[67] O. Lejeune, M. Tlidi, and P. Couteron. Localized vegetation patches: a self-organized response to resource scarcity. *Physical Review E*, 66:1–4, 2002.

[68] C. Li and Z. Zhao. Introduction to fractional integrability and differentiability. *The European Physical Journal Special Topics*, 193:5–26, 2011.

[69] Y. Li, Y. Chen, and I. Podlubny. Mittag–Leffler stability of fractional order nonlinear dynamic systems. *Automatica*, 45:1965–1969, 2009.

[70] W. Liu, C. Fu, and B. Chen. Hopf bifurcation for a predator–prey biological economic system with Holling type II functional response. *Journal of the Franklin Institute*, 348:1114–1127, 2011.

[71] C. Lubich. Discretized fractional calculus. *SIAM Journal on Mathematical Analysis*, 17:704–719, 1986.

[72] C. Magal, C. Cosner, S. Ruan, and J. Casas. Control of invasive hosts by generalist parasitoids. *Mathematical Medicine and Biology*, 25:1–20, 2008.

[73] D. Matignon. Stability results for fractional differential equations with applications to control processing. *Computational Engineering in Systems Applications*, 2:963–968, 1996.

[74] R. May. *Stability and Complexity in Model Ecosystems*. Princeton University Press, 2001.

[75] R. May and A. McLean. *Theoretical Ecology: Principles and Applications*. Oxford University Press, New York, 2007.

[76] S. McNaughton. Serengeti grassland ecology: the role of composite environmental factors and contingency in community organization. *Ecological Monographs*, 53:291–320, 1983.

[77] G. Melgoza, R. Nowak, and R. Tausch. Soil water exploitation after fire: competition between *bromus tectorum* (cheatgrass) and two native species. *Oecologia*, 83:7–13, 1990.

[78] K. Miller and B. Ross. *An Introduction to the Fractional Calculus and Fractional Differential Equations*. Wiley-Interscience Publication, 1993.

[79] J. Milton. Time delays and the control of biological systems: An overview. *IFAC-PapersOnLine*, 48:87–92, 2015.

[80] B. Morgan. Stochastic Models of Grouping Changes. *Advances in Applied Probability*, 8:30–57, 1976.

[81] A. Nayfeh. *Perturbation Methods*. John Wiley & Sons, 2008.

[82] T. Okayasu and Y. Aizawa. Systematic analysis of periodic vegetation patterns. *Progress of Theoretical Physics*, 106:705–720, 2001.

[83] K. Oldham and J. Spanier. *The Fractional Calculus Theory and Applications of Differentiation and Integration to Arbitrary Order*. Academic Press, 1974.

[84] A. Ouannas, Z. Odibat, A. Alsaedi, A. Hobiny, and T. Hayat. Investigation of Q-S synchronization in coupled chaotic incommensurate fractional order systems. *Chinese Journal of Physics*, 56:1940–1948, 2018.

[85] Y. Pachepsky and D. Timlin. Water transport in soils as in fractal media. *Journal of Hydrology*, 204:98–107, 1998.

[86] Y. Pachepsky, D. Timlin, and W. Rawls. Generalized Richards' equation to simulate water transport in unsaturated soils. *Journal of Hydrology*, 272:3–13, 2003.

[87] R. Pearl and L. Slobodkin. The growth of populations. *The Quarterly Review of Biology*, 51:6–24, 1976.

[88] I. Petras. Stability of fractional-order systems with rational orders: A survey. *Fractional Calculus & Applied Analysis*, 12:269–298, 2009.

[89] C. Pinto and A. Carvalho. The HIV/TB coinfection severity in the presence of TB multi-drug resistant strains. *Ecological Complexity*, 32:1–20, 2017.

[90] C. Pinto and A. Carvalho. A latency fractional order model for HIV dynamics. *Journal of Computational and Applied Mathematics*, 312:240–256, 2017.

[91] I. Podlubny. *Fractional Differential Equations*. Academic Press, 1999.

[92] S. Pooseh, H. Rodrigues, and D. Torres. Fractional derivatives in dengue epidemics. *AIP Conference Proceedings*, 1389:739–742, 2011.

[93] P. Raats. Steady flows of water and salt in uniform soil profiles with plant roots 1. *Soil Science Society of America Journal*, 38:717–722, 1974.

[94] P. Raats. Developments in soil-water physics since the mid 1960s. *Geoderma*, 100:355–387, 2001.

[95] P. Raats, D. Smiles, and A. Warrick. Contributions to environmental mechanics: Introduction. *Geophysical Monograph 129*, 129:1–28, 2002.

[96] H. Richard. *Fractional Calculus: an Introduction for Physicists*. World Scientific Publishing, 2014.

[97] L. Richards. The usefulness of capillary potential to soil-moisture and plant investigations. *Journal of Agricultural Research*, 37:719–742, 1928.

[98] L. Richards. Capillary conduction of liquids through porous mediums. *Applied Physics*, 1:318–333, 1931.

[99] M. Rietkerk, M. Boerlijst, F. van Langevelde, R. HilleRisLambers, J. van de Koppel, L. Kumar, H. Prins, and A. de Roos. Self-organization of vegetation in arid ecosystems. *The American Naturalist*, 160:524–530, 2002.

[100] M. Rietkerk, S. Dekker, De R., and J. van de Koppel. Self-organized patchiness and catastrophic shifts in ecosystems. *Science*, 305:1926–1929, 2004.

[101] M. Rietkerk and J. van de Koppel. Alternate stable states and threshold effects in semi-arid grazing systems. *Oikos*, 79:69–76, 1997.

[102] F. Rihan. Numerical modeling of fractional-order biological systems. *Abstract and Applied Analysis*, 2013:1–11, 2013.

[103] T. Roose and A. Fowler. A model for water uptake by plant roots. *Journal of Theoretical Biology*, 228:155–171, 2004.

[104] T. Roose, A. Fowler, and P. Darrah. A mathematical model of plant nutrient uptake. *Journal of Mathematical Biology*, 42:347–360, 2001.

[105] T. Roose and A. Schnepf. Mathematical models of plant–soil interaction. *Philosophical Transactions of the Royal Society A: Mathematical, Physical and Engineering Sciences*, 366:4597–4611, 2008.

[106] Y. Rubin and D. Or. Stochastic modeling of unsaturated flow in heterogeneous soils with water uptake by plant roots: The parallel columns model. *Water Resources Research*, 29:619–631, 1993.

[107] P. Saco, G. Willgoose, and G. Hancock. Eco-geomorphology of banded vegetation patterns in arid and semi-arid regions. *Hydrology and Earth System Sciences*, 11:1717–1730, 2007.

[108] T. Saha and M. Bandyopadhyay. Dynamical analysis of a plant-herbivore model bifurcation and global stability. *Journal of Applied Mathematics and Computing*, 19:327–344, 2005.

[109] S. Samko, A. Kilbas, and O. Marichev. *Fractional Integrals and Derivatives*. Gordon and Breach Science Publishers, 1993.

[110] G. Schoups and J. Hopmans. Analytical model for vadose zone solute transport with root water and solute uptake. *Vadose Zone Journal*, 1:158–171, 2002.

[111] R. Scott, W. Shuttleworth, D. Goodrich, and T. Maddock III. The water use of two dominant vegetation communities in a semiarid riparian ecosystem. *Agricultural and Forest Meteorology*, 105:241–256, 2000.

[112] N. Shnerb, P. Sarah, H. Lavee, and S. Solomon. Reactive glass and vegetation patterns. *Physical Review Letters*, 90:038101, 2003.

[113] R. Srivastava and T. Yeh. Analytical solutions for one-dimensional, transient infiltration toward the water table in homogeneous and layered soils. *Water Resources Research*, 27:753–762, 1991.

[114] J. Stewart, D. Clegg, and S. Watson. *Calculus: Early Transcendentals*. Cengage Learning, 2020.

[115] N. Sweilam, A. Nagy, T. Assiri, and N. Ali. Numerical simulations for variable-order fractional nonlinear delay differential equations. *Journal of Fractional Calculus and Applications*, 6:71–82, 2015.

[116] M. Tavazoei and M. Haeri. A necessary condition for double scroll attractor existence in fractional-order systems. *Physics Letters A*, 367:102–113, 2007.

[117] M. Tavazoei and M. Haeri. Chaotic attractors in incommensurate fractional order systems. *Physica D: Nonlinear Phenomena*, 237:2628–2637, 2008.

[118] M. Tavazoei and M. Haeri. A proof for non existence of periodic solutions in time invariant fractional order systems. *Automatica*, 45:1886–1890, 2009.

[119] S. Taylor and S. Campbell. Approximating chaotic saddles for delay differential equations. *Physical Review E*, 75:046215, 2007.

[120] J. Thiery, J. d'Herbes, and C. Valentin. A model simulating the genesis of banded vegetation patterns in Niger. *Journal of Ecology*, 83:497–507, 1995.

[121] A. Tsoularis and J. Wallace. Analysis of logistic growth models. *Mathematical Biosciences*, 179:21–55, 2002.

[122] P. Turchin. *Complex Population Dynamics: A Theoretical/Empirical Synthesis*. Princeton University Press, 2003.

[123] R. Upadhyay and S. Iyengar. *Introduction to Mathematical Modeling and Chaotic Dynamics*. CRC Press, 2013.

[124] N. Ursino and S. Contarini. Stability of banded vegetation patterns under seasonal rainfall and limited soil moisture storage capacity. *Advances in Water Resources*, 29:1556–1564, 2006.

[125] B. van der Waerden. *Algebra*. Springer Science & Business Media, 2003.

[126] J. von Hardenberg, E. Meron, M. Shachak, and Y. Zarmi. Diversity of vegetation patterns and desertification. *Physical Review Letters*, 87:198–101, 2001.

[127] B. Wang, L. Zhao, and Z. Liu. Robust H_∞ observer-based synchronization for a class of incommensurate fractional chaotic systems. In *Proceedings of the 35th Chinese Control Conference*, pages 10532–10537, 2016.

[128] C. Wang, B. Fu, L. Zhang, and Z. Xu. Soil moisture–plant interactions: An ecohydrological review. *Journal of Soils and Sediments*, 19:1–9, 2019.

[129] Y. Xu and Z. He. Synchronization of variable-order fractional financial system via active control method. *Central European Journal of Physics*, 11:824–835, 2013.

[130] J. Yu, H. Hu, S. Zhou, and X. Lin. Generalized Mittag-Leffler stability of multi-variables fractional order nonlinear systems. *Automatica*, 49:1798–1803, 2013.

[131] F. Yuan and Z. Lu. Analytical solutions for vertical flow in unsaturated, rooted soils with variable surface fluxes. *Vadose Zone Journal*, 4:1210–1218, 2005.

[132] K. Zhang, H. Wang, and H. Fang. Feedback control and hybrid projective synchronization of a fractional-order Newton–Leipnik system. *Communications in Nonlinear Science and Numerical Simulation*, 17:317–328, 2012.